NTNU
Norwegian University of
Science and Technology

Functionalization of Silica Aerogels and AlPO-5 with Molybdenum, Rhenium

A Study on Metal Introduction Methods

Tengzhi Liu

Chemistry
Submission date: May 2018
Supervisor: Karina Mathisen, IKJ

Norwegian University of Science and Technology
Department of Chemistry

Functionalization of Silica Aerogels and AlPO-5 with Molybdenum, Rhenium

A Study on Metal Introduction Methods

Tengzhi Liu

Department of Chemistry

Norwegian University of Science and Technology

This dissertation is submitted for the degree of

Master of Science in Chemistry

2018

Acknowledgements

This master project was supported by the Department of Chemistry at the Norwegian University of Science and Technology (NTNU), Trondheim, Norway. Funding from the university for both theoretical studies and experimental works to this project is greatly appreciated.

Foremost, I would like to express my sincere and immense gratitude toward my thesis supervisor Associate Professor Karina Mathisen for the continuous supports and encouragements throughout my entire master study. The insights and expertise she provided are invaluable both to this project and to myself, without which this work certainly could not have been completed.

I would also like to specially thank Ph.D. candidate Karsten Granlund Kirste and Ph.D. candidate Guro Sørli for their assistance in laboratory works and thorough explanations of all the questions I had during my master study.

In addition, I am also especially grateful to all the other members of the structural chemistry group, in particular to Post Doctoral Fellow Tina Kristiansen Voss, for sharing valuable opinions on aerogel synthesis and interpretation of results, to Ph.D candidate Stian Forselv for his comments on my presentations, to formal master student Sondre Håbrekke and Joakim Tafjord, for their assistance and comments during my first year of the study, and to master student Anders Hutcheson, for being a faithful friend and participated in some of the discussions during my study.

Thanks also to other employees at the Faculty of Natural Science, including Syverin Lierhagen for ICP-MS analysis, Kristin Høydalsvik-Wells and Magnus Rotan for assistance with XRD, Elin Harboe and Laura Rioja-Monllor for assistance with BET, and anyone else who in one way or an other provided assistance in my study.

Last but not least, I am always grateful to my family, who continuously supported my studies and always willing to provide wise consultation for my success.

May 15, 2018

Trondheim, Norway

Abstract

In the present work possible routes for the introduction of Mo and Re into silica aerogels and aluminophosphate AlPO-5 have been investigated. Parameter studies on the influence of synthesis conditions including metal precursor, metal molar ratio, sol pH, gelation mechanism, and post treatments have been performed on the synthesis of Me-aerogels. Parameter studies on the synthesis of MeAlPO-5 have been performed with varying metal precursor, sol preparation method, sol pH, choice of structural directing agent, and crystallization conditions. Both Mo and Re have been introduced into silica aerogels following the sol-gel route and ambient pressure drying method, in which the metal (Mo or Re) precursor was added during the sol stage before gelation. The as-prepared Mo-aerogels were all amorphous with metal content up to 0.56 wt.%, whereas all as-prepared Re-aerogels contain both amorphous and crystalline phases with metal content up to 6.61 wt.%. Direct introduction of Mo into AlPO-5 by isomorphous substitution obtained phase pure samples with metal content up to 0.12 wt.%. Direct introduction of Re into AlPO-5 produced samples either contain significant amount of extra phases, or with negligible amount of metal content. An indirect method to introduce Re into AlPO-5 through the intermediate GeAlPO-5 has been attempted in the first stage, where GeAlPO-5 was synthesized with the precursor GeO_2, yielding Ge content up to 0.84 wt.%.

Table of Contents

List of Figures

List of Tables

Nomenclature and Abbreviations

AFI : AlPO-5 framework

AM : Ammonium molybdate

APD : Ambient pressure drying method

APR : Ammonium perrhenate

BET : Brunauer–Emmett–Teller theory

BJH Barrett-Joyner-Halenda theory

CP : Co-precursor route

DEA : Diethylamine

$DIPA$: Diisopropylamine

DPA : Dipropylamine

$FT-IR$: Fourier transform infrared spectroscopy

$HMDS$: Hexamethyldisilazane

$HMDSO$: Hexamethyldisiloxane

$ICP-MS$: Inductively coupled plasma mass spectrometry

$IUPAC$: International Union of Pure and Applied Chemistry

$MDCHA$: N,N-Dicyclohexylmethylamine

$MeAERO/Me-aerogel$: Metal ion introduced silica aerogels, Me = Mo, Re

$MeAlPO-5$: Metal ion introduced AlPO-5 framework, Me = Mo, Re, Ge

MTO : Molybdenum trioxide, MoO_3

NPs : nanoparticles.

SA : Silicic acid

SD : Surface derivatization route

SDA : Structure directing agent

TEA : Triethylamine

TEAOH : Tetraethylammonium hydroxide solution

TEPA : Tetraethylenepentamine

TPA : Tripropylamine

XRD/*PXRD* : X-ray diffraction/Powder X-ray diffraction

Amo : Amorphous

AP : As-prepared

Cal : Calcined

Crys. : Crystalline

TMCS : Trimethylchlorosilane

Chapter 1

INTRODUCTION

1.1 Background and Motivation

Ever since the industrial revolution, the rapid advance in science and technology has forever changed the condition and ways of living for human beings. Energy and energy technology are the fundamental driving force that continuously powers the development of science and technology. Today, 79% of the world total energy consumption is still from fossil fuels (coal, oil, and natural gas, 2017)[1]. However, the ever growing use of fossil energy has led us into two major obstacles: the limited energy resources, and climate change due to influence including air pollution and CO_2 emissions. Extensive efforts have been made in searching for clean and renewable energy sources and carriers for the future. One possibility for clean and renewable energy is through the use of hydrogen technology, where hydrogen acts as a carrier for clean energy generated from renewable sources such as solar panels, wind turbines, etc[2]. Using hydrogen to power applications such as vehicles has the advantage that the only reaction product is water, effectively eliminates any on-site emission of CO_2, NO_x, and volatile organic compounds (VOCs), providing a viable path to a carbon neutral future society and reducing the climate impact due to human activities[2].

The current application of hydrogen for vehicles is to a large extend limited. One of the major challenges is the on-board storage of hydrogen, which has a relatively small volumetric energy density compares to gasoline, even when it is stored in a compressed tank or as a liquid in a cryogenic container[3][4]. One other issue concerning the production methods is the purity of the hydrogen. Conventional methods, which predominantly use steam reforming of fossil fuels, may produce hydrogen contains hydrocarbon and other impurities (such as methane, ethane, CO) that are toxic to the fuel cell catalyst[5]. Recent advances in hydrogen storage technology shown that storing hydrogen in the form of ammonia, which can be easily

liquefied at room temperature, can significantly improve the volumetric energy density of hydrogen, as well as having ultra-high purity[6][7][8]. On-site hydrogen production can be performed via the catalytic decomposition of ammonia. The development of effective and versatile while economically feasible catalysts is therefore a critical factor. However, studies on existing commercial catalysts for ammonia decomposition has shown limitations in achieving the necessary performance[9]. New catalytic materials that can eventually meet with the requirements are therefore in need.

Recently, in catalytic materials there has been a growing interest in using porous oxide materials as catalytic supports for more effective catalytic reaction processes, which increases the catalytic efficiency and decrease the overall costs[10][11][12]. Using porous oxides as catalytic supports has the advantages for its large inner surface area and pore volume, possible shape and size selectivity [12]. Roughly speaking there are two categories of different types of porous materials that can be used as catalytic supports, crystalline (or ordered) porous materials such as zeolites, zeotypes, and amorphous materials such as silica. However traditionally the application of these porous materials are limited by the challenges that they are easily deactivated due to sintering effects of the active metals [13]. Fortunately, newly developed synthesis methods in which the metal is introduced together with the precursors of the supports have shown promising results in overcoming these challenges in both silica aerogels and zeotypes, despite their difference in structures [14][15]. Meanwhile, prior studies have shown that molybdenum (Mo) and rhenium (Re) are active toward ammonia decomposition[16][17][18][19–21]. Using porous oxide materials for catalytic supports of Mo and Re may thus lead to new solutions for more effective catalysts for ammonia decomposition.

Silica aerogels are a class of porous amorphous materials (2-50 nm) that have extremely high surface area (500-1200 m^2/g) and porosity, in which 99% of the occupied volume is air, and consisting both mesopores and micropores[22][23]. The featuring of mesopores and the ability to manipulate the pore architectures are attractive properties for the design and synthesis of new catalytic materials[14][24]. On the other hand, zeolites and zeotypes are a class of microporous crystalline materials that emphasizes the catalytic selectivity[15]. The structure and property of zeolites/zeotype can be fine tuned to include pores with different dimensions (1-D to 3-D), sizes, and shapes, therefore by functionalizing the porous surface they can be designed as reactant/product specific catalysts[25]. These functionalized zeolite/zeotype structures can essentially act as true molecular micro-reactors and become highly selective toward certain desirable reactions[25].

The main focus of this study is to introduce transition metal Mo and Re into silica aerogels and aluminophosphate AlPO-5 (a zeotype). Although there has been some studies using aerogels or zeotypes as catalytic supports, most of the prior works involved using post-synthesis functionalization methods, such as ion-exchange, incipient wetness impregnation, or deposit-precipitation[26][27][28][29]. These methods have the advantages that they have straightforward procedures, but also have the drawback that the distribution of the active metal ions is low and lacking the interaction between the active phase and the support materials [26][27][30][31]. On the other hand, other works have shown that incorporation of single-site active atoms into the support structure can maximize the dispersion of the active phase and ensure an even distribution, as well as avoiding potential sintering effects[13][26]. However, the possible synthesis routes of Me-aerogels (Me=Mo, Re) have not been thoroughly studied; no synthesis of ReAlPO-5 has been reported, one report claimed to synthesized MoAlPO-5, but the authors admitted that no direct proof of incorporation was given, and the results are inconclusive[32]. This project is therefore to investigate the possibility of introducing Mo and Re species into silica aerogels and AlPO-5 following similar methods for the incorporation. In the most ideal case the single-site incorporated samples are desired; however no experiment in this study is to confirm the existence of single-site active metals, therefore no conclusion will be drawn with respect to single-site speciation. Instead this work will be dedicated to exploring the possible routes and investigating the influencing factors for the introduction, which will lay down the ground work for future studies to synthesize possible metal incorporated samples.

1.2 The Project Scope

The general goal of this project is two fold. First, to explore the possibility and investigate the influencing factors for the introduction of molybdenum and rhenium into silica aerogels and AlPO-5, based on previously developed new methods[14][33][34][35][36]. Second, to investigate if the introduction can be controlled for possible incorporation of the metal species into the supports.

In the attempt to introduce metal ions (Mo, Re) into silica aerogels, the experiments will follow the sol-gel route and ambient pressure drying (APD) method based on the prior work by Kristiansen et al., which has reported successful incorporation of Cu(II) into the silica aerogel network through the sol-gel route and ambient pressure drying method [14][26]. The investigation will focus on the influence of varying the molar ratio between the added

metal ion and silicon ions (Me:Si), varying the metal precursors, varying the pH of the sol, using different surface modification agents, and the effects of post-synthesis treatments, to the phase of the samples (crystalline or amorphous), metal loading, and surface and pore characteristics. The results will be compared with similar prior studies in the literature.

The introduction of metals into aluminophosphate AlPO-5 (MeAlPO-5) will be based on a series of prior studies that have led to successful incorporation of several different metal ions (including (Cu(II), V(IV), Fe(III), etc.)) through isomorphous substitution with hydrothermal synthesis[15][33][37][38]. The varying parameters include the precursor of the metal ion, the preparation method of the suspension, the choice of the structure directing agent (SDA), the crystallization temperature, and the crystallization time. The samples will be characterized by their phases, metal contents, and surface and pore characteristics. The results will also be compared with literature to determine the quality of the samples.

The characterization of the samples will be focused on using powder X-ray diffraction (XRD) for phase determination, inductively coupled plasma mass spectroscopy (ICP-MS) for the elemental composition analysis, N_2- Brunauer-Emmett-Teller (BET) adsorption-desorption method for the surface area and porosity analysis. The pore size distribution, average pore size, and cumulative pore volume will also be calculated based on the Barrett-Joyner-Halenda (BJH) theory[39].

Chapter 2

THEORY

2.1 Molybdenum and Rhenium as Catalysts

This section serves as a basic introduction of molybdenum/rhenium and their active species in catalysis. The detail mechanisms of catalytic activities have been well described in the literature such as [16][40], but the description is beyond the scope of this study. The introduction will focus on the known active species in catalysis, and how they relate to the materials in this study.

2.1.1 Molybdenum and molybdenum catalysts

Molybdenum is a transition metal element located in group six on the fifth period of the periodic table. It has an atomic number of 42 and an abundance-weighted average atomic mass of 95.96 atomic units[41]. It was first discovered by German-Swedish chemist Carl Wilhelm Scheele in 1778 and later isolated by Peter Jacob Hjelm in 1781[42][43]. Molybdenum and molybdenum compounds have a wide range of applications in catalysis, such as in the ammonia decomposition for hydrogen production, selective oxidation of propylene to acrolein and acrylic acid, conversion of synthesis gas to alcohol, etc. [16][44][45]. In particular the catalytic activity toward ammonia decomposition for hydrogen production is of particular interest for this study, being a part of the joined effort in the development of clean energy, as previously described.

Molybdenum processes rich and versatile chemical properties, forming compounds from oxidation state of -2 to +6. The most active molybdenum compound studied toward ammonia decomposition is the molybdenum nitride, MoN_x [16], which is formed when the trioxide MoO_3 reacts with NH_3 in a series of temperature programs (600 K to 900 K)[40]. In a

fresh catalyst the active species is therefore MoO_3, which can be formed via thermal decomposition of ammonium molybdate through different polymolybdate intermediate products upon annealing at approximately 400°C [16][46]. MoO_3 is insoluble in water, but can react with alkaline solutions to form soluble molybdates[47]. Therefore, molybdate salts such as ammonium molybdate would be a natural choice for syntheses of Mo(VI) containing samples in aqueous solution, which will be used in this study.

2.1.2 Rhenium and rhenium catalysts

Rhenium was discovered by the German chemists Walter Noddack, Otto Carl Berg, and Ida Tacke in 1925 as the last element found with stable isotopes [48]. It is a transition metal element locates at the sixth period of the seventh group on the periodic table of elements. It is a precious metal with a variety of applications, such as making alloys for the turbine blades, combustion chambers, exhaust nozzles of jet engines, which is the single largest application and accounted for over 80% of annual consumption of rhenium [49]. It is also catalytic active toward different reactions and used as catalysts in the petroleum industry, which accounted for approximately 10% of annual consumption [49]. Similar to Mo, this study is based on its catalytic activity toward ammonia decomposition for the application in hydrogen production, which has been shown in previous works[18] [19–21].

The active rhenium species for ammonia decomposition is the metallic rhenium [18]. The most convenient method to introduce rhenium into catalyst supports is through impregnation with the perrhenate acid, $HReO_4$, or its soluble salts [50]. Therefore to be catalytic active the fresh catalysts will need to be treated with H_2 at 400 to 450°C which will reduce rhenium from Re(VII) to its metallic form[51]. Previous studies have also shown that it can also be introduced in bi-metallic system with another component such as cobalt, as a promoter, in which both metals are reduced upon treatment with H_2, forming a metal alloy [51]. This work will focus on introducing rhenium alone into the supports. Re(VII) species Re_2O_7 and NH_4ReO_4 will be used as precursors.

2.2 Porous Materials as Catalytic Supports

2.2.1 Porous materials

Porous materials are a type of solid materials in which the structure contains a large number of pores (or voids), either they are channels, cavities, or interstices[52][53]. Porous materials can be either organic or inorganic, and in this study the term limits to inorganic porous oxides. There are different ways to classify porous materials, including by their pore sizes and shapes, ordered (crystalline) or disorder (amorphous), and different compositions[53]. A schematic illustration of some different types of pores is shown in Figure 2.1.

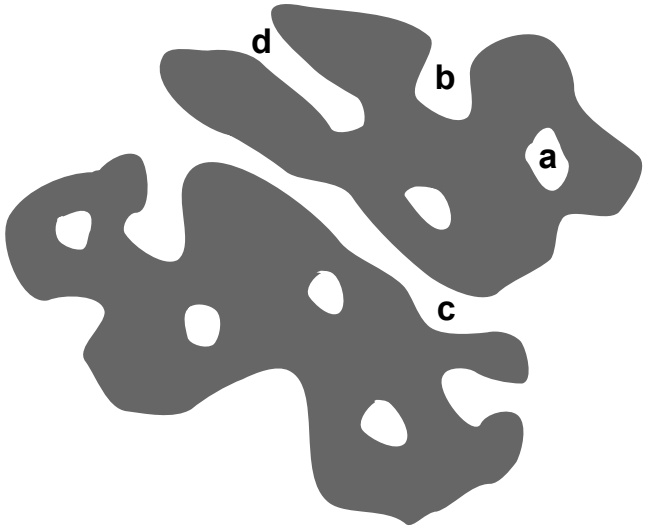

Figure 2.1 A schematic illustration of different types of pores. (a) A close pore. (b) An ink-bottle shaped open pore. (c) An open channel. (d) A cylindrical open pore. Figure adapted from[53].

Porous materials with open pores are excellent candidates for the supporting materials of catalysts, as they typically have very large surface area and provides maximum dispersion for the active materials[31]. The size of the pores is usually consider an important factor of porous materials, since it not only affects the specific surface area of the materials, but also has substantial influence on the catalytic activities of the materials toward different chemical reactions by selecting specific size of molecules to enter/exit the pores[54][55]. However, the pore size is usually difficulty to define, because of the diverse variety of pore shapes and the possible broad distribution of sizes[53], as illustrated in Figure 2.1 above. IUPAC defined three different kinds of pores based on their sizes compare to the mean free path of a typical gas, For instance, the mean free path of air at ambient condition is approximately 68 nm[56]. Macropores are defined as cavities or voids that are larger than 50 nm in diameter, in which case the pores are much larger than the mean free path of a typical gas fluid, resulting in

high permeabilities but low or none permselectivities[53][57]. Mesopores occupy the range of 2 - 50 nm, they have sizes comparable to the mean free path of a typical gas fluid and Knudsen diffusion is significant, in which the gas flux is dependent on the inverse-square-root of the molecular weight [53][57]. And finally, micropores refer to pores with diameter less than 2 nm, much smaller than the mean free path of a typical gas, which leads to high permselectivities[53][57]

The two different porous materials in this study contain quite different pore systems. Silica aerogels are a class of mesoporous materials, with both micropores and mesopores present and a relatively broad pore size distribution[23]. On the other hand, AlPO-5 is a crystalline material features micropores with a narrow pore size distribution[58]. A schematic illustration of pore sizes and pore size distributions of some different types of porous materials is shown in Figure 2.2. Actual pore sizes and pore size distributions may vary due to different preparation and measurement methods.

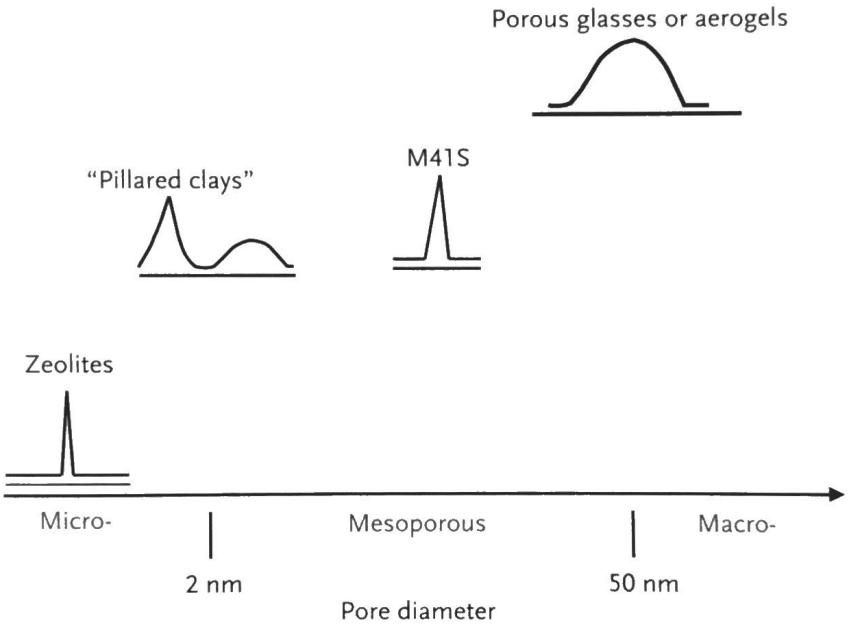

Figure 2.2 Some different types of porous materials and their typical pore sizes. Materials relevant to this study are zeolites (similar to zeotypes) and aerogels. Figure re-printed from[53] with permission.

2.3 Silica Aerogels

2.3.1 Structure and properties

Silica aerogels are a type of porous amorphous materials derived from the wet silica gels (or silica hydrogels). First synthesized by S. S. Kistler in 1931[22], it features some very impressive properties, such as ultra-high specific surface area (500 - 1200 m^2/g), very high porosity and extremely low density (0.003 - 0.05 g/cm^3), low thermal conductivity and dielectric constant[23]. These properties of silica aerogel attract a variety of applications, from thermal insulation, catalyst supports, to space dust collection[59]. In this project silica aerogel will be used as a new type of catalyst support, to be functionalized with metals Mo or Re.

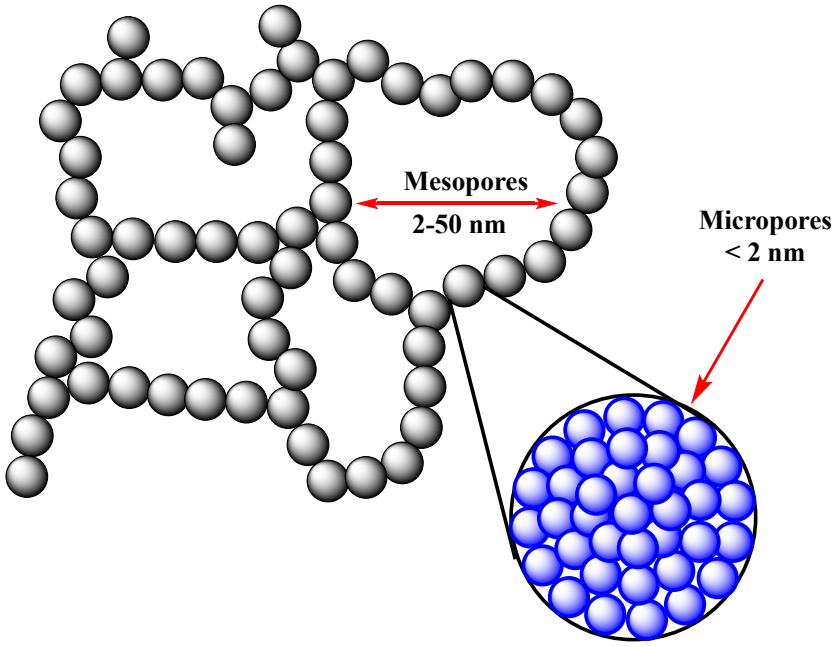

Figure 2.3 A schematic illustration of silica aerogels showing the mesopores and micropores. Figure adapted from[14].

The primary structure of a silica aerogel is a 3-dimensional interlinked SiO_2 network, which consists of silica nanoparticles (NPs), as shown in the schematic illustration in Figure 2.3 as the blue spheres. It differs from the conventionally dried silica gel (or the xerogel) that although both an aerogel and a xerogel are porous materials consist of silica, the mesopores in an aerogel are preserved whereas in a xerogel the mesopores are mostly collapsed or shrank. The primary reason for the mesopore shrinkage or collapse is because when water is evaporated from the mesopores of the hydrogel, the hydrophillic surface of the gel network is subject to substantial stress from the surface tension of water, which eventually

causing the mesopores to collapse[24]. Replacing water with a different solvent that has less surface tension by solvent exchange can significantly reduce the shrinkage and prevent collapse of the mesopores, resulting an aerogel. This is also the reason that xerogels are mostly microporous, while aerogels are both microporous and mesoporous: in xerogels the larger mesopores collapsed during the drying process, and in aerogels the mesopores are preserved[14][23][60][61].

The structure and surface characteristics of silica aerogels are largely dependent on the methods that it is prepared. Conventionally, silica aerogels are prepared by the so-called supercritical drying (SCD) method. In the SCD method, water is first washed away with an alcohol, then the alcohol is replaced with liquid CO_2 at high pressure, which then transformed into a supercritical fluid[62]. As the pressure gradually released, the dried aerogels can be obtained[62]. Replacing the water in the pores with a supercritical fluid, which has zero surface tension, can fully preserves the gel network without collapsing the pores[24][63]. However the use of supercritical fluids is costly and requires complicated process, limiting its application and commercial availability[24]. Since then various methods to synthesize aerogels with ambient pressure drying (APD) method have been developed, and dramatically simplify the synthesis process and lowered the costs while preserving the special properties[24][64][65].

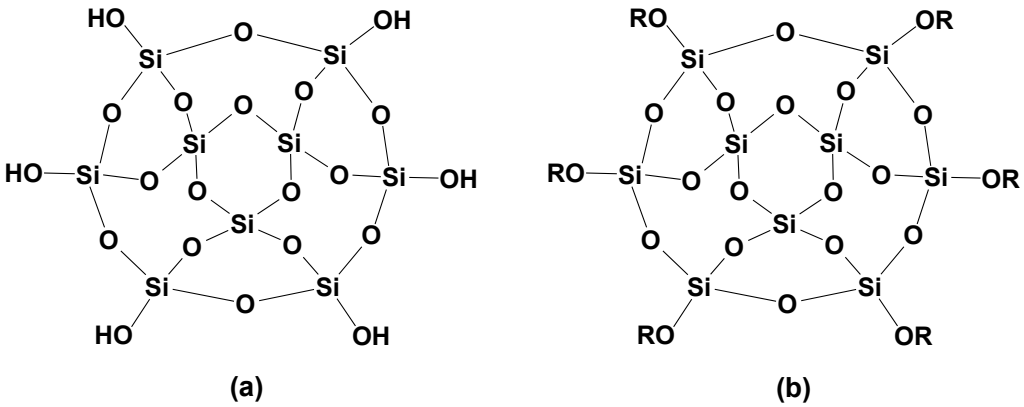

Figure 2.4 A schematic illustration of (a). A hydrophilic silica nanoparticle and (b). A hydrophobic silica nanoparticle. These nanoparticle are the building blocks of the aerogel structure, represented in Figure 2.3 as the blue spheres.

In this study, all aerogel sample will be synthesized using the APD method. Figure2.4 a shows an example of a hydrophilic silica nanoparticle, which constitutes the silica gel network by interlinkages with other nanoparticles. The core of the APD method is to modify the surface of the aerogel from hydrophilic to hydrophobic. By modifying the hydrophilic surface to hydrophobic as shown in Figure 2.4b, it will repel water and when a non-polar

solvent is present, water can be pushed out of the pores in exchange of the non-polar solvent. The non-polar solvent can be chosen to have a small surface tension and therefore when it is evaporated, the surface will be subject to much less stress and pore collapse can be prevented. Further discussion of the APD method will be given in the following sections.

2.3.2 Aerogel preparation: the ambient-pressure drying method

To compensate the disadvantages of the SCD method and to expend the study and utilization of silica aerogels, various ambient-pressure drying (APD) methods of silica aerogel synthesis had been developed[60][65][66] [67][68][69]. The key idea of the APD method is that the surface of the aerogel is modified with silylation agents to become hydrophobic, and in the presence of another (typically nonpolar) organic liquid phase which has lower surface tension, the water can be expelled by the surface in exchange with the organic solvent. The organic solvent will have much less surface tension upon drying, therefore prevents the shrinkage of the pores and the collapse of the gel network. Another advantage of surface modification is that although the hydrophobic surface of aerogel still experiences some compressive stress when the solvent is removed, the inert surface will prevent collapse of the pores by forbidding the formation of siloxane bonds, and the pores can relax back to the original position when the solvent is removed [14][64][68][70][71][72].

The first step of the synthesis following the sol-gel route is the preparation of the sol. The sol is essentially a colloidal solution of silicic acid. Traditionally the silicon precursor is a silicon alkoxide, such as tetraethyl ortho-silicate (TEOS)[71]. In such case the silicon precursor will first been hydrolyzed in the presence of either an acid or a base, which will replace the organic -R group. However TEOS is also a costly precursor. In this study a much cheaper precursor, sodium silicate (water glass), will be used. The structure of sodium silicate in a solution is shown in Figure 2.5.

The water glass colloidal solution will be ion-exchanged with a proton source, such as a column of sulfonic acid immobilized in a styrene-divinylbenzene matrix. The ion-exchange replaces the Na^+ with protons which combine with oxygen atom to become hydroxyl groups and the silicic acid is obtained. It is also important to monitor the pH during these process. Typically the water glass solution will have a pH of approximately 11.5, and when the ion-exchange with proton is completed, the colloidal solution should have a pH of around 2-3[14][71].

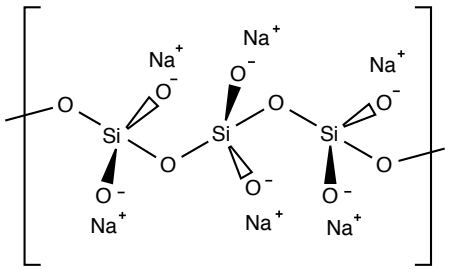

Figure 2.5 A simple sketch of the general structure of sodium silicate, the terminal oxygen is connected to the next silicon atom at the both ends.

The gelation of silicic acid is essentially a polycondensation reaction in which the monomer $Si(OH)_4$ condenses into a large network of silica polymer[73]. During the process, the colloidal solution system losses its fluidity as the SA molecules condense into large polymer structures[74]. Upon completion of the reaction, the gel can be seen as a single macroscopic molecules as all the monomers condensed and connected to each other, which is essentially a polymer with infinite size[75]. This reaction can be catalyzed by either an acid or a base. The reaction between two monomers is shown in Figure 2.6.

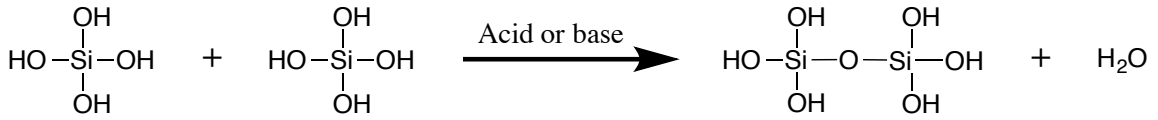

Figure 2.6 Polycondensation reaction of silicic acid monomers to form a large interconnected network. The reaction can be catalyzed either by an acid or a base, which eventually produces a network consists of $[SiO_4]$ units.

The pH of the sol is a crucial parameter for the gelation, since it will affect whether the gelation is catalyzed by an acid or a base. Different catalytic mechanisms will lead to different structure of the gel, which eventually resulting different morphology of the samples (i.e. pore sizes, surface area). Studies have shown that the base catalyzed reaction is a kinetic favored mechanism, which leads to larger pore, narrow distribution of pore size, and higher porosity[60][76]. In comparison, the acid catalyzed reaction follows a slower reaction mechanism. The resulting gel is more of a polymer like species, which contains a large number of micropores and high surface area, but lack of mesopores compares to the base-catalyzed reaction[14]. A schematic illustration of gelation catalyzed by acid or base is shown in Figure 2.7 .

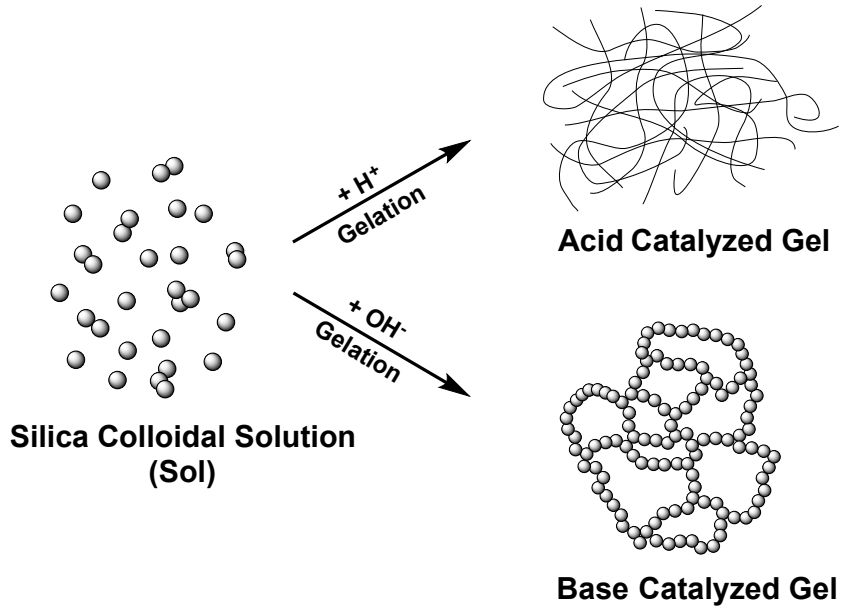

Figure 2.7 Illustration of silica aerogels produced by acid catalyzed or base catalyzed gelation.

The essence of the aerogel preparation is to prevent the collapse of the pores when the liquid is removed. There are two ways of doing so, either use a fluid that has very low or none surface tension, like the SCD method as previously mentioned, or alternatively, modify the surface of the gel (which consists of hydroxyl groups) to hydrophobic and allows the water to be expelled, as in the APD method. In the APD method, one or more surface modification agent(s) will be used to replace the hydroxyl groups with silyl groups via the silylation reactions. To achieve the hydrophobicity, the silylation agents are often chosen to have bulky organic nonpolar endings, such as HMDS, HMDSO, TMCS. In this case when the silyl groups are attached, the surface of the gel will be full of -CH_3 groups, which rapidly repels water. In this study for most of the samples the silylation agents will be HMDS and HMDSO for base catalyzed gelation by generating the reaction product NH_3. TMCS may be also used for a comparison sample following the acid catalyzed gelation. The surface modification with TMCS that will trigger acid catalyzed gelation involves the reaction shown in Figure 2.8.

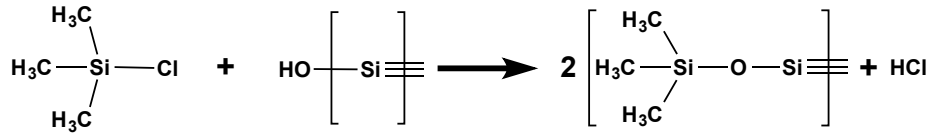

Figure 2.8 Surface modification with TMCS, which will trigger the acid catalyzed gelation.

Similarly, when HMDS and HMDSO are used for surface modification, the reaction produces NH_3, which subsequently triggers the base catalyzed gelation. The surface modification reactions involved in this case are shown in Figure 2.8.

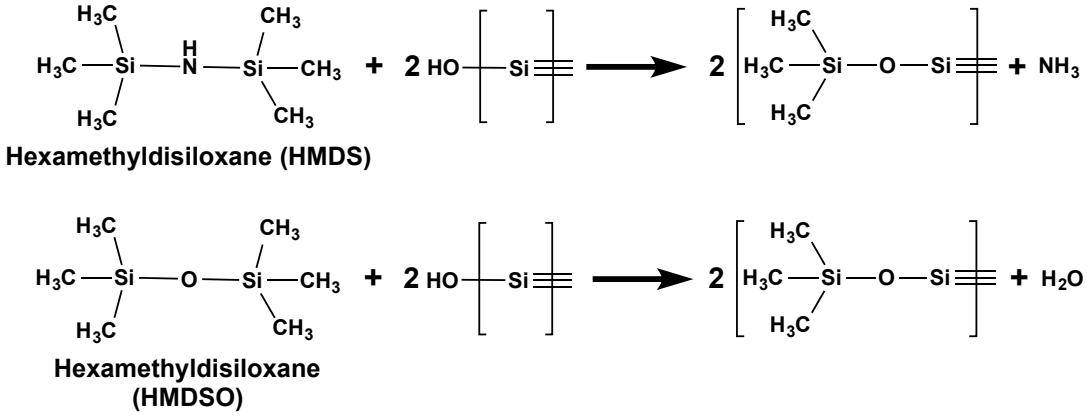

Figure 2.9 Surface modification with HMDS and HMDSO, which will trigger the base catalyzed gelation.

As previously mentioned, the pH conditions in which the samples are prepared will have strong influence on the morphology of the samples. Furthermore, the pH of the sol may also have strong influence to the interaction between SA and the speciation of the precursor. During the experiments the pH of the sol will be closely monitored, and in some of the experiments it will be adjusted to either be more acidic or basic. It is important to mention that the gelation mechanism in this experiment depends on the choice of silylation agent but not necessarily on the sol pH.

The steps of the APD method with base catalyzed gelation are as follow: Once the surface modification agents are added into the silica colloidal solution, the reactions begin as shown in Figure 2.9. The reaction with HMDS produces ammonia, which is basic in aqueous solution. The sudden increase of pH catalyzes and triggers the polycondensation reaction of the silica, which is shown in Figure 2.6. The resulting product is the base catalyzed formation of the hydrogel, or the gelation process, which is illustrated in Figure 2.7. However, at this stage the silylation reactions are still not completed. When the nonpolar solvent is added, solvent exchange starts to take place inside the pores, which allows the reaction to continue and eventually, a hydrophobic surface is obtained, where water is repelled out of the pores, which will then be filled with the nonpolar solvent (heptane), as illustrated in Figure 2.10. In the acid catalyzed mechanism the steps are similar, but instead the reaction produces HCl, which causes the pH the decrease and triggers the acid catalyzed gelation.

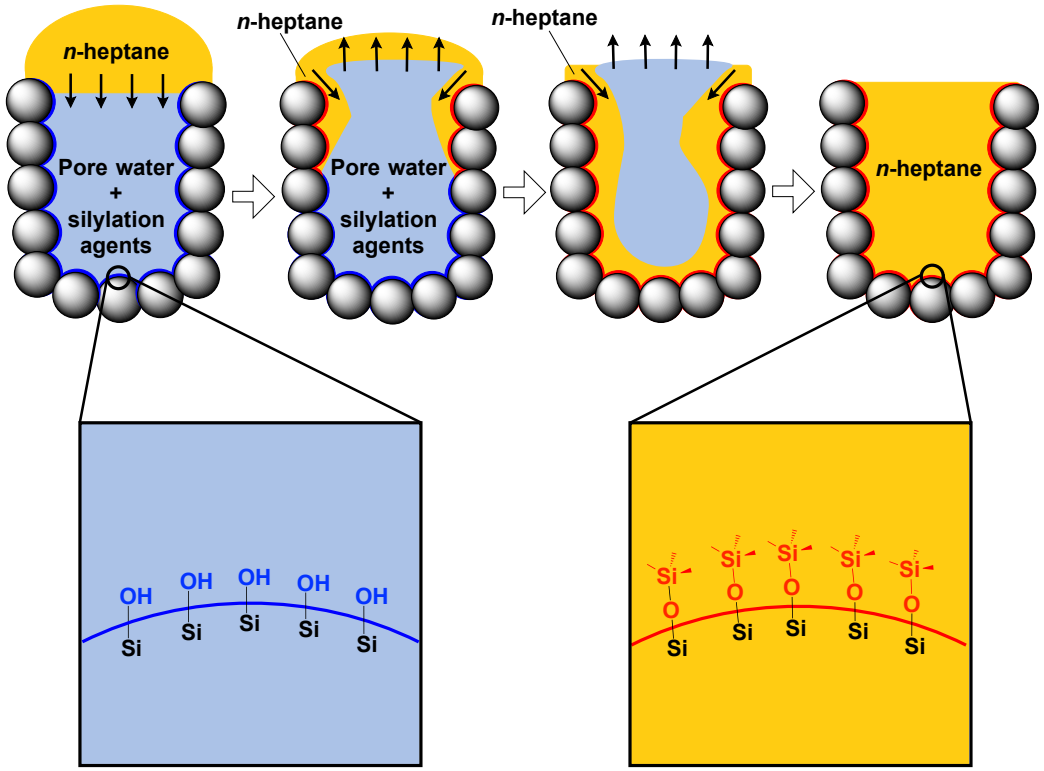

Figure 2.10 A schematic illustration of aerogel synthesis with APD method.

2.3.3 Incorporation with metal ions

Because of the unique structure of silica aerogels (large surface area with open channels and mesopores), it has recently been thought as a new class of supports for catalysts[14]. Previous work has shown that following the sol-gel route it is possible to obtain metal-incorporated silica aerogels. One such successful example is the incorporation of single-site Cu (II) into silica aerogels for catalytic reduction of NOx, as described in[26]. In this example, silica aerogels were synthesized using ambient-pressure drying method following the sol-gel route. Unlike introducing metal ions with ion-exchange or incipient wetness impregnation methods, incorporation requires that the metal ion become part of the framework. The precursor therefore is added before the formation of the gel structure, typically dissolved in the silica colloidal solution during the sol stage [77]. Before gelation, the metal ion can react with the siloxy groups in the sol, connect to the silicon atoms with bridging oxygen atoms. Upon gelation, the metal ion together with the silica undergo polycondensation reaction to form the gel structure. Prior work also shown that the uptake of metal ion is better when the polycondensation reaction was base catalyzed[78].

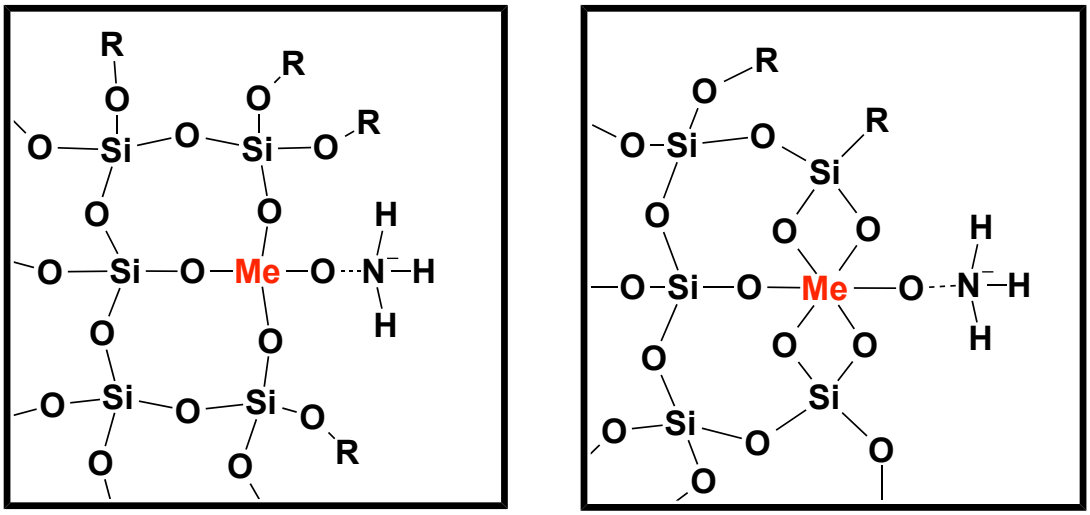

Figure 2.11 Proposed possible models of incorporation of metal ions into the silica network (a). With tetrahedral geometry (b). With Octahedral geometry. Note that the surface is hydrophobic with the -R groups.

One important aspect to consider for incorporation is the coordination number. Ideally, since silicon has the coronation number of four with tetrahedral geometry in the gel structure, incorporating a metal ion that has the same geometry will introduce less stress in the structure than metal ions with other geometries. However, it has also been reported that metal ions with coordination number of six, such as Cu(II), can also be incorporated [26]. In this study, the possibility of controlling the introduction for incorporation of ReO_4^- and MoO_4^{2-} will be investigated. Such control meaning that the metal ion should exist inside the aerogel network and not as a separate phase. ReO_4^- has the tetrahedral geometry in aqueous solution in pH = 0-14[79], therefore it is expected that the perrhenate ion should not have the restrain due to the ionic geometry. In the case of the Mo(VI), the chemistry of molybdate in aqueous solution is rather complex, depend strongly on the pH. The geometry of ortho-molybdate is tetrahedral, but as the pH decrease below 6, it starts forming polyoxomolybdate ions, such as the heptamolybdate and octamolybdate, and the geometry will change from tetrahedral to octahedral. Possible outcomes of the incorporation are shown in Figure 2.11a for tetrahedral geometry and Figure 2.11b for octahedral geometry. The $-NH_3$ groups are stemmed as a byproduct from the reaction between HMDS and the siloxy groups, which is present before gelation[13][14]. In previous study to incorporate copper, it has been shown that the ammine group can be removed by annealing the sample, departing in the temperature range between 200°C to 250°C, and in the copper case the local surrounding of the metal remains unchanged after the departure [26].

2.3.4 Treatments of the samples

A. The post-gelation wash method

The "wash" method is a post-synthesis treatment of the sample to eliminate unreacted chemicals and other byproducts. It was developed by S. Habrekke [13] by modifying the techniques described in [67] and [80]. The wash method aims to remove unreacted silylation agents and possible reaction products resides in the pores prior to drying[13]. Prior experiments show that silica aerogels undertaken this treatment exhibit considerably higher level of hydrophobicity, have a observably different "rubbery" texture, and appear to have much less of shrinkage of pores comparing to the silica aerogels synthesized without this treatment using the ambient pressure drying method [13].

B. Annealing

Annealing is a method to further modify the hydrophobic aerogel surface and to evaluate the interaction between the metal ions and the aerogel systems[26][81]. Following the sol-gel route and ambient pressure drying method, the resulting aerogels have hydrophobic surface, due to the -CH_3 groups attached by the silylation agents. It has been reported that annealing of the hydrophobic aerogels in the air at temperature above 300°C will increase the specific surface area but weaken or eliminate the hydrophobicity, due to the oxidative removal of organic -CH_3 groups[82][83].

2.4 Aluminophosphate AlPO-5

2.4.1 Introduction

Aluminum phosphate AlPO-5 is a molecular sieve first synthesized by S. T. Wilson et al. in 1982 [84]. It belongs to a class of novel crystalline microporous materials that are isomorphic to zeolites yet structured with other atoms, which collectively called zeotypes. Zeolite and zeotypes are of high interests in synthesizing functionalized catalytic supports because firstly, they can act as molecular micro-reactors that provide channels to allow gas reactants to enter the pores, react, and depart; secondly, they can also be structured to contain different sized and shapes of channels and cavities (or "cages") that are comparable to the size of molecules, therefore can be tuned to be highly selective toward certain desired products [15] [25]. The difference between zeolites and zeotypes is that zeolites are aluminosilicates that consist only of [AlO_4] and [SiO_4] tetrahedra, while zeotypes can be partially or entirely substituted by other atoms. One such example would be the aluminophosphate $AlPO_4$-n, in which -n indicates a specific type of structure. AlPO-5 is a pure aluminophosphate and contains no silicon atom. It belongs to a type of structure denoted by the code AFI, as shown in Figure 2.12.

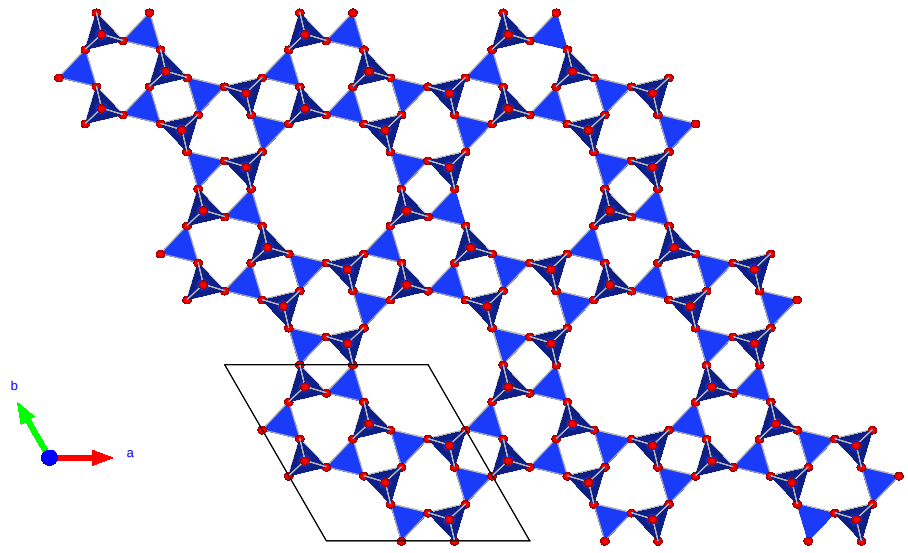

Figure 2.12 The AFI structure along the [001] plane. The 1-D cylindrical pores are constructed by the 12-member rings with alternating [AlO_4] and [PO_4] tetrahedra. Figure plotted with VESTA.

The AFI structure represents a large pore zeotype containing 1-D channels along the c-axis consists of 12-member rings with pore opening of 7.3 Å[85]. In AlPO-5 the 12-member rings are consist of alternating [AlO_4] and [PO_4] tetrahedra[84]. The crystal structure of AlPO-5

was determined by single-crystal X-ray diffraction, which is reported to have hexagonal space group symmetry (P6/mcc) with lattice parameters of a = 13.827Å, b = 13.827Å, c = 8.580Å[58]. AFI has been in particular interests in catalysis for its ability to incorporate hetero-atoms into the framework through isomorphous substitution[36][38]. Previous studies have reported successful incorporation of Cu, Fe, Co, etc. into the framework[33][35][37][86]. In this work, AlPO-5 will be used as support in the attempt to incorporate active metal ions Mo (VI) and Re(VII) via isomorphous substitution.

2.4.2 Isomorphous substitutions

Isomorphous substitution of AlPO-5 replaces a T-atom (tetrahedral) with a hetero-atom, typically a transition metal ion (TMI). Incorporation of the framework with TMIs has the advantage that the framework is itself functionalized and catalytic active, which increases the dispersion of the active TMIs, and provides a better interaction between the support and the TMIs. As mentioned previously, TMIs including Cu, Fe, Co, etc. had been successfully incorporated into different structures of aluminophosphates, such as AFI, CHA, AEL, etc[33][35][37][86]. Hartmann et al. reviewed the incorporation of TMIs into aluminophosphates (AlPOs) and silicoaluminophosphates (SAPOs) in details, as well as the spectroscopic characterization of these materials[38]. Some of the key factors that influence the ability and positions of a framework to incorporate with hetero-atoms are firstly, the electric-charge of the metal ion. In the case of aluminophosphate, the T-atom to be substituted is either Al or P. Although the AlPO-5 framework has zero net charge, locally the Al atom bares a negative charge and the P atom bares a positive charge. Substitution of T-atoms with TMIs at either the Al or P position results in different charge distribution of the framework. It was proposed that it is unlikely to have a framework that is overall positively charged, although not impossible[38]. For TMIs with valence of +1, +2, or +3, it is more likely to take the position of Al and avoids a positively charge framework, while for the position of P, it is possible to replace with TMIs baring charges from +1 to +5, although with lower valence TMIs it would generate a relatively large negative charge on the overall framework, which is also unlikely[38]. Note that if a negative charge is introduced into the framework, a positively charge counter ion must also be present outside of the framework to balance the charge. This positive extra-framework counter ion could typically be a proton, which links to the neighbouring bridging oxygen and create a hydroxyl group, forming a Brønsted acid site[15]. Dehydration at the acid site is also possible, which forms a Lewis acid site[15][87].

A second important factor to consider that influences the incorporation is the radius of the incoming TMI. In most cases the TMI will have a larger radius than Al (r = 0.39 Å) or

P (r = 0.17 Å), therefore introduction of TMI may also introduce strain on the surrounding lattice and distort the framework[15]. Subsequently the introduction could be consider easier if the TMI has similar dimension compares to Al or P. One example would be in the case of Cu(II), which has an ionic radius of 0.73 Å, considerably larger than the native atoms (Al or P), had been a challenge to incorporate, though the incorporation was successful. However it is worth to mention that in the case of copper although ionic radius is one factor for the difficulty, there are other restrains, such as the coordination number, which will be discussed in the following paragraph. A list of ionic radius of Al, P and some TMIs are shown in Table 2.1 [47].

Table 2.1 A list of ionic radius of selected elements. Data obtained from [47].

Element	Coordination number	Ionic radius (Å)
Al(III)	4	0.39
P(V)	4	0.17
Cu(II)	6	0.73
Fe(III)	4	0.49
Co(II)	4	0.56
Mo(VI)	4	0.41
	6	0.59
Re(VII)	4	0.38
	6	0.53
Ge(IV)	4	0.39
	6	0.53

Thirdly, one should also consider the coordination number of the TMI. In the AFI framework both the Al and the P atom have the tetrahedral geometry. Therefore, TMIs with coordination number of four and have the tetrahedral geometry are considered easier to incorporate, since they would introduce less stress on the framework[38]. If the TMI has other coordination number, it could be challenging for the incorporation since the position of the ion in the framework will be tetrahedral. However, it does not mean that it is impossible to incorporate TMIs with other geometries. Cu(II) typically has the square planar (D_{4h}) geometry, which is a distorted octahedral structure, with coordination number of six and has been successfully incorporated into the AFI framework previously by carefully choosing the structure directing agent (SDA) and a slow ramp rate for calcination [15][33]. This might partially attribute to the flexibility of the AFI framework due to its large pore size (7.3 Å) therefore smoother pore walls, more tolerant to a local distortion[38].

The elements of interests in this study are Mo(VI) and Re(VII). There has been reported challenges to introduce Mo(VI) and Re(VII) into the zeotype structure through isomorphous substitution[88]. The first reason being that both molybdenum and rhenium have high valence number (+6 and +7, respectively); although they exist in aqueous solution as the oxo-anion (i.e. molybdate and perrhenate), the incorporation will either create net positive charges on the framework, regardless either substituting the Al or P position, or causing a breakage/terminal position in the framework by forming one or more Me=O double bonds. The microporous positively-charged framework would likely be destabilized because the positive charge would be screened by the surrounding oxide ions, which are negatively charged, and hence limiting the access of the extra-framework counter ions [88]. This was one of the issues encountered in other studies related to the hydrothermal incorporation of V(V) ions into the MEL and MFL frameworks[89][90], which usually result in low metal contents and often time the metal ions are loosely bounded on the wall of the pores, and can be easily washed away in aqueous solution[91]. On the other hand, the incorporation of V(IV) is considerably easier, since a positively charged framework can be avoided[88].

The introduction of Mo into AlPO-5 by isomorphous substitution has been previously attempted and reported, but the species of Mo in the AlPO-5 framework was not specified [32]. The authors also admitted that although there were circumstantial evidence, there was no direct poof of any element studied incorporated into the framework [32]. In another study, it has been reported that Mo can be introduced into the silicon containing AFI molecular sieves (SAPO-5) using solid state reactions with the precursor MoO_3, by physically mixing pure SAPO-5 and MoO_3 and heated to 723 K with the presence of water vapor, which yielded a Mo(V) species MoH-SAPO-5 in the framework, characterized by EPR (electron paramagnetic resonance) studies [88][92][93]. In that study it was proposed that oxidation of the Mo(V) species in the framework may lead to Mo(VI)[38], but no definitive evidence was reported.

The molybdate has a rather complex behavior in aqueous solution to form polyoxoanions with bridging oxygens, depending on the pH[94]. Molybdate can refer to a series of compounds, from the simplest form of the ortho-molybdate, MoO_4^{2-}, to larger cluster polyoxoanions such as the heptamolybdate $Mo_7O_{24}^{6-}$. An XAS study show that in hydrothermal chloride solution MoO_4^{2-} and $HMoO_4^{-}$ are the dominating species at near neutral to basic environment, while decreasing the pH will produce a series of species including the formation of polyxoxanions or ligand attachment to the Mo atom[95]. This will also cause a change of geometry from tetrahedral to octahedral. Further, the presence of phosphate ions will complex with the molybdate ions and form heteropolymetalate ions. Nevertheless if

considering only the monometric ortho-molybdate anion MoO_4^{2-} the framework would most likely prefer to minimize the baring positive charges and therefore substitute the position of P atom.

Similarly, incorporation of Re(VII) into AlPO-5 will also introduce positive charges on the framework, therefore imposing a challenge. There has been debates in the early time about the ionic species of perrhenate ions in dilute solution, either it exist as the tetrahedral ReO_4^- or the octahedral ReO_6^{5-}, especially at high pH environment[96][97]. Later and more recent studies shown that given the solution is not in a strongly reducing condition, the predominate species is the tetrahedral ReO_4^- over the pH range 0-14[96][98]. The ionic radius of Re in this species is 0.38 Å, as shown in Table 2.1, which is very close to the radius of the native atom Al(III), and therefore it should not be a limiting factor. In general similar to the case of molybdenum, the biggest challenge to incorporate Re(VII) into AlPO-5 would be its high valence number, which will certainly introduce positive charges on the framework, assuming the framework is able to maintain its structure.

An possible indirect method to synthesize MeAlPO-5 is through the intermediate product GeAlPO-5, based on an prior work on another zeotype ITQ-33[99]. This method was designed as an alternative in the case that the direct synthesis method do not produce desirable samples, considering the challenges it faces, as mentioned previously. Prior work has shown that Re(VII) can be incorporated into the the framework of ITQ-33, in which Ge(IV) is a major component, by post-treatment of the molecular sieve with a ethanol solution of the rhenium precursor Re_2O_7 or NH_4ReO_4, to reach up to 4 wt.% of Re content[99]. AlPO-5 and ITQ-33 share some structural similarities as they both contain large size pores (12 member rings for AlPO-5, 18 and 10 member rings for ITQ-33), and therefore it can be hypothesized that similar method to replace Ge(IV) with Re(VII) may also be conducted with AlPO-5. In the study of ITQ-33, the benefits to incorporation Re(VII) into the framework are two-fold: firstly, since calcined ITQ-33 is unstable for more than 30 days because of its large germanium content and the subsequent formation of the so-called silanol nests, replacing Ge(IV) with Re(VII) may stabilized the structure; and secondly, incorporation of Re(VII) also functionalizes the structure to be catalytic active toward such as methanol to hydrocarbon conversion (MTH) reactions [99] [100][101]. In the case of GeAlPO-5, the molecular sieve has shown good thermal stability and the catalytic reactions had been well studied [102]. Therefore, replacing the Ge(IV) with Re(VII) will be mainly for the introduction of Re(VII) into the AFI framework.

The synthesis of GeAlPO-5 has been previously reported and patented with the precursor $GeCl_4$[102][103][104]. $GeCl_4$is a liquid that will fume in the air, and in contact of water,

it will hydrolyze to form GeO_2[102][105]. In this study GeAlPO-5 will be attempted to synthesize directly using the precursor GeO_2, which is powder, easier to handle and control during the synthesis. The possible substitution model of Ge into AlPO-5 is shown in Figure 2.13. Substitution of Al atom is highly unlikely, since it will leave a positive charge on the framework.

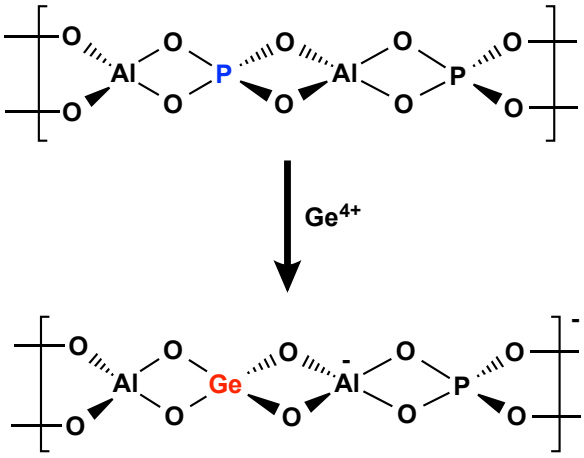

Figure 2.13 A possible resulting structure of GeAlPO-5 by isomorphous substitution.

The major reason for this two-step isomorphous substitution is that Re(VII) has relatively high valence number; direct incorporation of Re(VII) may face difficulties because of the positive charge it will create on the framework, as previously discussed. On the other hand, Ge(IV) has proven to be able to incorporate into AlPO-5, and if it can then be replaced by Re(VII), which can enter the pores together with the counter ions, a Re(VII) incorporated framework can be obtained. Several properties of Ge(IV) and Re(VII) may be considered favorable for the substitution of Ge(IV) with Re(VII). First of all, Ge(IV) and Re(VII) have very similar ionic radius (with tetrahedral geometry), which are 0.39 Å and 0.38 Å, respectively, as shown in Table 2.1 [47]. Secondly, they both exist in aqueous solution with coordination number of 4 and tetrahedral geometry[106]. Finally, since Re(VII) will be introduced into the already-exist AFI framework, both ReO_4^- and the counter ion (such as OH^- or Cl^-) can enter the relatively large pores (7.3 Å) freely, and upon completion of the replacement, the counter ion will already exist near the replacement sites and therefore stabilize the positively framework, preventing the collapse.

2.5 Characterization Techniques

2.5.1 Powder X-ray diffraction

X-ray diffraction refers to a kind of scattering process when the scattered X-ray waves are coherent, which will occur when the Braggs' condition is satisfied [107][108]. The diffraction patterns are a result of constructive and destructive interference between diffracted waves. XRD uses the diffraction between the incoming X-ray electromagnetic waves and the electrons in the electron cloud of the sample to determine the structure of the materials. The fundamental condition for diffraction to occur is described by the Braggs' Law[108]:

$$n\lambda = 2dsin(\theta) \qquad \text{(Eq. 2.5.1)}$$

where λ is the wavelength of the incoming X-ray beam, θ is the incident angle, d is the lattice constant, and n is the order of the diffraction. Since the both the X-ray wavelength and the lattice spacing d do not change in the course of an XRD experiment, the data is recorded with varying incident angles. An important approximation in XRD is that the interaction is considered kinematic, i.e. each photon only scatter once by the sample, and the beam do not significantly attenuated by the material[107]. The intensity of diffraction is proportional to the square of structure factor S(q), which is related to the electron density by Fourier Transformation[107]. Note that in Fourier space the independent variable is the the magnitude of the scattering vector **q**, which is equivalent to the scattering angle by $q = \mid \mathbf{q} \mid = 4\pi sin(\theta)/\lambda$. An illustration of the Braggs' Law in real space is shown in Fig.2.14.

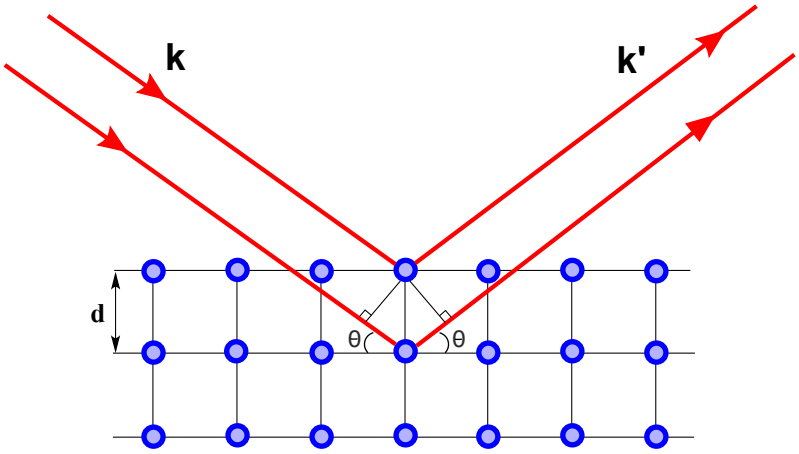

Figure 2.14 An illustration of Braggs' Law in real space, with the lattice parameter d, incident angle ϑ, the incoming wave **k** and diffracted wave **k'**. Note that the positions of the arrows indicate the phase of the wavefronts, which are different in the diffracted waves. The interference of the waves caused by this phase shift produces the diffraction patterns.

Powder X-ray diffraction, or PXRD, uses fine powders instead of a single crystal to determine the structural composition and morphology of materials[109]. Similar to single crystal XRD, PXRD is also a very versatile and non-destructive technique and therefore became very convenient and popular, widely used in structural determination of materials, especially for materials that are impossible or difficult to grow single crystals that are sufficiently good for single-crystal X-ray diffraction[108]. In the phase characterization experiments, the presence of the Braggs' peaks (typically sharp and intense peaks) indicates that the material has long-range order and it is crystalline, while the absence of Braggs' peaks shows that the material has no long-range order and it is amorphous[109]. Amorphous materials however will still have some broad features in the powder XRD diffractogram, which is from the short-range orders[109]. The position and relative intensity of the peaks are determined by the structure (such as space group) of the crystal and therefore can be used to identify the crystal structure of materials[109]. However, one limitation of powder XRD is that as the particle size become smaller, the Braggs' peaks will be broadened; at particle size below 2 nm, the peaks may not be able to identify[110].

In this study powder XRD will be used as the primary tool to characterize the phase structure of the samples. For silica aerogel samples, there should be no Braggs' peak present in the powder XRD patterns, since it is an amorphous material and has no long-range orders. However, short range order still present in silica aerogels, which will result in a broad bump in the powder XRD patterns, and will be used to identify the aerogel structure. An example of powder XRD patterns of a silica aerogel sample is shown in Figure 2.15 (Figure reprinted from [111] under the Creative Commons Attribution License).

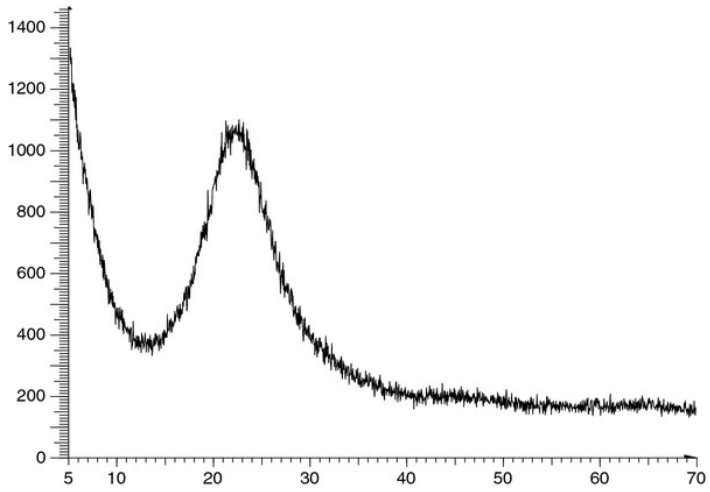

Figure 2.15 A typical powder XRD diffractogram of a silica aerogel sample, which features a broad bump from the short-range order of silica. The absence of Braggs' peak indicates that it is an amorphous materials. Figure re-printed from [111].

In the phase characterization of silica aerogel experiments, when Braggs' peaks are present a sample, it is an indication that there is at least one extra crystalline phase in the sample and therefore it is not phase pure. Single-site incorporation of hetero-atoms in the silica structure should not produce any crystalline structure, therefore the powder XRD patterns should still show an amorphous phase and no crystalline phase. If crystalline phases are present, it is typically due to the precursor not being able to incorporate into the network, or the addition of precursor reacted with other reactants and produced a crystalline product (which is also not in the network).

In the experiments to synthesize MeAlPO-5 samples, the samples should be crystalline and therefore should produce specific Braggs' peaks, of which the reflection conditions will depend on the crystal structure. Incorporation of hetero-atoms into the framework through isomorphous substitution should retain the crystal structure AFI and therefore produce reflections at the same diffraction angles (given the X-ray wavelength constant). The crystal parameters of phase pure AlPO-5 (AFI) was found on the zeolite database[85] and the powder XRD data using the X-ray from Cu-$K_{\alpha 1}$ is shown in Figure 2.16.

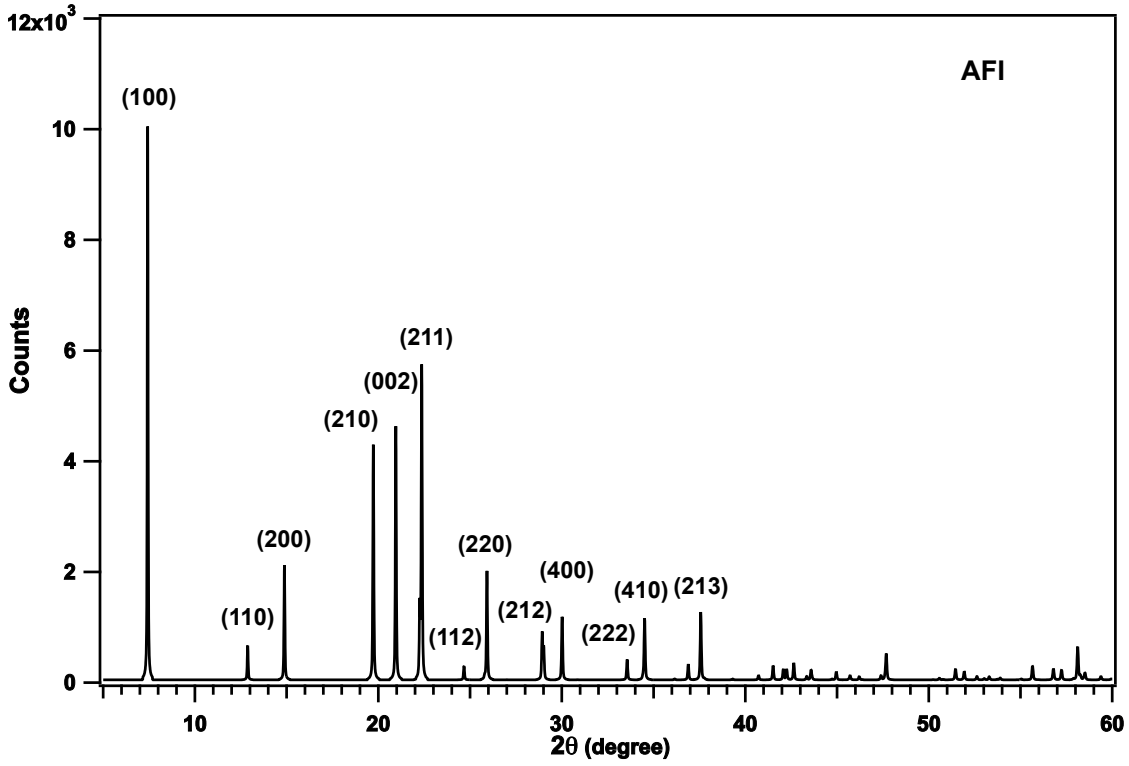

Figure 2.16 Powder XRD patterns of phase pure AFI structure using X-ray from Cu-$K_{\alpha 1}$ ($\lambda = 1.5406$). Powder data acquired from zeolite database[85].

2.5.2 N_2 Adsorption-desorption analysis

The Brunauer-Emmett-Teller (BET) theory was first established by Stephen Brunauer, Paul Hugh Emmett, and Edward Teller in 1938[112]. Based on the Langmuir theory, BET theory is a model to describe the physical adsorption of gas molecules onto solid surfaces. It further extends the Langmuir theory, which only assumes single layer physical adsorption of gas molecules on the surface, to a model that can describe multilayer gas physical adsorption [113] [114].

In order to determine the surface area of a material, one can in principle follow a simple approach: if there is a type of inert gas (such as nitrogen or argon) that can adsorb onto the surface universally and forms a complete monolayer of the gas molecules, the surface area can be simply calculated by counting the number of the gas molecules used to form the monolayer and multiply by the area occupied by one such molecule. However in reality the gas molecules will easily adsorb beyond the first layer and have multiple layers of molecules on the surface. For porous systems, the gas molecules will also condense and fill in the pores. In facts, the narrower the pores, the easier nitrogen gas will condense into them, which is called the capillary condensation effect and can be described by the Kelvin equation [113]. One can in facts take advantages of this effect to determine the surface area. For mesoporous materials (which is relevant to this project), a monolayer will form at relatively low relative pressure, and as the pressure approaches the saturation pressure, multilayers will build up until all the pores are fully filled by the gas due to the capillary condensation effect, which arrives at the saturation pressure. When the pressure of the gas is reduced, the departure of gas molecules from the pores will show a hysteresis effect, in which case the gas molecules have to overcome the capillary condensation energy in order to leave the pores, resulting a "delay" of the gas molecules departing the pores (the gas leave the pores at a lower equilibrium pressure, compares to the pressure it enters) [113]. This hysteresis forms a type IV isoterm, and can be used to determine the surface area and pore distribution. The resulting BET specific surface area equation can be written as [115]:

$$\frac{p}{V_{ads} \cdot [(p^o - p)]} = \frac{c-1}{c \cdot V_m}(\frac{p}{p^o}) + \frac{1}{c \cdot V_m} \qquad \text{(Eq. 2.6.2)}$$

where V is the total volume of the gas adsorbed, V_m is the quantity of gas adsorbed in monolayer, p is the equilibrium pressure of the adsorbate at a certain temperature, p^o is the saturation pressure at this temperature, and c is the BET constant.

Using the BET equation above, one can generate a linear plot of $\frac{p}{V_{ads}\cdot(p^o-p)}$ for the dependent variable vs. the independent variable $\frac{p}{p^o}$, which is the relative pressure. An example of a typical BET plot of a real sample is shown in Fig.2.17

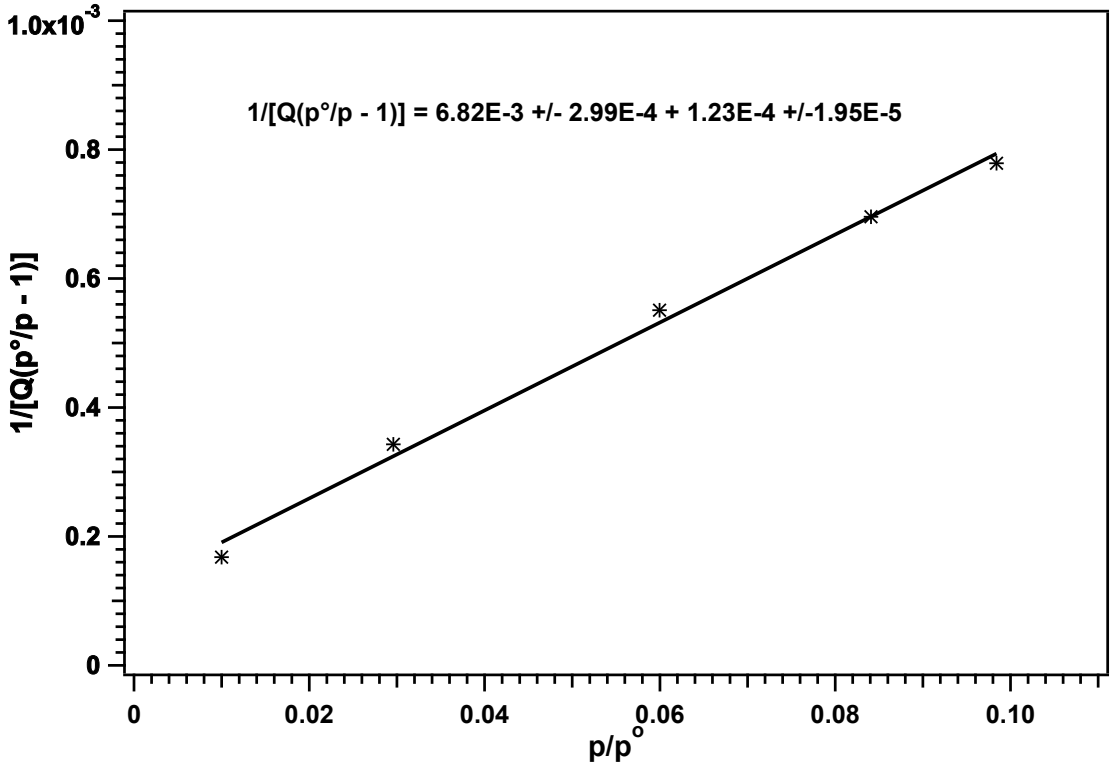

Figure 2.17 An example of BET plot to determine the specific surface area.

The quantity of gas adsorbed in monolayer, V_m, and the BET constant c, can be related to the slope and intercept of the fitted line, k and b, respectively, by

$$V_m = \frac{1}{k+b} \qquad \text{(Eq. 2.6.3)}$$

$$c = 1 + \frac{k}{b} \qquad \text{(Eq. 2.6.4)}$$

The total surface area can then be calculated from the value of the slope and intercept, which can be written as:

$$S_{total} = \frac{v_m \cdot a_o \cdot N_A}{V} \qquad \text{(Eq. 2.6.5)}$$

Where S_{total} is the total surface area of the sample, a_0 is the adsorption cross section of the gas molecule (i.e. nitrogen), N_A is the Avogadro's number, and V is the molar volume of

the adsorbed gas. Subsequently, the specific area can be simply calculated by dividing the total area by the mass of the sample:

$$S_o = \frac{S_{total}}{m} = \frac{v_m \cdot a_o \cdot N_A}{m \cdot V} \qquad \text{(Eq. 2.6.6)}$$

In this study BET analysis will be used to determine the specific surface area and porosity of the samples. According to IUPAC, in most cases the physisorption isotherms can be classified into 6 different types[116], as shown in Figure 2.18a.

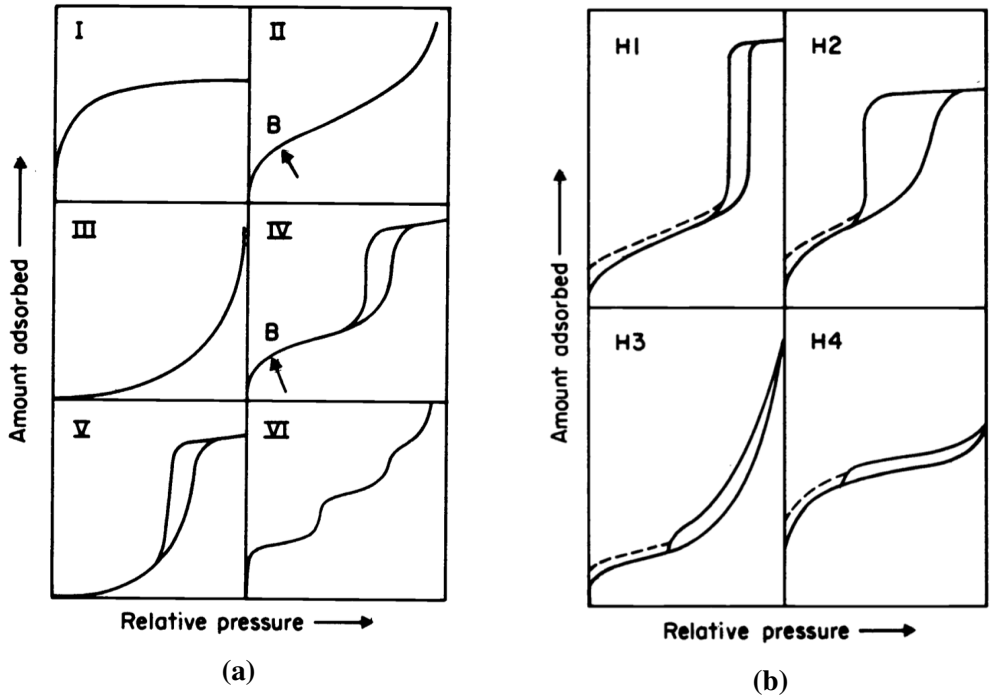

Figure 2.18 IUPAC classification of physisorption isotherms. (a). The 6 types of adsorption-desorption isotherms. (b). The 4 types of hysteresis. Figure re-printed from [116], copyright ©1985 IUPAC).

Among the six types of physisorption isotherms, the most relevant ones for this study is the type I isotherm and type IV isotherm. Type I isotherm typically represents a microporous material, in which the limiting uptake of the gas is from the micropore volume instead of the surface area[116]. This would likely be the case of AlPO-5 samples, which is a microporous material. Type IV isotherm features a hysteresis loop between the adsorption and desorption curves, which is due to the capillary condensation within the mesopores and limits the uptake at higher relative pressure[116]. This would be in the case of silica aerogel samples, where mesopores are abundant and has a large surface area.

IUPAC also classified the hysteresis into four categories, as shown in Figure 2.18b[116]. Type H1 hysteresis is believed to be an indication that the porous material may be consists of

uniformly sized sphere, with relatively narrow pore size distribution[116]. Type H2 hysteresis is said to be not completely understood, but in a simplified picture it was understood as corresponding to the difference between the mechanism of the condensation process and the evaporation process[116]. Type H3 hysteresis was understood to be associated with the aggregation of particles with plate-like shape[116]. Finally, type H4 hysteresis was understood as from slit-like pores and indicating the microporosity of the material[116].

The pore size distribution will also be plotted in this work, as it is a useful tool to characterize the types of pores present in the sample by their sizes. A classical model will be used in this work for the pore size distribution, based on the Kelvin equation by Barret, Joyner, and Halenda (BJH) to interpret the adsorption-desorption isotherms[39]. This model has accounted for the effect of multilayer adsorption and has been widely used to illustrate the average pore size and pore size distribution, although having the limitation that it cannot confirm the presence of micropores below approximately 1 nm[14][117]. The pore size distribution can be calculate from either the adsorption or the desorption branch of the isotherms; for historical and thermodynamic reasons the desorption branch was usually favored in deriving the distribution of mesoporous materials from the isotherms[14][117]. However, using the desorption branch is also subject to misinterpretation of the pore size distribution due to the so-call tensile strength effect (TSE) by showing a narrow peak at approximately 3.8 - 4 nm, which is a result of forced closure of the hysteresis loop, commonly observed when using the desorption loop[117][118]. Therefore in this study, the BJH pore size distribution, average pore size, and cumulative pore volume will be calculated with the adsorption branch of the isotherm.

2.5.3 Inductively coupled plasma mass spectroscopy

Inductively Coupled Plasma Mass Spectroscopy, or ICP-MS, is a sensitive and versatile instrumental technique for analyzing the elemental compositions of samples. ICP-MS finds a wide range of diverse applications in trace element analysis, including within materials chemistry, water and food chemistry, environmental chemistry and toxicology, geochemistry, etc. [119]. The advantage of using ICP-MS for trace element analysis includes ultra-low limit of detection and higher spectral resolution, long linear range, and unlike atomic absorption spectroscopy, in which only one element can be analyzed at a time, ICP-MS can simultaneously analyze all elements of interests at the same time[119].

The principle of ICP-MS is straight forward. A solution containing the sample matrix is first injected into the ionization chamber, mix with Ar gas to form an aerosol. The aerosol is

then passes through a temperature Ar plasma, where it decomposed, atomized and ionized, producing positively charged ions. After passing through a series of ion lenses, the ions enter the quadrupole mass analyzer, which only allows ions at a certain m/z ratio to pass through at a time[120][121]. Ions with different m/z ratios are analyzed sequentially in one experimental run by tuning the AC-DC frequency of the quadrupole mass analyzer. Finally, the ions arrive at the detector and register as electronic signal.

ICP-MS will be used in this project to analyze the elemental composition of the samples in metal weight percentages (Me wt.%). The metal weight percentage is an important quality factor of the sample, as it directly illustrate the among of the desired metal is actually been introduced into the porous materials.

Chapter 3

EXPERIMENTAL

3.1 Functionalization of Silica Aerogels

3.1.1 The sol-gel procedure

The general synthesis procedures for aerogels using the sol-gel route with ambient-pressure drying method were developed from Bhagat et al.[122][123] and further modified by Kristiansen et al.[26]. There are two different routes for the sol-gel APD method, which are the co-precursor(CP) route and the surface derivatization route (SD). In this study only the CP route was used. The general synthesis procedures are shown in Figure3.1 as a flow chart illustration. The synthesis can be separated into 4 stages: preparation of the sol (including the addition of the metal precursor), adjustment of the pH (optional), surface modification and gelation, and finally solvent evaporation. The chemical reagents involved in the synthesis of aerogels following the sol-gel route and ambient pressure drying method are: sodium silicate solution (Na_2SiO_3, 26.5 wt.%, Sigma-Aldrich), Amberlite IR 120 Hydrogen Form (Sigma-Aldrich), hexamethyldisilazane (HMDS, 99.9%, Sigma-Aldrich), hexamethyldisiloxane (HMDSO, 98.5%, Sigma-Aldrich), trimethylchlorosilane (TMCS, 99%, Sigma-Aldrich), ammonia hydroxide stock solution (NH_4OH, 28%, Sigma-Aldrich), nitric acid stock solution (HNO_3, 65%, Sigma-Aldrich), n-heptane ($CH_3(CH_2)_5CH_3$, 99%, Sigma-Aldrich), ethanol (C_2H_5OH, absolute, Sigma-Aldrich). The metal precursor for Mo-aerogels is ammonium heptamolybdate tetrahydrate ($(NH_4)_6Mo_7O_{24}$ •$4H_2O$, 99.98%, Sigma-Aldrich). The metal precursor for the synthesis of Re-aerogels is either rhenium(VII) oxide (Re_2O_7, 99.9%, Sigma-Aldrich), or ammonium perrhenate (NH_4ReO_4, 99%, Sigma-Aldrich).

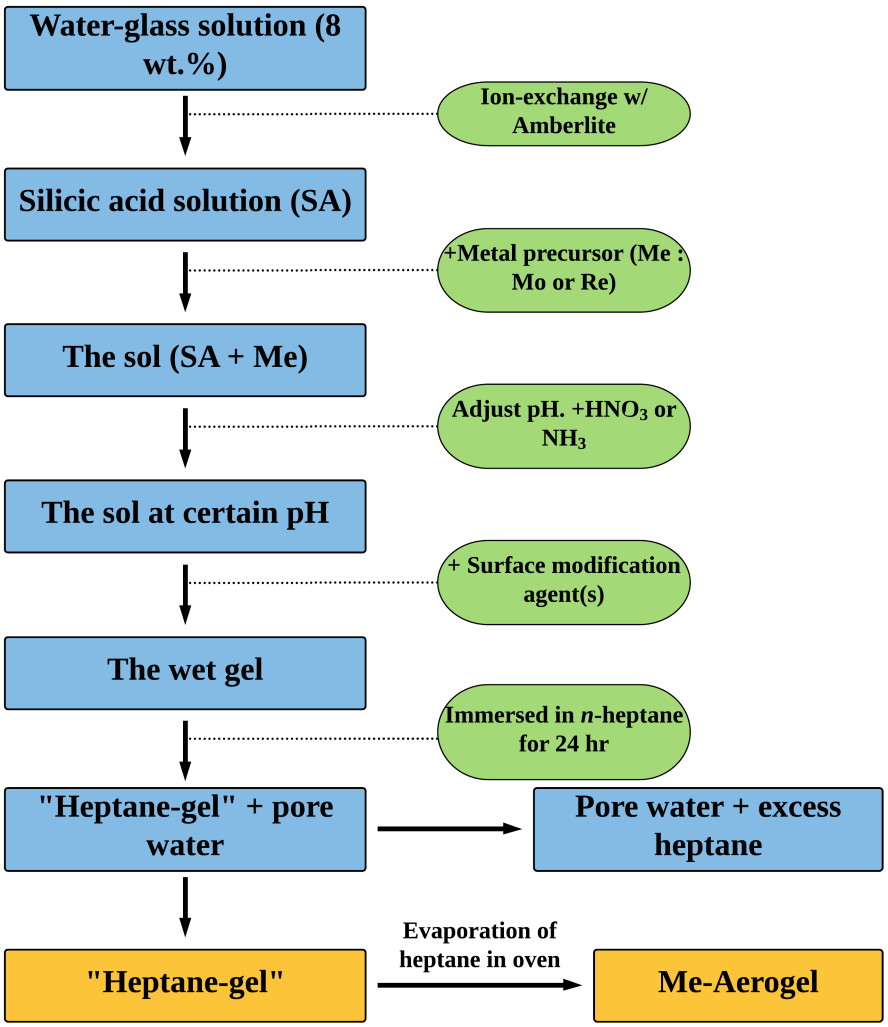

Figure 3.1 A flowchart illustration of the synthesis procedures of Me-aerogels using the sol-gel and ambient pressure drying method

A. Preparation of the sol

The preparation of the sol is described as the following. In a typical synthesis, approximately 24.2g of concentrated sodium silicate solution was diluted with Di-water to a 8 wt.% solution. The ion-exchange was performed using a glass column filled with approximately 80 ml of Amberlite IR 120 Hydrogen Form. The pH of the solution was monitored both before and after the ion-exchange, changed from approximately 13 to a final pH of 2, consistent with previous studies[26][124][125].

Once the silicic acid colloidal solution was obtained, water soluble metal precursor (as mentioned previously) was added into the solution. The molar relationship of each component is shown in Table 3.1.

Table 3.1 Molar ratio of each component in a typical synthesis of Me-aerogels using the co-precursor route

Sample	Si	Me (Mo or Re)	H_2O	HMDS	HMDSO
MeAERO-n	1	x	166	3.30	3.40

B. Adjustment of the pH

The pH of the sol was measured and controlled after the metal precursor was added and fully dissolved in the colloidal solution. In the experiments where the sol pH was increased, 5 M ammonia solution prepared from the stock solution was added into the solution drop-wise. In the experiments where the sol pH was decreased, 5 M nitric acid prepared from the stock solution was added drop-wise.

C. Surface modification and gelation

Once the preparation of the sol was finalized, the surface modification (silylation) agent(s) was added into the colloidal solution to modified the surface and catalyzed (either acid or base) the polycondensation reaction to form the gel.

In a typical synthesis the surface modification silylation agents HMDS (99%, 3.48 g) and HMDSO (99%, 3.56 g) were measured in two separate beakers and added into the sol with simultaneously. The gelation typically occurred within 1-2 minutes, and has a distinct appearance as the liquid solution turned into a form of jelly. The mixture was kept stirring for 10 minutes to allow the gelation to complete. Subsequently, n-heptane (99%, 100 mL) was added into the gel and allowed to stay for 24 hours at room temperature in the sealed container.

After 24 hours, the gel was then removed from heptane and the solvent was evaporated in an oven first at 65°C for 1080 minutes (18 hours) at a ramp rate of 5°C/min, then 85°C for 180 minutes and 150 °C for 120 minutes. The temperature program is illustrated in Figure 3.2.

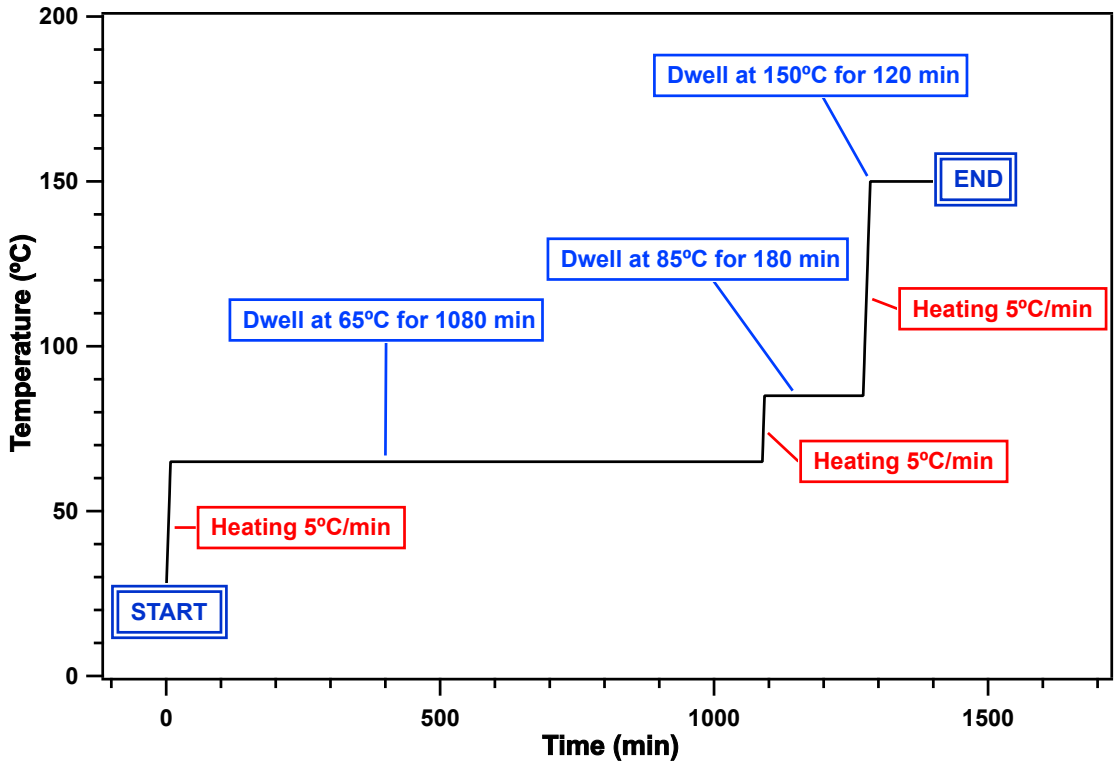

Figure 3.2 Temperature program of the final drying process to evaporate the n-heptane inside the pores

Finally, when the dried sample was obtained, it was grounded into a fine powder. The hydrophobicity of the sample was confirm using a simple test with water droplets, from that the water droplets appear "floating" on the surface of the container which has some remain of the aerogel and can move freely, instead of stick on the surface.

3.1.2 Synthesis of Me-aerogels

A. Synthesis of Mo-aerogels

Mo-aerogels were synthesized following the procedures as described in the previous section. Two experimental parameters were varied, the Mo:Si molar ratio, and the pH of the sol before gelation. As shown in Table 3.2. Sample MoAERO-1 to sample MoAERO-4 were synthesized at the sol pH of 5, and varied the molar ratio from 0.05 to 0.4. Sample MoAERO-5 and MoAERO-6 were synthesized at the molar ratio 0.2 with the sol pH adjusted to pH = 1 and pH =3, respectively. All Mo-aerogel samples were synthesized using the Mo precursor ammonium molybdate and the silylation agents HMDS and HMDSO.

Table 3.2 Summary of Mo-aerogel samples.

Sample	Re:Si	pH	Silylation
MoAERO-1	0.05	5	HMDS+HMDSO
MoAERO-2	0.10	5	HMDS+HMDSO
MoAERO-3	0.20	5	HMDS+HMDSO
MoAERO-4	0.40	5	HMDS+HMDSO
MoAERO-5	0.20	1	HMDS+HMDSO
MoAERO-6	0.20	3	HMDS+HMDSO

B. Synthesis of Re-aerogels

Re-aerogels were synthesized following the procedures as described in the previous section. Four experimental parameters were varied during the synthesis, Re : Si molar ratio, choice of Re precursor, sol pH, and silylation agent(s), as shown in Table 3.3.

Table 3.3 Summary of Re-aerogels

Sample	Re:Si	sol pH	Silylation	Precursor
ReAERO-1	0.05	2	HMDS+HMDSO	Re_2O_7
ReAERO-2	0.10	2	HMDS+HMDSO	Re_2O_7
ReAERO-3	0.20	2	HMDS+HMDSO	Re_2O_7
ReAERO-4	0.40	2	HMDS+HMDSO	Re_2O_7
ReAERO-5	0.05	2	HMDS+HMDSO	NH_4ReO_4
ReAERO-6	0.10	2	HMDS+HMDSO	NH_4ReO_4
ReAERO-7	0.20	2	HMDS+HMDSO	NH_4ReO_4
ReAERO-8	0.40	2	HMDS+HMDSO	NH_4ReO_4
ReAERO-9	0.20	7	HMDS+HMDSO	NH_4ReO_4
ReAERO-10	0.20	8	HMDS+HMDSO	NH_4ReO_4
ReAERO-11	0.20	9	HMDS+HMDSO	NH_4ReO_4
ReAERO-12	0.20	12	HMDS+HMDSO	NH_4ReO_4
ReAERO-13	0.20	1	HMDS+HMDSO	NH_4ReO_4
ReAERO-14	0.20	2	TMCS	NH_4ReO_4

ReAERO-1 to ReAERO-2 were synthesized with the metal precursor Re(VII) oxide, the sol pH = 2, the silylation agents HMDS and HMDSO, with varied molar ratio from 0.05 to

0.40. Sample ReAERO-5 to ReAERO-8 were synthesized with the metal precursor ammonium perrhenate, the sol pH = 2, the silylation agents HMDS and HMDSO, and also with varied molar ratio from 0.05 to 0.40. Sample ReAERO-9 to ReAERO-13 were synthesized using the molar ratio 0.2, the metal precursor ammonium perrhenate, the silylation agents HMDS and HMDSO, but with the sol pH varied at pH = 7, pH = 8, pH = 9, pH = 12, pH = 1, respectively. Lastly, sample ReAERO-14 were synthesized with the metal precursor ammonium perrhenate, the sol pH = 2, but with a different silylation agent TMCS.

3.1.3 The post-gelation wash method

The washing method was performed on one sample (ReAERO-5) during the stage in which the gelation has completed and before heptane was added for drying. Immediately upon completion of the gelation, the samples were immersed and washed, separately and independently, in ethanol (approximately 75 - 100 ml) for a few minutes, before the ethanol was decanted. This wash was repeated and performed to a total number of 4 times. The second step of the wash was to use of heptane (approximately 75 - 100 ml) to wash the samples for 4 times, following the similar procedure as in the first step. When this was completed, the samples were immersed in an approximately 100 ml solution, consists of 20 vol.% of HMDS and 80 vol.% of heptane. The samples were kept in this solution for 24 hours.

In the final step of the wash, the liquid was decanted and the samples were washed again with 75 - 100 ml of dry heptane, following the similar procedure as the second step, to remove the unreacted excess silylation agent. Upon completion of this wash treatment, the samples were dried in the oven following the procedure described previously.

3.1.4 Annealing

The annealing of the aerogel samples were performed as the following: a portion of the as-prepared sample in a container was placed inside the annealing furnace at room temperature in the air. The furnace was programmed to achieve 450°C at a ramp rate of 5°C/min, and to dwell for 3 hours. After the program was completed, the sample was left inside the furnace until cooled to room temperature.

3.2 Functionalization of AlPO-5

3.2.1 Synthesis procedures of MeAlPO-5

The introduction of metal ions (Me) into the aluminophosphate AlPO-5 molecular sieves was attempted by isomorphous substitution following the modification of synthesis conditions as described in [35], in which the metal precursor was added into the reactant mixture before crystallization by hydrothermal synthesis. In the study to synthesize MeAlPO-5, the SDAs attempted were triethylamine (TEA, 99%, Sigma-Aldrich), tetraethylammonium hydroxide solution (TEAOH, 40 wt.%, Sigma-Aldrich), tripropylamine (TPA, 98%, Sigma-Aldrich), N,N-Dicyclohexylmethylamine (MDCHA, 97%, Sigma-Aldrich), Tetraethylenepentamine (TEPA, 99%, SigmaAldrich). An overview of the synthesis parameters is shown in Table 3.4, in which x is the molar composition of Me in relation to Al and was varied between 0.05 to 0.1, and SDA is the choice of structure directing agent.

Table 3.4 Molar ratio of each component in a typical synthesis of MeAlPO-5.

Sample	Al	P	Me	SDA	H_2O
MeAlPO5-n	1	1	x	0.675	20

Two different synthesis methods have been attempted in order to introduce Me into AlPO-5, the 1-solution method and the 2-solution method. The 1-solution method follows a similar procedure as described in [35]. In such a typical synthesis ortho-phosphoric acid (H_3PO_4, 85%, 11.60 g, Sigma-Aldrich) was added into Di-water (31 g) under gentle stirring, followed by the metal precursor. Once the metal precursor was fully dissolved and a homogeneous solution was formed, pseudoboehmite (AlOOH, 71.8 wt.%, 7.11 g) was added into the mixture with vigorous stirring until a uniform suspension is formed. Subsequently, the selected SDA was added into the reactant mixture. The beaker was then sealed with parafilm and kept stirring for an addition of 3 hours to obtain a homogeneous gel. The resulting gel was transferred into a 100 mL stainless steel autoclave with a Teflon liner, and placed into an oven for crystallization at selected temperatures. A flowchart illustration of the one solution method is shown in Figure 3.3.

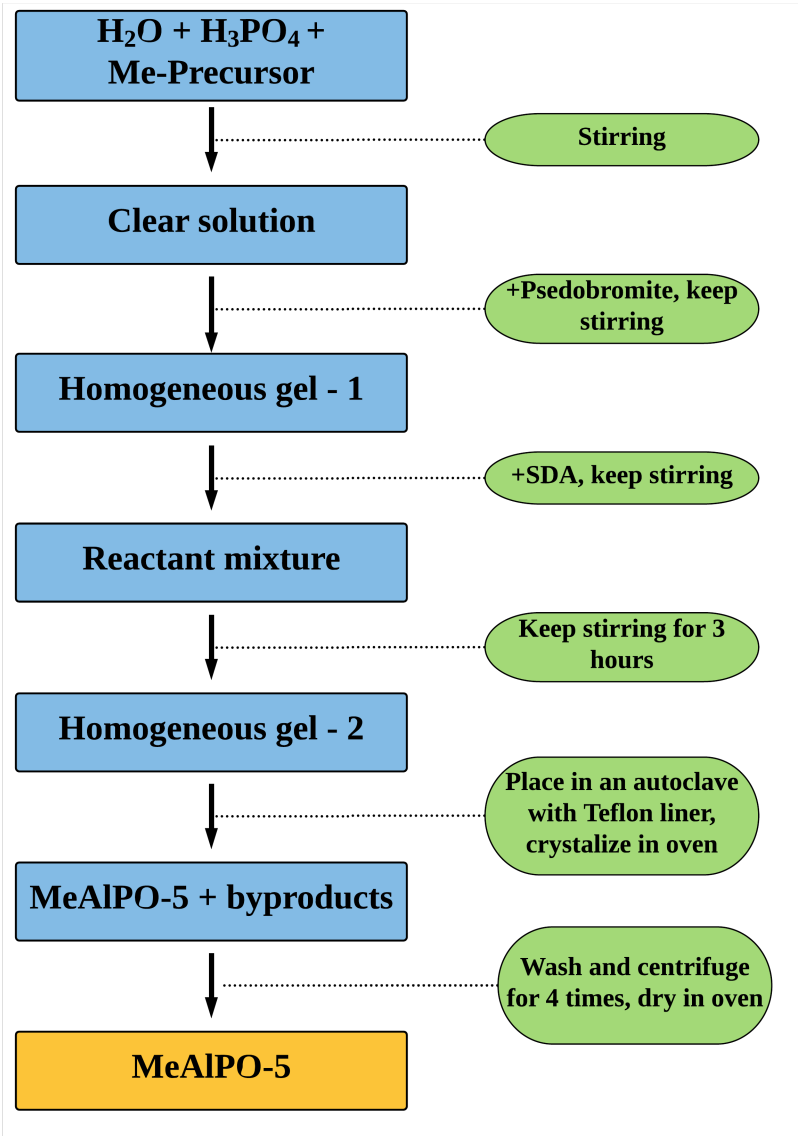

Figure 3.3 A flowchart illustration of the synthesis procedures of MeAlPO-5 using the one-solution method.

The 2-solution method was attempted in the synthesis of MoAlPO-5, ReAlPO-5, and GeAlPO-5. In this method, instead of adding all the components in one suspension mixture, the metal precursor was first dissolved into the SDA. In a typical synthesis using the 2-solution method, solution A was prepared by adding ortho-phosphoric acid (H_3PO_4, 85%, 11.60 g, Sigma-Aldrich) into Di-water (17.60 g), followed by pseudoboehmite (AlOOH, 71.8 wt.%, 7.11 g) under vigorous stirring. Solution B was prepared by dissolving the metal precursor into the SDA to form a homogeneous and clear solution. Once both solutions were ready, solution B was added into solution A, and allowed to stir for 3 hours until a homogeneous gel was obtained. Subsequently, the gel was transferred into a 100 ml stainless

steel autoclave with Teflon liner and crystallized in the oven with selected temperature and time. A flowchart illustration of the one solution method is shown in Figure 3.4

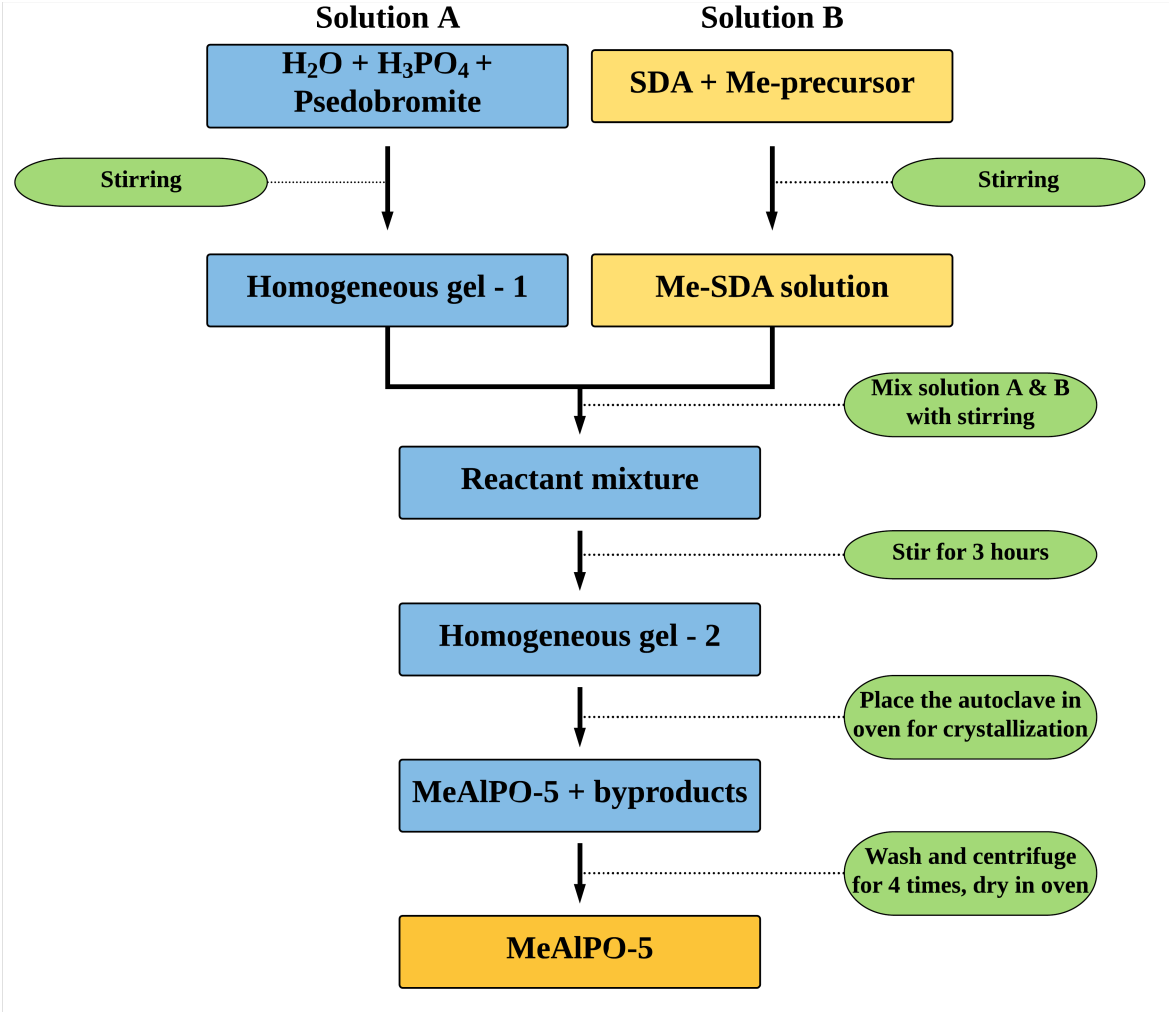

Figure 3.4 A flowchart illustration of the synthesis procedures of MeAlPO-5 using the two-solution method.

In the case of insoluble metal precursor with the 1-solution method, HF was used to assist the dissolution. GeAlPO-5 samples were synthesized using the Ge(IV) precursor GeO_2, which is insoluble in water, common acids and alkali, but it is soluble in HF. GeAlPO-5 samples synthesized using the 1-solution method used HF to dissolve GeO_2 in a separate beaker, then added into the reaction mixture and follows the subsequent synthesis procedures.

After the crystallization the obtained samples were washed and centrifuged for sedimentation for 4 times with approximately 80 ml of Di-water, then dried in an oven at 70°C overnight.

3.2.2 Synthesis of MeAlPO-5 (Me=Mo, Re, Ge)

In the attempt to achieve the isomorphous substitution of Me into AlPO-5, several synthesis parameters have been varied. The parameter study includes using different metal precursors, SDAs, crystallization temperatures, crystallization times, and synthesis methods (1-solution or 2-solution methods). 2-solution method was attempted with the SDA MDCHA, while 1-solution method was attempted with TEAOH, TEA, MDCHA, and TPA. A summary of the parameter study in the attempt to synthesize MoAlPO-5 is shown in Table 3.5. All the MoAlPO-5 attempted used the molar ratio Mo:Al = 0.05.

Table 3.5 An overview of the parameter study to synthesize MoAlPO5 using isomorphous substitution.

Sample	Precursor	SDA	Sol. Method	Temp.	Time (hr)
MoAlPO5-1	MTO	TEAOH(40%)	2-Sol	150	24
MoAlPO5-2	AM	TEAOH(40%)	2-Sol	150	24
MoAlPO5-3	MTO	TEAOH(40%)	2-Sol	200	24
MoAlPO5-4	AM	TEAOH(40%)	2-Sol	200	24
MoAlPO5-5	AM	MDCHA	1-Sol	150	48
MoAlPO5-6	AM	TEAOH(40%)	1-Sol	180	24
MoAlPO5-7	AM	TEAOH(40%)	1-Sol	180	48
MoAlPO5-8	AM	TPA	1-Sol	180	24
MoAlPO5-9	AM	TEA	1-Sol	200	24
MoAlPO5-10	AM	TEA	1-Sol	200	72
MoAlPO5-11	AM	TEA	1-Sol	200	96
MoAlPO5-12	AM	TEA	1-Sol	200	168
MoAlPO5-13	AM	MDCHA	1-Sol	150	24
MoAlPO5-14	AM	MDCHA	1-Sol	150	96
MoAlPO5-15	AM	MDCHA	1-Sol	200	24
MoAlPO5-16	AM	MDCHA	1-Sol	200	48
MoAlPO5-17	AM	MDCHA	1-Sol	200	96

Similar experiments were performed in the first attempt to search direct synthesis routes for ReAlPO-5. The available precursors were rhenium (VII) oxide and ammonium perrhenate (APR). The 1-solution method was attempted using the SDA TEA, while the 2-solution method was attempted using the SDAs TEPA and TPA. In all synthesis the precursor used was Re_2O_7. An overview of synthesis parameters of ReAlPO-5 in this study is shown in Table 3.6.

Table 3.6 An overview of synthesis parameters of ReAlPO5 using isomorphous substitution. All samples were synthesized using the precursor rhenium(VII)oxide.

Sample	Re:Al	SDA	Sol. Method	Temp.	Time (h)
ReAlPO5-1	0.05	TEA	1-Sol	200	16
ReAlPO5-2	0.05	TEA	1-Sol	200	24
ReAlPO5-3	0.05	TEA	1-Sol	200	48
ReAlPO5-4	0.05	TEA	1-Sol	200	96
ReAlPO5-5	0.05	TEA	1-Sol	150	96
ReAlPO5-6	0.10	TEA	1-Sol	200	96
ReAlPO5-7	0.03	TEPA	2-Sol	200	48
ReAlPO5-8	0.03	TPA	2-Sol	200	48

An indirect route to synthesize ReAlPO-5 was also attempted via the intermediate product GeAlPO-5. The synthesis procedures for GeAlPO-5 followed slightly modified 1-solution method. In a typical synthesis ortho-phosphoric acid (85%, 11.60 g) was added into Di-water (25 g) under gentle stirring in a plastic beaker, followed by pseudoboehmite (71.8 wt.%, 7.15 g). GeO_2 (99%, Sigma-Aldrich, 0.53 g) was added into HF (40 wt.%, Sigma-Aldrich, 0.25 g) in a separate plastic beaker, followed by of Di-water (6 g). The mixture of GeO_2 and HF was transferred into the beaker containing the rest of reactants, and kept stirring for one hour. Sample GeAlPO5-3 was heated to 95 °C during the stirring, while the other were at room temperature. Afterward the SDA TEA was added into the reaction mixture and allowed to stir for another 2 hour until a homogeneous gel was obtained. Subsequently the gel was transferred into a 100 mL stainless steel autoclave with Teflon liner and put in the oven for hydrothermal crystallization. The washing and centrifuging of the samples were the same as described previously. A summary of GeAlPO-5 samples is shown in Table 3.7.

Table 3.7 An overview of synthesis parameters of GeAPO5 using isomorphous substitution.

Sample	Ge:Al	Precursor	SDA	Sol. Method	Temp.	Time (hr)
GeAlPO5-1	0.10	GeO_2	TEAOH	2-Sol	200	90
GeAlPO5-2	0.05	GeO_2	TEA	1-Sol	200	90
GeAlPO5-3	0.05	GeO_2	TEA	1-Sol	200	90
GeAlPO5-4	0.05	GeO_2	TEA	1-Sol	200	180
GeAlPO5-5	0.05	GeO_2	TEA	1-Sol	180	90

3.2.3 Calcination

To remove the template (SDA) and evacuate the porous structure, the as-prepared samples were calcined in the air inside a calcination oven. The temperature profile is shown in Figure 3.5: heating at 1°C/minute to 550 °C and dwelled for 6 hours. The calcined samples were allowed to cool down to room temperature inside the oven.

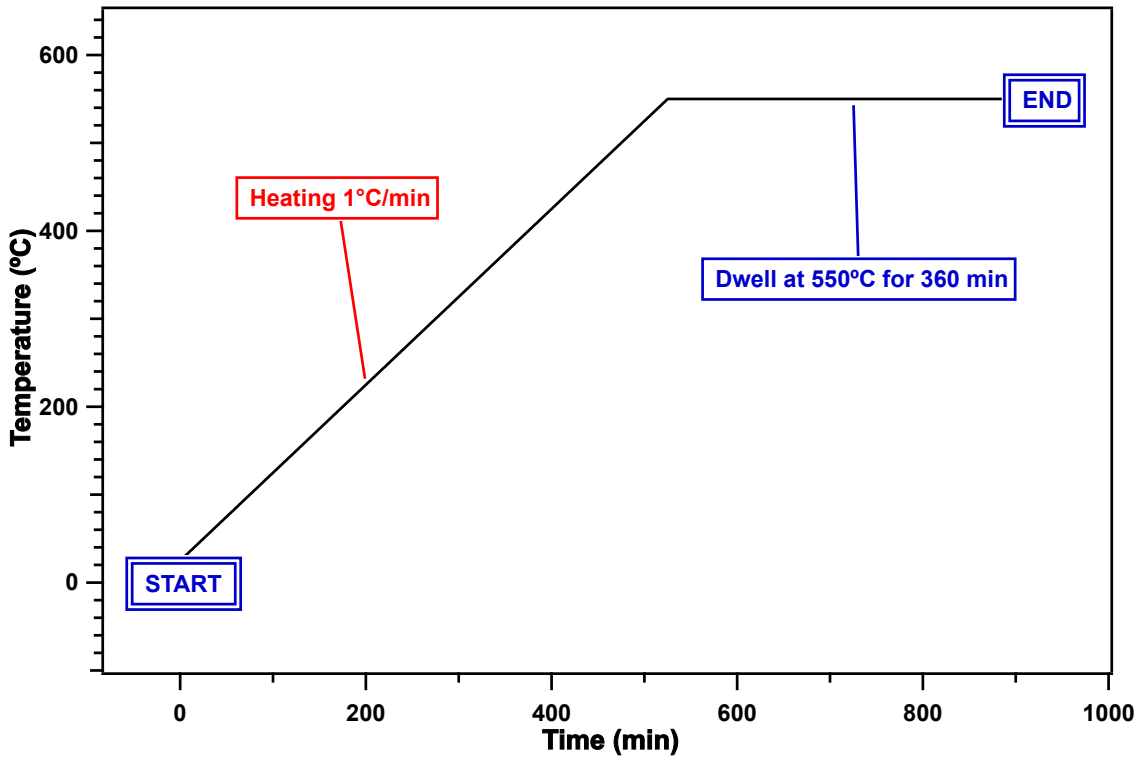

Figure 3.5 Temperature program to the template (SDA).

3.3 Structure Characterization

3.3.1 Powder X-ray diffraction

The samples for powder XRD measurements were prepared by grinding the original materials to a fine powder, and distributed onto Si sample holder plates with a flat surface. The sample holders were placed on the operation sample charger of the instrument and subsequently placed to the detection channel sequentially and automatically.

The measurements were performed on a Bruker AXS D8 Advance diffractometer. The instrument operated with a Cu target X-rays tube with 40 kV plate voltage and 40 mA current. The X-rays used is Cu $k_{\alpha 1}$ line at 1.5406 Å. The scans were set to record intensity data from 2θ = 5 - 75 degrees, with 0.01°step size and variable divergence slit such that the illuminated length on the sample always remain 6 mm. The data collection was set to record for 30 minutes for each sample.

3.3.2 ICP-MS

A. Sample decomposition

The sample decomposition was performed using a mixture of ultra-pure 40% HF and 65% HNO_3. Since HF was used, all the sample preparation containers used were made of Teflon. In a typical sample preparation, 20-35 mg of a sample was dissolved in a mixture of 0.7 g of 40% HF and 2.1 g of 65% HNO_3 acid solution. The sample was mixed in this acid solution for at least 30 minutes for a complete digestion. The fully-digested sample mixture was diluted with di-ionized water to a final volume of approximately 216 mL, and was stored in a sealed Teflon sample tube for instrumental analysis.

B. Instrumental analysis

The instrumental analysis was conducted using a Thermo Scientific ELEMENT-2 ICP-MS spectrometer equipped with prepFAST sample autodilution system (Elemental Scientific) and SC-2 DX autosampler (Elemental Scientific). Instrumental analysis was operated by Senior Engineer Syverin Lierhagen at the Department of Chemistry, NTNU.

3.3.3 Surface and porosity characterization

The surface and porosity measurements were conducted using a Micromeritics TriStar 3000 Surface Area and Porosity Analyzer. In a typical experiment, approximately 0.02 - 0.5 g of

the sample was used for a measurement. Prior to the analysis, the samples were degassed using a Micromeritics VacPrep 061 degaser. The degassing was conducted at 250°C, under a vacuum of approximately 150 mbar pressure for 24 hours.

Upon completion of the degassing, the sample tubes were attached to the analyzer. The adsorption-desorption isotherm was obtained using N_2 gas at liquid nitrogen temperature (78 K). The BET specific surface area was calculated according to the BET theory using 5 points at low pressure from the adsorption isotherm.

The adsorption-desorption isotherm was obtained using 48 points measurement for adsorption, from P/P^o = 0.01 to 0.98, and 25 points for desorption. The shape of the isotherm was used to determine the type of adsorption and therefore giving information about the characteristics of the pores. The pore size distribution was determined by employing the Barrett-Joyner-Halenda (BJH) method to the adsorption-desorption isotherm.

Chapter 4

RESULTS

4.1 Functionalization of Silica Aerogels

4.1.1 Observations of the aerogel synthesis

A. Preparation of the sol

In the first step of the aerogel synthesis, the ion-exchange of the sodium silicate solution yielded a clear and colorless silicic acid solution with a pH approximately equals to 2. In the Mo-aerogels experiments after the precursor ammonium molybdate was added, the solution has no apparent change and remains a clear and colorless liquid. In the Re-aerogels experiments, both rhenium precursors dissolved quickly in the silicic acid solution and yielded a clear and colorless liquid. In the Mo-aerogel synthesis the pH of the colloidal solution raised to approximately 5 after the precursor was added. On the other hand in the Re-aerogel synthesis the pH of the colloidal solution remains at 2 after the Re precursor (either Re_2O_7 or NH_4ReO_4) was added.

B. Adjustment of sol pH

In the Mo-aerogel experiments, when HNO_3 was added into the solution to lower the pH, the color of the solution changed to a bright yellow. It appeared that as more HNO_3 was added into the solution, the yellow color became deeper. After gelation, the gel first took a bright yellow color the same as the solution before gelation, then in the period of approximately 10 minutes, the colors became fainter and fainter, eventually turned into a hint of light blue. The color was more noticeable when comparing to an unmodified pH (pH=5) sample, which remains colorless during the entire synthesis. On the other hand, in the Re-aerogels

experiments, neither increasing the pH using ammonia solution nor decreasing the pH using HNO_3 changed the color of the solution and the subsequent gel, which are both colorless.

C. Gelation

The gelation happened relatively fast after the surface modification agents were added, typically within 1-2 minutes. In both Mo and Re experiments, as more metal precursor was added, the gelation time decreased. It is worth mention that Mo-aerogel colloidal solution will turn into a gel relatively fast within 1 minute after the precursor was added, even without adding the surface modification agents, yielding a hydrogel. One possible reason for this phenomena is because the precursor raised the pH of the solution and therefore triggered the base-catalyzed polycondensation reaction of silicic acid. In comparison, the Re-aerogel sol with either precursors was relatively stable within the time of the experiment before solvent exchange (1-2 hours), although it will eventually turn into a hydrogel after 1-2 days if no silylation agent is added. In all experiments following the co-precursor route it has been given particular caution that that the solution remained a liquid when the surface modification agents were added.

D. Solvent exchange

Solvent exchange happened as the obtained gel was quickly immersed in n-heptane, and no apparent change was observed during this process. The surface modification reaction typically happens within 3 hours, but the aerogels were allowed to stayed immersed in heptane for 24 hours to assure the completion of the reaction. In all the Mo-aerogel experiments which the pH are unmodified, as well as all the Re-aerogel experiments which included modified pH samples, the obtained "heptane-gel" (since the pores are now filled with heptane) appeared to be colorless. In the Mo-aerogel experiments which the pH were modified with HNO_3, it appeared that the light blue color was transferred to the aqueous phase, and the organic phase as well as the heptane-gel appeared colorless.

E. Sample appearance

After drying in the oven to evaporate the heptane, all the obtained aerogel samples were white solids. The hydrophobicity of the aerogels was confirmed with a simple test, by pipetting small drops of water onto a container which has some residue aerogel sample. The appearance of a typical sample and the hydrophobic test is shown in Figure 4.1.

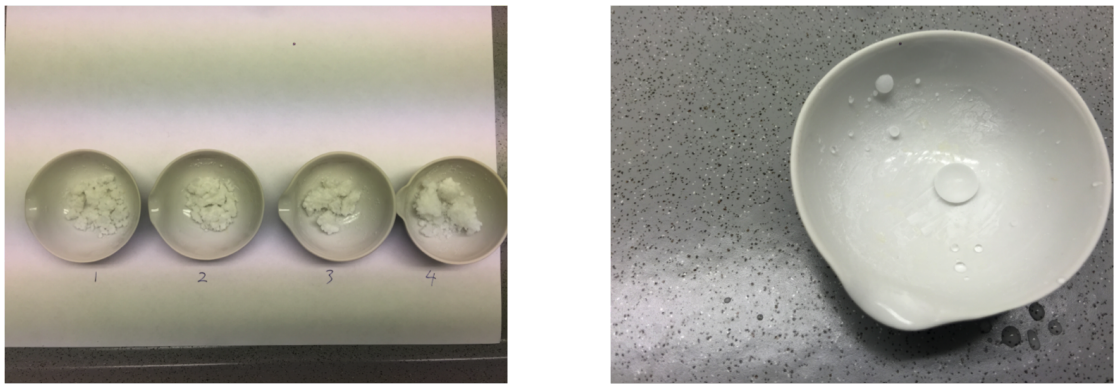

(a) **(b)**

Figure 4.1 (a). After evaporation of the n-heptane, a white solid was obtained. All the solids were then further ground into fine powders (b). A simple test with water confirmed the obtained sample is hydrophobic.

4.1.2 Powder XRD phase determination of Me-aerogels

A. Phase determination of Mo-aerogels

The phase of the Me-aerogel samples was characterized using powder X-ray diffraction (PXRD). Sample MoAERO-1 to sample MoAERO-4 were synthesized at pH = 5 using ammonium molybdate as the metal precursor, at various Mo : Si molar ratios. The powder XRD patterns of these Mo-aerogel as-prepared and annealed samples are shown in Figure 4.2.

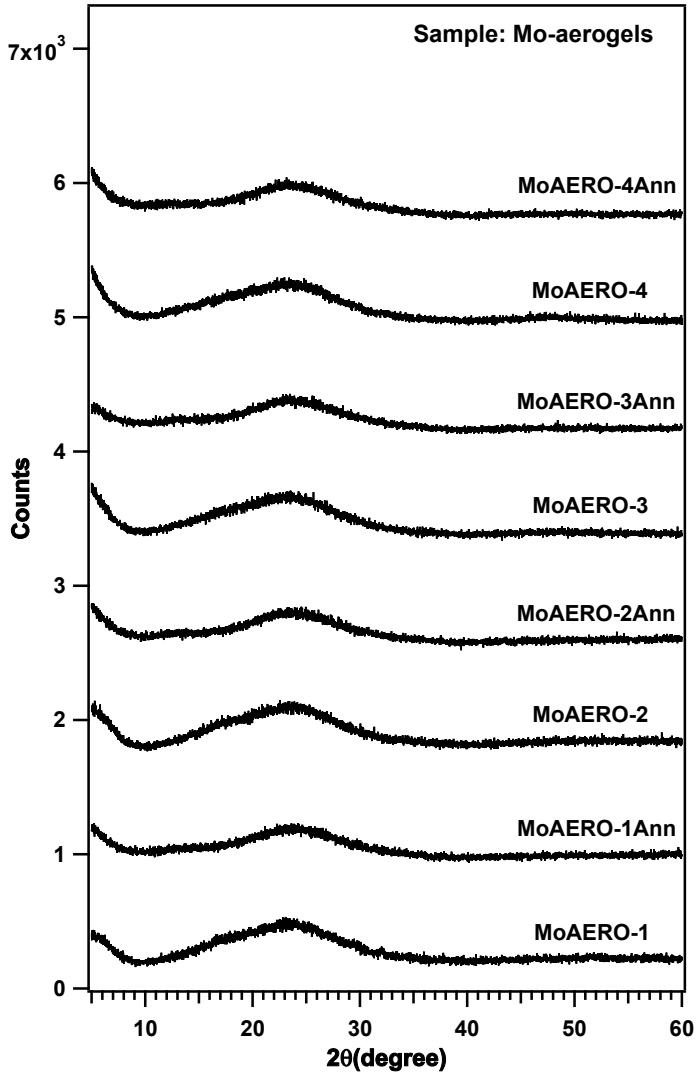

Figure 4.2 Powder XRD patterns of as-prepared and annealed Mo-aerogels synthesized at pH=5 with varying molar ratios.

The powder XRD patterns indicate that all the samples are amorphous and the reflections consistent with the reflection of plain silica aerogels as described in chapter 2. Changing the

Mo : Si molar ratio did not appear to affect the XRD patterns for the samples. After annealing at 450°C for 3 hours all these samples remain amorphous. Varying the sol pH during the syntheses, the diffraction patterns of sample MoAERO-5 (pH = 1) and MoAERO-6 (pH = 3) indicate that these samples are also amorphous with the absence of Braggs' peaks, as shown in Figure 4.3. The annealed samples are also amorphous, but the treatment seems to have some effects that altered the shape of the diffraction patterns.

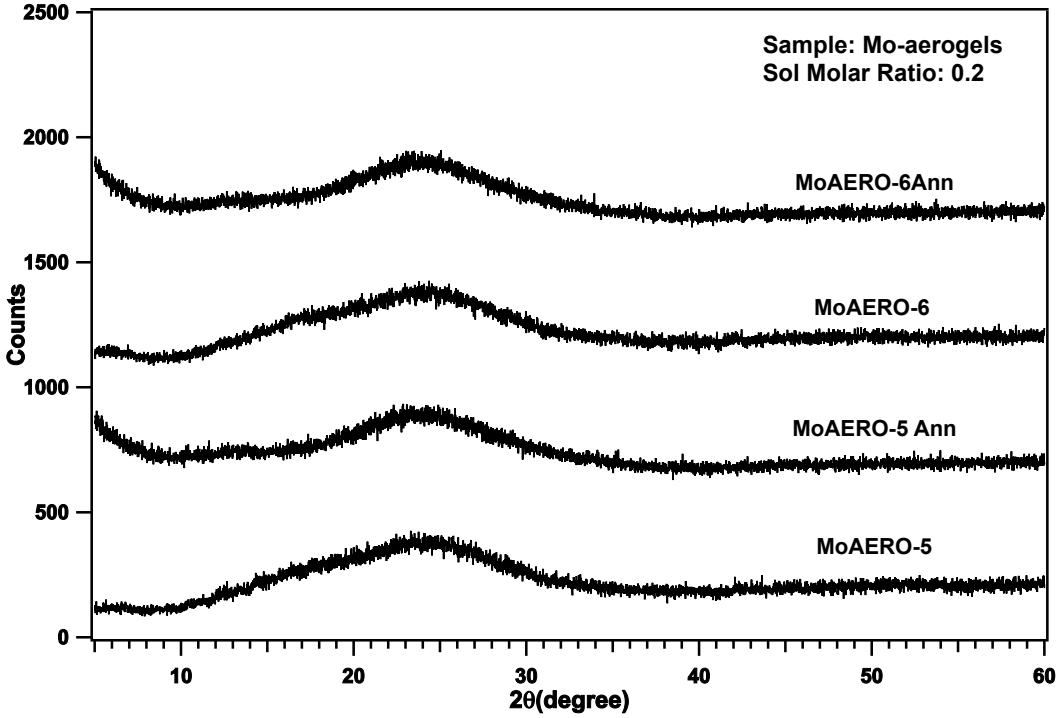

Figure 4.3 Powder XRD diffractogram of as-prepared and annealed Mo-aerogel samples synthesized at adjusted pH.

In summary, the phase analysis of all Mo-aerogel samples synthesized at various Me:Si molar ratio, various pH of the sol, and post-treatment with annealing, given no Braggs' peaks in the powder XRD patterns and therefore are amorphous.

B. Phase determination of Re-aerogels

The phase of Re-aerogel samples was also determined using powder X-ray diffraction. Sample ReAERO-1 to ReAERO-4 were synthesized using the Re(VII) precursor Re_2O_7 with the sol pH = 2 at various Re:Si molar ratios. The powder XRD patterns are shown in Figure 4.4, at all molar ratios the synthesis gives Re-aerogel samples with a combination of amorphous and crystalline phase.

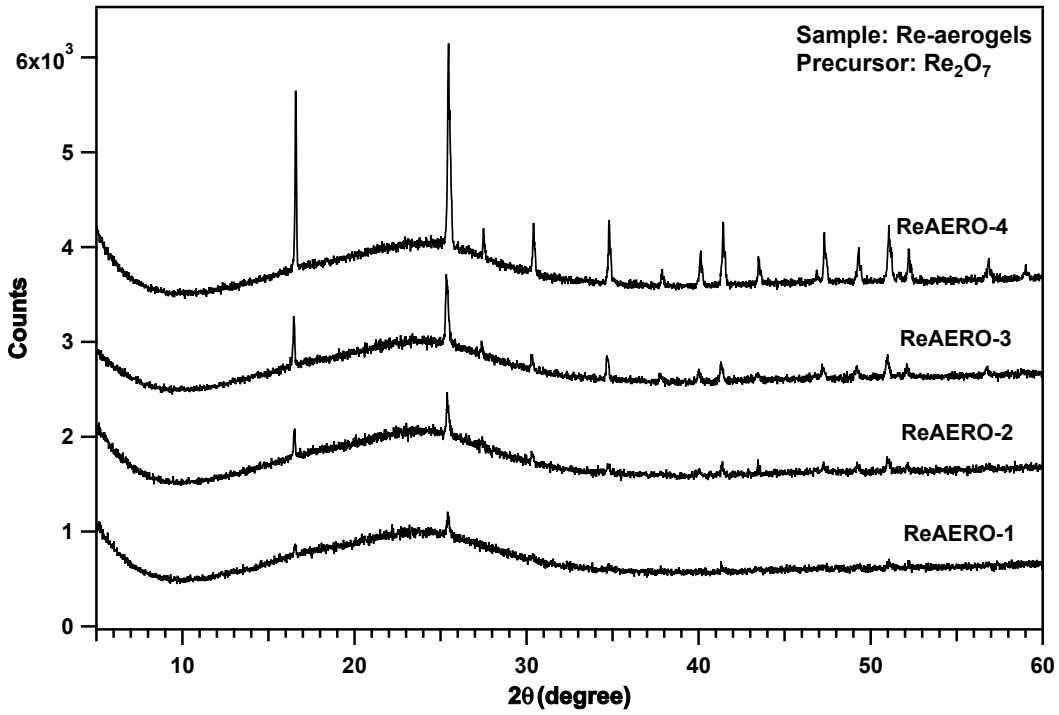

Figure 4.4 Powder XRD patterns of the as-prepared Re-aerogel samples with varying Re:Si molar ratios.

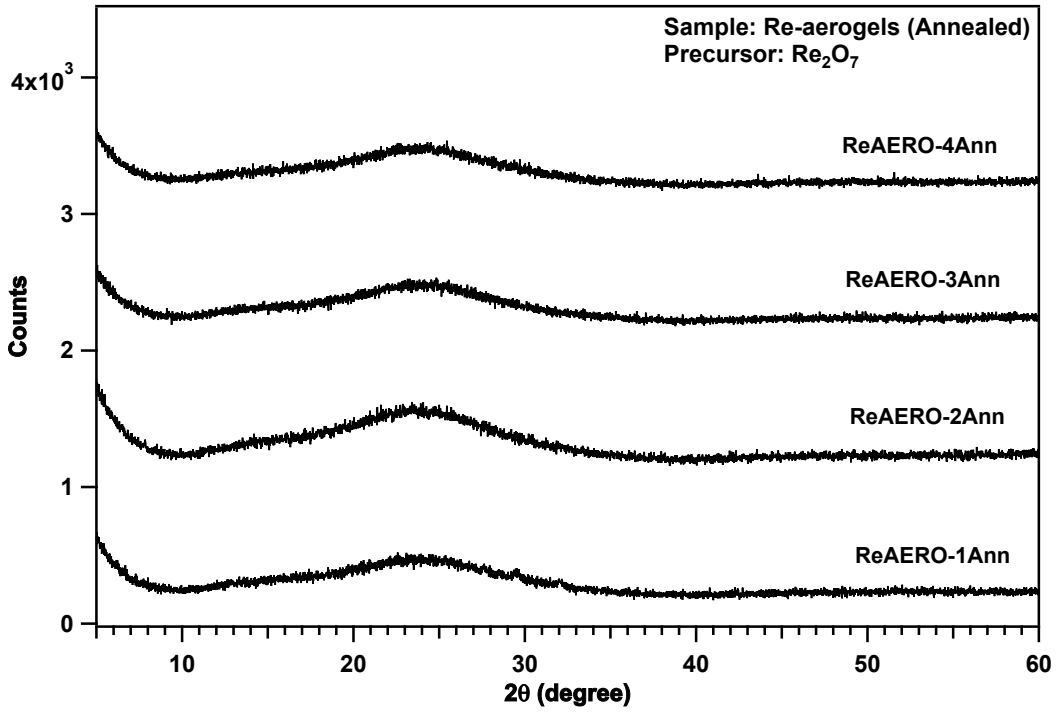

Figure 4.5 Powder XRD patterns of the annealed Re-aerogel samples using Re_2O_7 as the metal precursor and at various Re:Si molar ratios.

Annealing of sample ReAERO-1 to ReAERO-4 eliminated the crystalline phase and left only the amorphous phase present, as shown in Figure 4.5. The exact nature of this phenomenon is unknown, but it is likely because the instability of NH_4ReO_4 upon heating and becoming Re_2O_7, which is known to be volatile in the air, departing from the samples[126].

The amorphous phase was easily identified from the short range order of the silica aerogel. Using the powder diffraction database *The International Centre for Diffraction Data*, the crystalline phase which features the sharp Braggs' peaks was identified from the reflections of the rhenium salt NH_4ReO_4, as shown in Figure 4.6. The source of ammonia is believed to be from the surface modification reaction between silylation agent HMDS and the siloxy groups. From the powder XRD patterns of as-prepared ReAERO-1 to ReAERO-4 samples it can also be seen that as the molar ratio Re : Si increased, the intensity of the Braggs' peaks of ammonium perrhenate became higher.

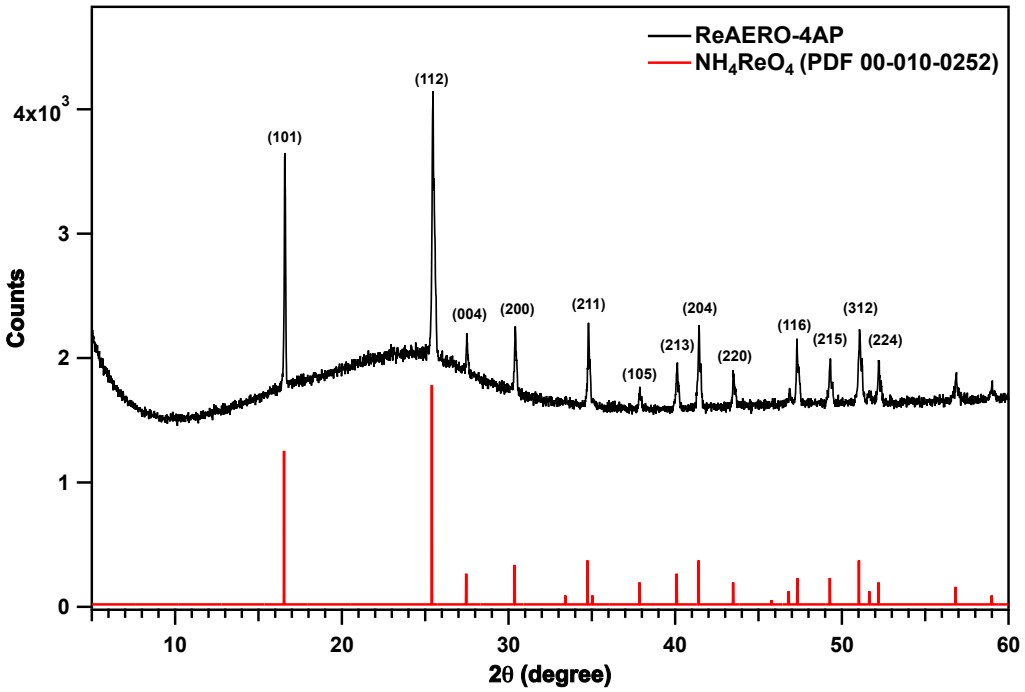

Figure 4.6 Analysis of the diffraction patterns with database shows that the Braggs' peaks matching with the powder diffraction patterns of ammonium perrhenate

Sample ReAERO-5 to sample ReAERO-8 were synthesized using a different Re(VII) precursor, ammonium perrhenate (APR), with other synthesis parameters identical to ReAERO-1 to ReAERO-4. The powder XRD patterns of these samples are similar to that of ReAERO-1 to ReAERO-4, and are shown in Appendix Figure A.1. The patterns show that using the precursor ammonium perrhenate also produced samples with a mixed phase of amorphous

silica aerogel and crystalline APR. Unlike in the synthesis when Re_2O_7 was used as the metal precursor, when APR was used, the intensity of the reflections did not follow a clear trend as the Re:Si ratio increases. Similar to when Re_2O_7 was used as precursor, annealing of sample ReAERO-5 to ReAERO-8 also eliminated the crystalline phase and left only the amorphous phase present, which are also shown in Appendix Figure A.2.

For the pH adjusted Re-aerogels, it appears that either increasing or decreasing the pH will still result in samples with a combination of amorphous and crystalline phase. The powder XRD patterns of as-prepared Re-aerogels synthesized with adjusted sol pH show similar reflections as ReAERO-1 to ReAERO-4, which are shown in Appendix Figure A.3. Sample ReAERO-12, of which the pH of the sol was adjusted to 12 using ammonia solution, was not formed and the sol remained liquid after silylation agents were added. After the annealing, the crystalline phase was eliminated, as shown in Appendix Figure A.4. Sample ReAERO-14 was synthesized with NH_4ReO_4 and at the Re:Si molar ratio 0.2, while changing the silylation agent to TMCS. The powder XRD patterns of both as-prepared and calcined samples are shown in Appendix Figure A.3 and Figure A.4. Similar to the base catalyzed aerogels, when TMCS was used, crystalline phase of NH_4ReO_4 was also present in the powder XRD patterns of the as-prepared samples, and after annealing, the crystalline phase was also disappeared.

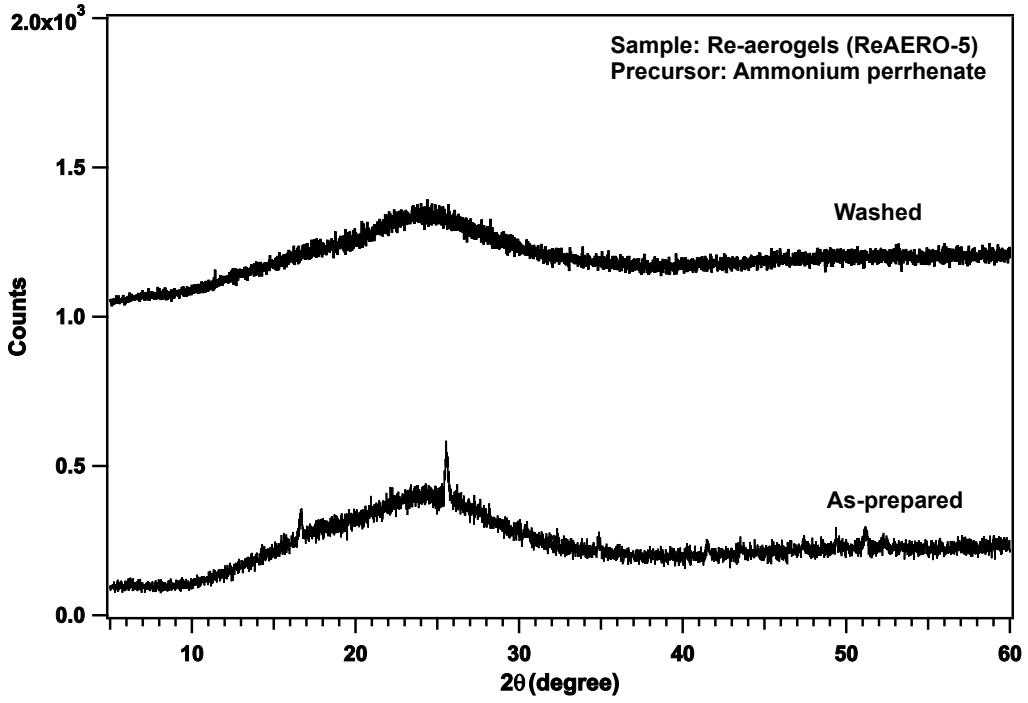

Figure 4.7 Powder XRD patterns of Re-aerogels with the wash post-treatment comparing to the as-prepared sample.

The post-gelation wash method was performed on sample ReAERO-5, and the powder XRD patterns comparison of as-prepared sample and washed sample are shown in Figure 4.7. The effect of washing appeared to be similar to annealing; both of them will eliminate the crystalline phase of NH_4ReO_4 and left only the amorphous phase from the aerogel.

In summary, the synthesis of Re-aerogels using the sol gel route and ambient pressure drying method resulted in a combination of both and amorphous and a crystalline phase in all the as-prepared samples. The ammonium perrhenate crystalline phase remains present in synthesis at various Re:Si molar ratio, metal precursors, and sol pH. For all samples annealing at 450°C eliminated the crystalline phase and left only the amorphous phase. An overview of all the Re-aerogel samples in the phase determination experiment is shown in Table 4.1.

Table 4.1 Summary of phase determination of Re-aerogels using powder X-ray diffraction.

Sample	Re:Si	pH	Silylation	Precursor	Phase
ReAERO-1	0.05	2	HMDS+HMDSO	Re_2O_7	Amo+Crys
Annealed					Amo
ReAERO-2	0.10	2	HMDS+HMDSO	Re_2O_7	Amo+Crys
Annealed					Amo
ReAERO-3	0.20	2	HMDS+HMDSO	Re_2O_7	Amo+Crys
Annealed					Amo
ReAERO-4	0.40	2	HMDS+HMDSO	Re_2O_7	Amo+Crys
Annealed					Amo
ReAERO-5	0.05	2	HMDS+HMDSO	NH_4ReO_4	Amo+Crys
Annealed/washed					Amo/Amo
ReAERO-6	0.10	2	HMDS+HMDSO	NH_4ReO_4	Amo+Crys
Annealed					Amo
ReAERO-7	0.20	2	HMDS+HMDSO	NH_4ReO_4	Amo+Crys
Annealed					Amo
ReAERO-8	0.40	2	HMDS+HMDSO	NH_4ReO_4	Amo+Crys
Annealed					Amo
ReAERO-9	0.20	7	HMDS+HMDSO	NH_4ReO_4	Amo+Crys
Annealed					Amo
ReAERO-10	0.20	8	HMDS+HMDSO	NH_4ReO_4	Amo+Crys
Annealed					Amo
ReAERO-11	0.20	9	HMDS+HMDSO	NH_4ReO_4	Amo+Crys
Annealed					Amo
ReAERO-12	0.20	12	HMDS+HMDSO	NH_4ReO_4	Not formed
ReAERO-13	0.20	1	HMDS+HMDSO	NH_4ReO_4	Amo+Crys
Annealed					Amo
ReAERO-14	0.20	2	TMCS	NH_4ReO_4	Amo+Crys
Annealed					Amo

4.1.3 ICP-MS elemental composition analysis of Me-aerogels

A. ICP-MS results of Mo-aerogels

The Mo-aerogel samples were analyzed using ICP-MS and an illustration of the results is shown in Figure 4.8. A complete summary of the results is shown in Table 4.2.

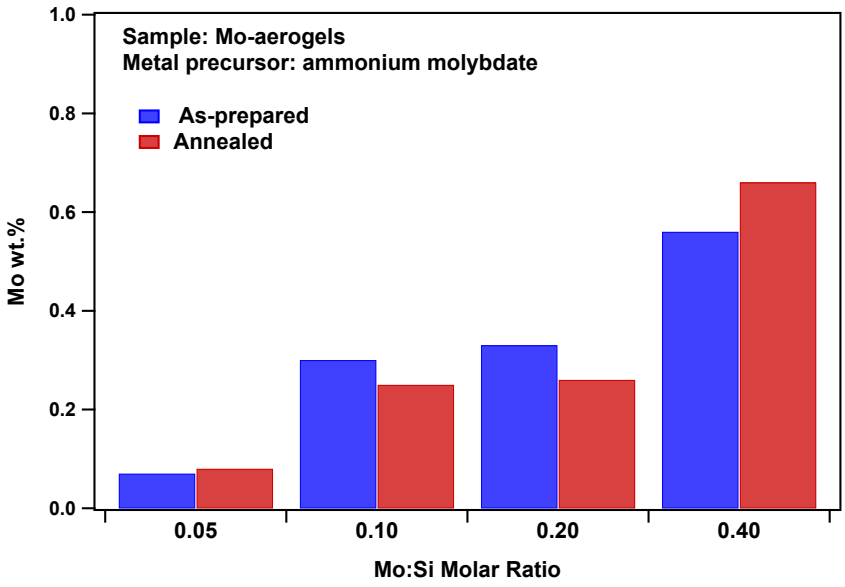

(a)

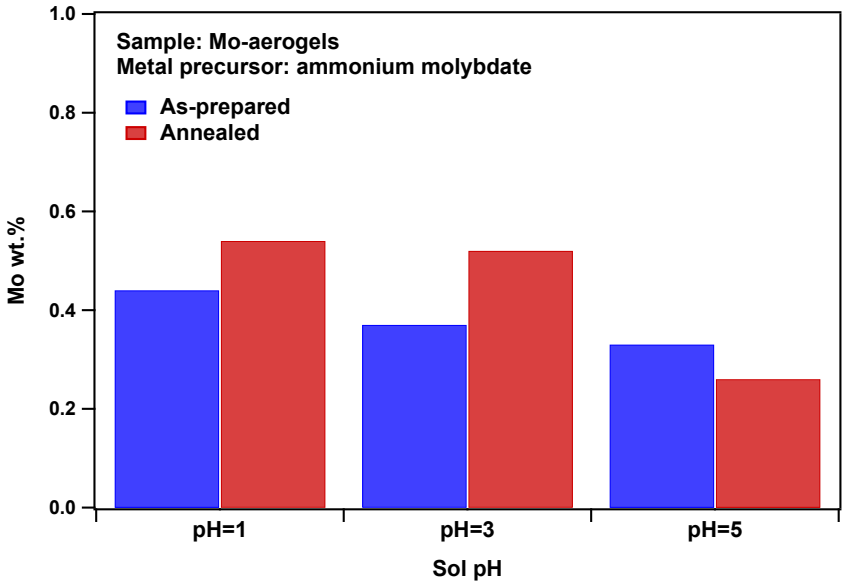

(b)

Figure 4.8 (a). Comparison of as-prepared and annealed Mo metal uptake in samples synthesized with different Mo:Si molar ratio. (b). Comparison of as-prepared and annealed Mo metal uptake in samples synthesized with different sol pH.

The ICP-MS results of Mo-aerogels show that the uptake of metal into the aerogel is relatively low (< 1 wt.%), indicating the the majority of molybdenum atoms were remain in the aqueous phase after gelation. Increasing the Mo : Si molar ratio in the sol resulted in higher metal content in the aerogels. Changing the pH of the sol before gelation appears to influence the metal uptake, but the difference is not significant. Annealing of the samples did influenced the metal content of the samples, but the trend is unclear.

Table 4.2 ICP-MS results of Mo-aerogels

Sample	Mo:Si	Sol pH	Mo wt.%	Si wt.%
MoAERO-1	0.05	5	0.07	34.4
Annealed			0.08	38.5
MoAERO-2	0.10	5	0.30	34.0
Annealed			0.25	35.0
MoAERO-3	0.20	5	0.33	34.7
Annealed			0.26	36.8
MoAERO-4	0.40	5	0.56	30.2
Annealed			0.66	43.3
MoAERO-5	0.20	1	0.44	26.7
Annealed			0.54	34.1
MoAERO-6	0.20	3	0.37	28.7
Annealed			0.52	40.4

B. ICP-MS results of Re-aerogels

In the Re-aerogel case, an illustration of the ICP-MS results is shown in Figure 4.9 and Figure 4.10. A complete summary of the ICP-MS analysis results is shown in Appendix Table 4.3

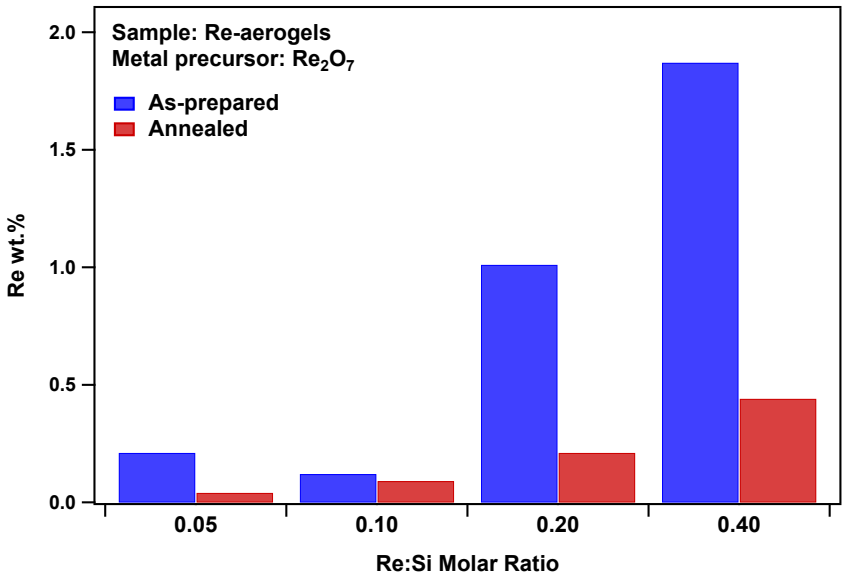

(a)

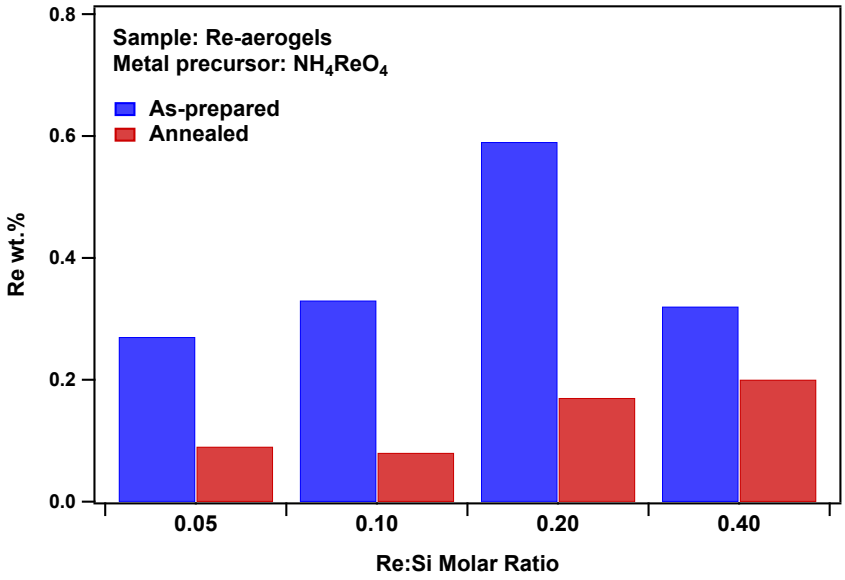

(b)

Figure 4.9 Comparison of Re metal uptake in as-prepared and annealed samples synthesized with the metal precursor (a). Re_2O_7 and (b). ammonium perrhenate.

As shown in Figure 4.9a, samples synthesized using the metal precursor Re_2O_7 at different $Re : Si$ molar ratios shown a trend that as the molar ratio increased, the metal content also

increased. Annealing of the samples at 450°C caused significant losses of the Re content. When synthesized with the metal precursor NH_4ReO_4, as shown in Figure 4.17b, although samples synthesized with higher molar ratio still have higher uptake, but the trend is not as obvious, since the uptake fluctuated as the molar ratio increased. Annealing of the samples at 450°C also caused significant decrease of the Re content.

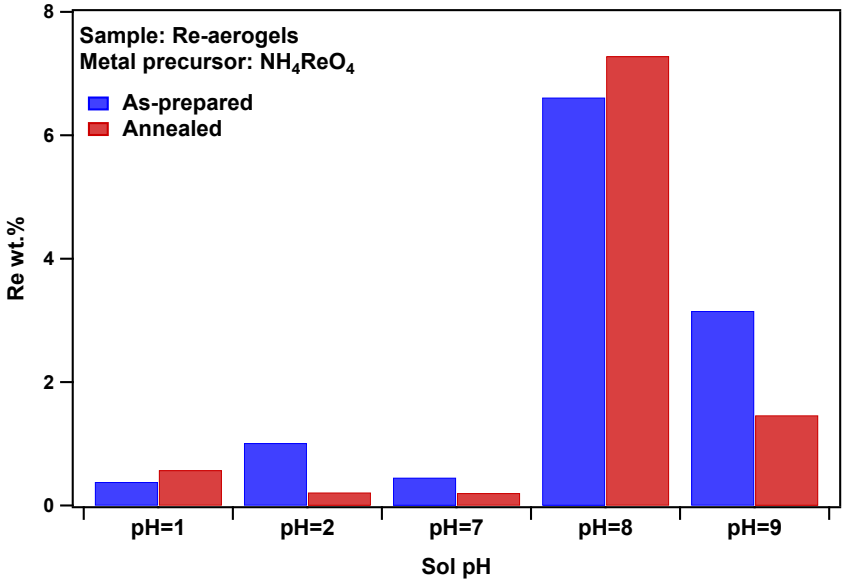

Figure 4.10 Comparison of Re metal uptake in as-prepared and annealed samples synthesized with different sol pH. The molar ratio in the sol was 0.2Re : Si.

The comparison of samples synthesized at different sol pH with other synthesis parameters constant is shown in Figure 4.10. Clearly, at higher pH (pH > 7), the uptake of Re increased significantly. The data suggested that at sol pH = 8 (sample ReAERO-10) the uptake of Re is at its maximum among the samples tested. For samples synthesized at pH = 1 (ReAERO-13) and at pH = 8 (sample ReAERO-10), it appears that after annealing, the Re content increased instead of decrease. The increase of metal content normally can be explained by the departure of the hydrophobic -R groups on the surface. However, since NH_4ReO_4 or Re_2O_7 are volatile upon heating, Re-aerogels typically have a lower Re content after annealing.

Table 4.3 ICP-MS results of Re-aerogels

Sample	Re:Si	Sol pH	Re wt.%	Si wt.%
ReAERO-1	0.05	2	0.21	35.2
Annealed			0.04	38.1
ReAERO-2	0.10	2	0.12	30.3
Annealed			0.09	39.9
ReAERO-3	0.20	2	1.15	31.1
Annealed			0.21	39.6
ReAERO-4	0.40	2	0.87	34.1
Annealed			0.44	37.7
ReAERO-5	0.05	2	0.27	32.8
Annealed/Washed			0.09/0.04	39.6/37.5
ReAERO-6	0.10	2	0.33	30.7
Annealed			0.08	34.9
ReAERO-7	0.20	2	0.59	26.5
Annealed			0.17	33.1
ReAERO-8	0.20	2	0.32	30.2
Annealed			0.20	35.8
ReAERO-9	0.20	7	0.45	33.3
Annealed			0.20	38.6
ReAERO-10	0.20	8	6.61	41.2
Annealed			7.28	34.8
ReAERO-11	0.20	9	3.15	34.8
Annealed			1.46	39.5
ReAERO-13	0.20	1	0.38	29.5
Annealed			0.57	41.8
ReAERO-14	0.20	2	3.52	27.2
Annealed			1.15	32.6

Lastly, ICP-MS analysis shown that the post-gelation wash method will eliminate almost all the Re in the sample, as shown in Figure 4.11. Clearly, after the washing, most of the Re

has been removed from the sample, consistent with the powder XRD results, which showing the disappearance of NH_4ReO_4 reflections after the washing. This is another evidence that the rhenium species exists in a separate phase residing in the pores of silica aerogels.

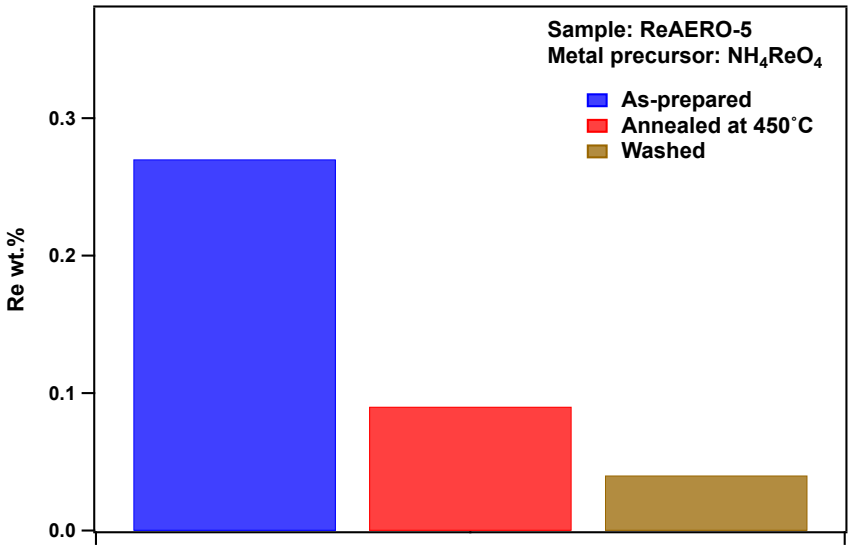

Figure 4.11 Comparison of Re metal uptake in as-prepared, annealed, and washed Re-aerogel samples. The sol molar ratio Re:Si was 0.05.

4.1.4 N_2 adsorption-desorption analysis of Me-aerogels

A. Analysis of Mo-aerogels

N_2 surface area and porosity analysis was performed on selected samples. The adsorption-desorption isotherms of as-prepared and annealed sample MoAERO-3 are shown in Figure 4.12a. Isotherms of other samples analyzed have similar features and are shown in Appendix. Figure 4.12b shows the pore size distribution of samples synthesized at sol pH = 5.

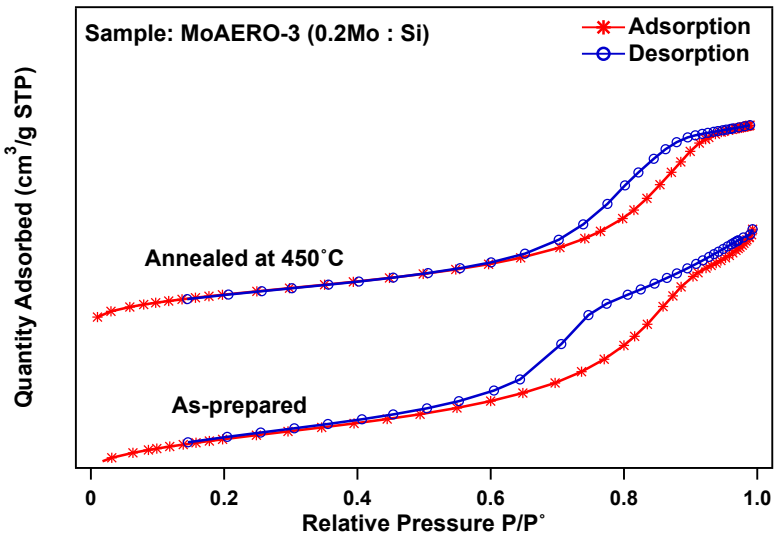

(a)

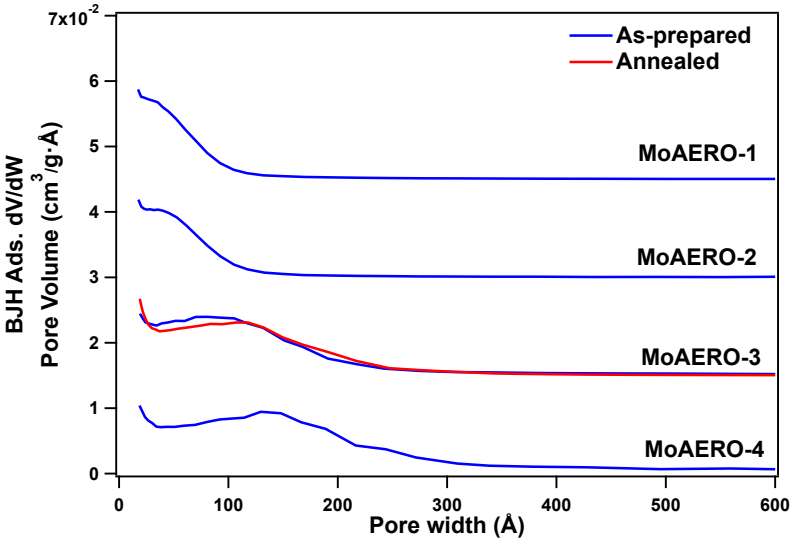

(b)

Figure 4.12 (a). N_2 adsorption-desorption isotherms of as-prepared and annealed sample MoAERO-3. (b). Pore size distribution of Mo-aerogels synthesized at molar ratio 0.05 - 0.40, corresponding to sample MoAERO-1 to MoAERO-4. The BET measurement of annealed Mo-aerogels was only performed on MoAERO-3.

As shown in the adsorption-desorption isotherms, both the as-prepared and annealed samples feature type IV adsorption-desorption isotherm with the presence of the hysteresis loop, which is caused by the capillary condensation of the mesopores [116]. In a more detail classification of hysteresis, it appears that the isotherm of the samples consistent with either Type I (H1) or Type II (H2) hysteresis, which implies either the materials consist of compact uniform spheres with narrow pore size distribution (H1), or pores with narrow necks and wide bodies (H2), although the distinction is difficult to make based on the isotherms [116]. It is also possible that it is a combination of both. Looking into the pore size distribution, as shown in Figure 4.12b, the samples contain mesopores with pore size distributed up to approximately 300 Å. Increasing the sol Mo:Si molar ratio resulted in larger pores and broader pore size distribution. For the annealed samples the BET measurement was only performed on sample MoAERO-3. Annealing of the sample did not significantly change the pore size distribution.

Comparing Mo-aerogel samples synthesized at different sol pH, the pore size distribution of both as-prepared and annealed samples are shown in Figure 4.13.

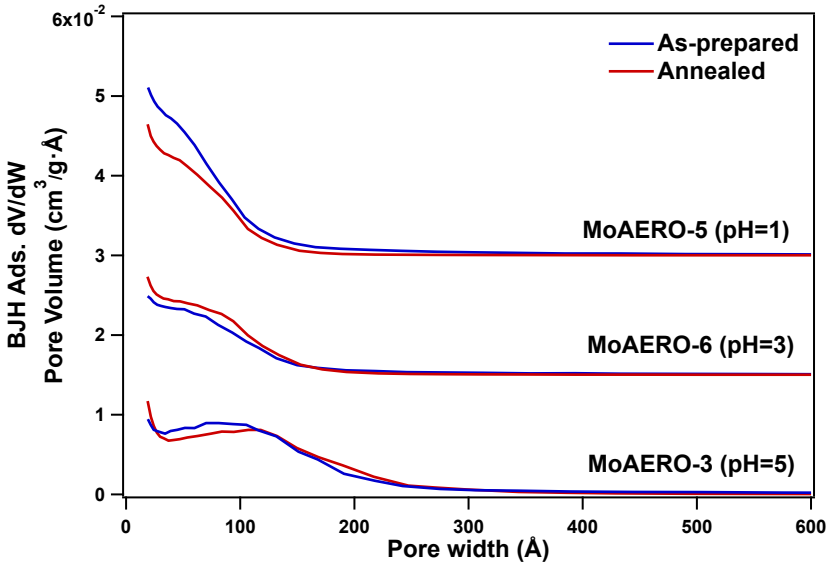

Figure 4.13 Pore size distribution of as-prepared and annealed Mo-aerogels synthesized at different sol pH.

Lowering the pH seems to decrease the pore size from up to approximately 300 Å (pH = 5) to 150 Å (pH = 1), but the effect is not very significant. Annealing of these samples also did not significantly change the pore size distribution. This is an interesting observation, because when molar ratio was increased, the metal content also increased and the pore size became larger; adjusting the sol pH to more acidic also increased the metal content, but the

pore size decreased. This suggests that both the metal precursor and the pH may influence the gelation process and hence the pore size distribution.

BET specific surface area and BJH average pore size/cumulative pore volume are also important properties of aerogel samples. The BET specific surface area of all the samples analyzed are illustrated in Figure 4.14 and summarized in Table 4.4.

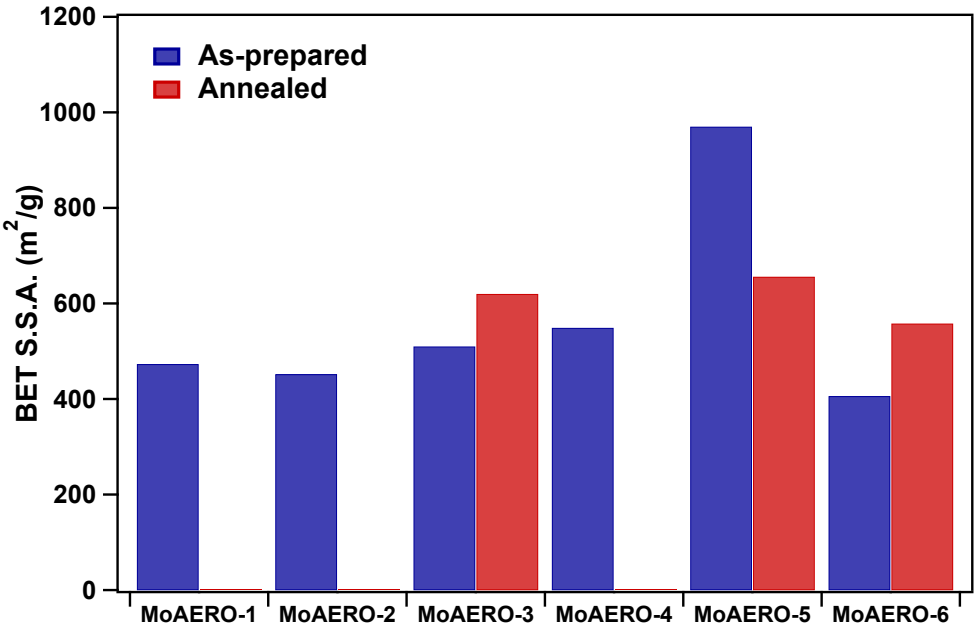

Figure 4.14 Illustration of BET specific surface area of Mo-aerogel samples.

The BET surface areas of most Mo-aerogels are lower than the literature value of approximately 600 m^2/g [26]. It appears that as the Mo : Si molar ratio of the sol increased, the surface area also increased. The effect of different sol pH to the BET surface area is unclear; when the pH decreased from 5 (MoAERO-3) to 3 (MoAERO-6), the BET surface area decreased, but when the pH further decreased to 1 (MoAERO-5), the surface area of the as-prepared sample increased significantly. After annealing, the BET surface area of MoAERO-3 and MoAERO-6 increased, but MoAERO-5 decreased substantially, which is rather strange behavior and the reason is unclear. The BJH adsorption average size and cumulative pore volume of Mo-aerogel samples are illustrated in Figure 4.15a and Figure 4.15b, and summarized in Table 4.4.

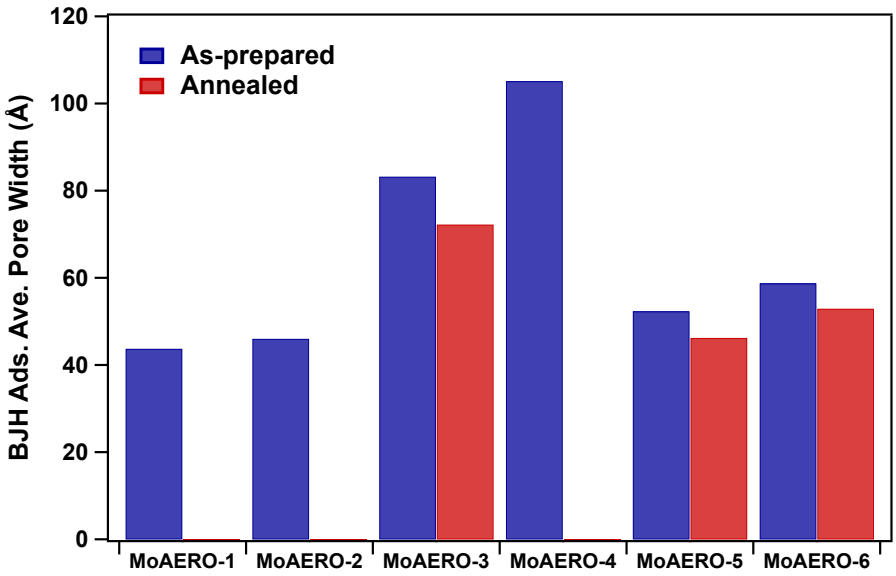

(a)

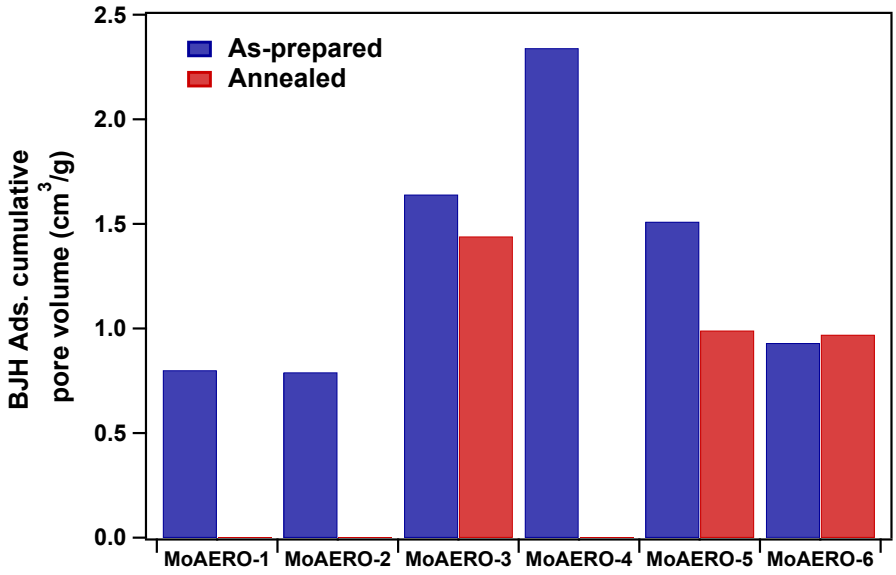

(b)

Figure 4.15 (a) Illustration of BJH adsorption average pore size of Mo-aerogel samples. (b) Illustration of BJH adsorption cumulative pore volume of Mo-aerogel samples.

As shown in Figure 4.15, increasing the sol molar ratio from 0.05 to 0.40 (MoAERO-1 to MoAERO-4) resulted in the increase of both BJH average pore size and cumulative pore volume. Increasing the sol pH from 1, 3 to 5 (MoAERO-5, MoAERO-6, MoAERO-3, respectively) appears to also resulted in higher pore sizes. However, the effects of changing pH on the cumulative pore volume did not seem to have a clear trend: at pH = 5, the

cumulative pore volume is relatively high at 1.64; at pH = 3, cumulative pore volume decreased to 0.93; further decreased to pH = 1, the cumulative pore volume increased again to 1.51. Annealing of the samples appears to decrease both the pore size and the cumulative pore volume.

Table 4.4 BET specific surface area, BJH average pore width, and cumulative pore volume of Mo-aerogels.

Sample	Mo:Si	Sol pH	S. S. A (m^2/g)	Pore width (Å)	Pore volume (cm^3/g)
MoAERO-1	0.05	5	473	43.7	0.80
Annealed			-	-	-
MoAERO-2	0.10	5	452	46.0	0.79
Annealed			-	-	-
MoAERO-3	0.20	5	510	83.2	1.64
Annealed			620	72.2	1.44
MoAERO-4	0.40	5	549	105.1	2.34
Annealed			-	-	-
MoAERO-5	0.20	1	970	52.3	1.51
Annealed			656	46.2	0.99
MoAERO-6	0.20	3	406	58.7	0.93
Annealed			558	52.9	0.97

B. Analysis of Re-aerogels

In the Re-aerogel case, the N_2 surface area and porosity analysis was performed on selected samples synthesized with different precursors and molar ratios. The adsorption-desorption isotherms of a sample synthesized with Re_2O_7 (ReAERO-3) are shown in Figure 4.17.

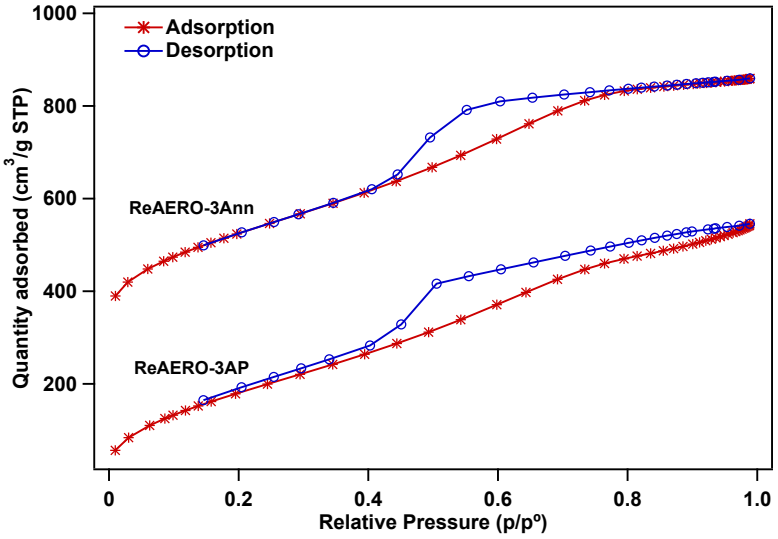

(a)

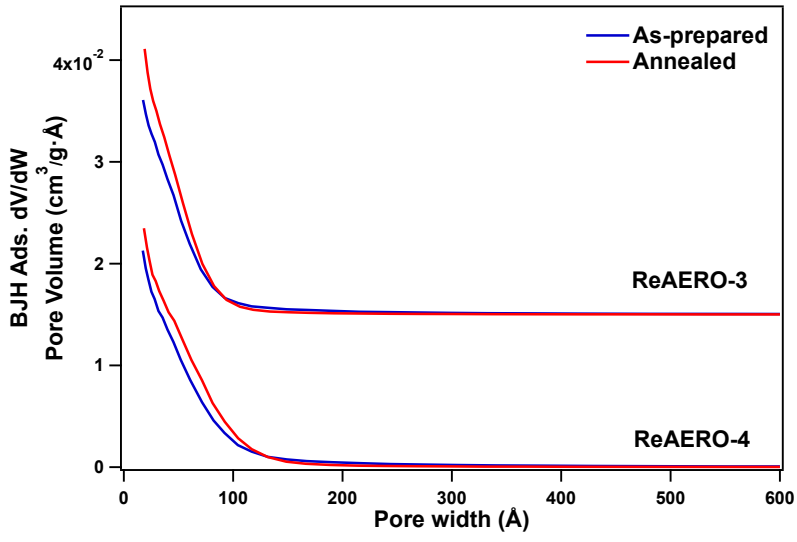

(b)

Figure 4.16 (a). N_2 adsorption-desorption isotherms of as-prepared and annealed Re-aerogels (ReAERO-3) synthesized with Re_2O_7. For clarity only one pair of samples is shown. Isotherms of other samples are shown in Appendix. (b). Pore size distribution of 2 samples synthesized at different molar ratios, 0.20 (ReAERO-3) and 0.4 (ReAERO-4)

The adsorption-desorption isotherms of Re-aerogels synthesized with Re_2O_7 show that both the as-prepared and annealed samples consistent with the Type IV isotherm, and

possibly a combination of H1 and H2 hysteresis. The pore size distributions of ReAERO-3 and ReAERO-4 show that in both samples mesopores up to 120 Å are present. Annealing seems to slightly increase the pore size, but the effect is not significant.

Similarly, the adsorption-desorption isotherms and pore size distribution of Re-aerogels as-prepared samples synthesized with NH_4ReO_4 are shown in Figure 4.17.

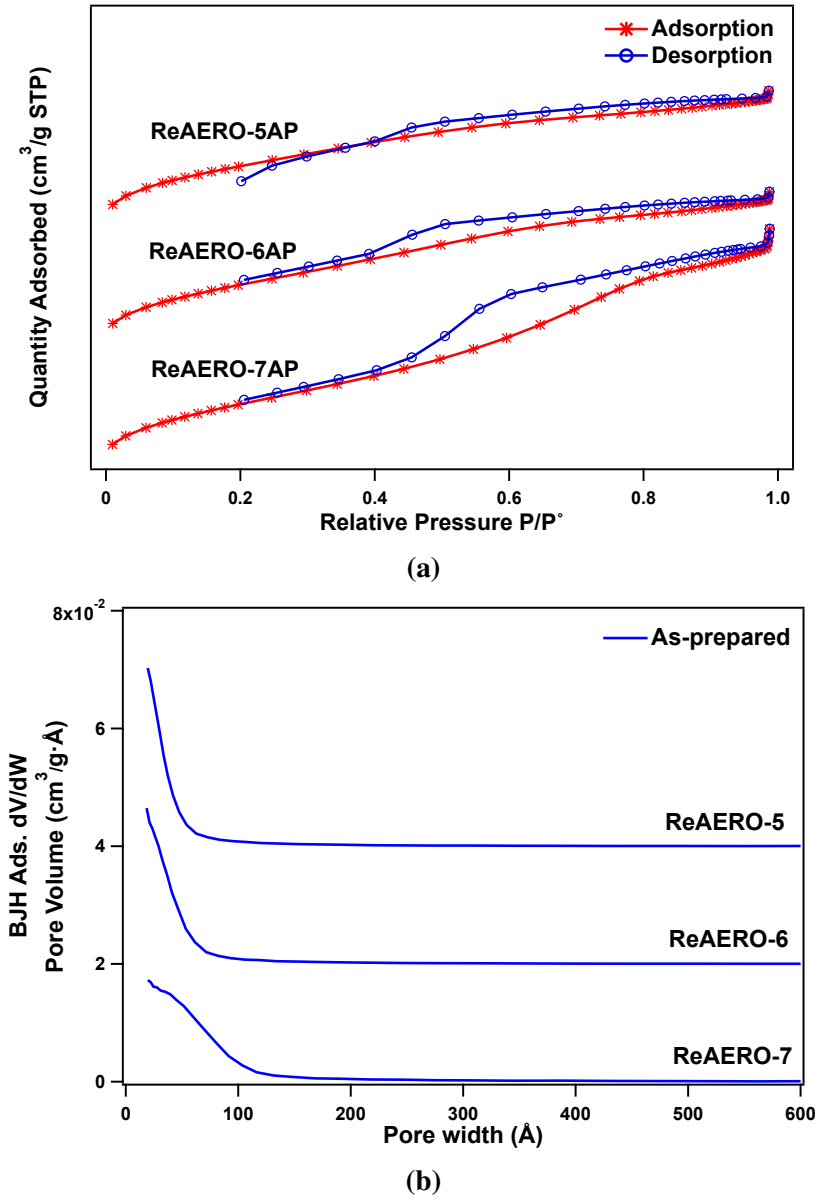

Figure 4.17 (a). N_2 adsorption-desorption isotherms of as-prepared Re-aerogels synthesized with NH_4ReO_4 The annealed samples were not analyzed.

As shown in the isotherms, all three as-prepared samples that are analyzed features hysteresis loops and are consistent with the IUPAC type IV isotherm and either H1 or H2

hysteresis classification, or a combination of both. The pore size distribution shows that all three samples have mesopores with distribution up to approximately 120 Å. It appears that increasing the Re : Si molar ratio of the sol resulted in slightly larger pores. To further illustrate the surface properties, the BET specific surface area results are shown in Figure 4.18. All BET/BJH results are summarized in Table 4.5.

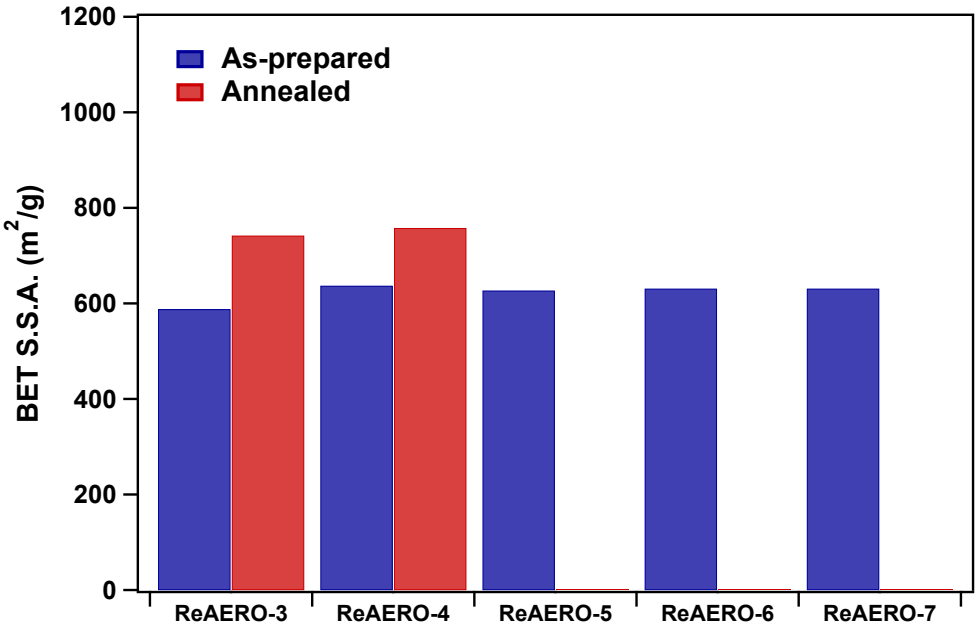

Figure 4.18 Illustration of BET specific surface area of Re-aerogel samples.

The BET specific surface area of Re-aerogels are comparable to the literature value of approximately 600 m^2/g [26], slightly higher than those of Mo-aerogels. The 2 analyzed annealed samples have higher surface area at over 700 m^2/g, which may be understood by the oxidative removal of the surface -CH_3 groups at temperature above 300°C[82][83]. Varying the sol molar ratio and changing the precursor did not appear to significantly affect the surface area, which all have the BET surface area at approximately 600 m^2/g, as shown in Figure 4.18. Further analysis using the BJH theory shows the average pore size and cumulative pore volume of the Re-aerogels, which seems to have some interesting trends, as illustrated in Figure 4.19.

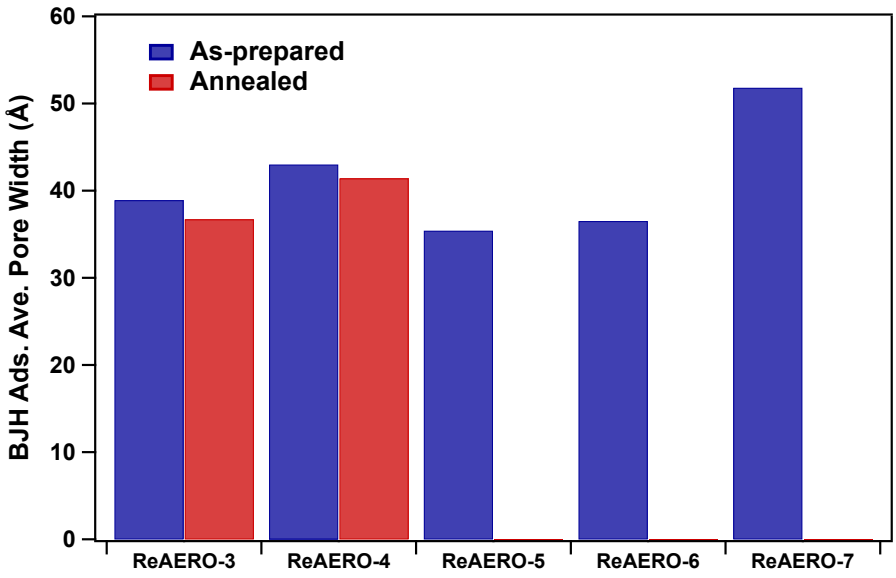

(a)

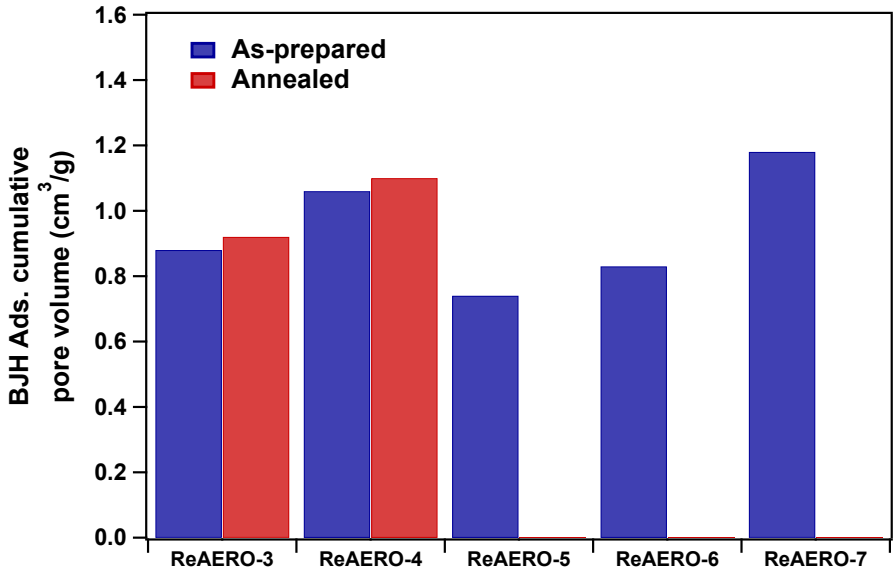

(b)

Figure 4.19 (a) Illustration of BJH adsorption average pore size of Re-aerogel samples. (b) Illustration of BJH adsorption cumulative pore volume of Re-aerogel samples.

Among the Re-aerogels, it appeared that both the average pore size and the cumulative pore volume are correlated with the sol molar ratio: at higher molar ratio, both of them increased, regardless of either using Re_2O_7 or NH_4ReO_4 as the metal precursor. Comparing the samples synthesized using different metal precursors at the same sol molar ratio, using Re_2O_7 resulted in Re-aerogels with higher pore size and cumulative pore volume. Furthermore,

it seems like the cumulative pore volume increase is due to the higher molar ratio, but not necessarily the metal content. Sample ReAERO-3 was synthesized at molar ratio 0.2, which has higher metal content (1.15 wt.%) than sample ReAERO-4 (0.87 wt.%), but ReAERO-4, which was synthesized at higher molar ratio of 0.4, has higher cumulative pore volume.

Table 4.5 BET specific surface area, BJH average pore width, and cumulative pore volume of Re-aerogels.

Sample	Re:Si	S. S. A.(cm^2/g)	Pore width (Å)	Pore volume (m^3/g)
ReAERO-3	0.20	588	38.9	0.88
Annealed		742	36.7	0.92
ReAERO-4	0.40	637	43.0	1.06
Annealed		758	41.4	1.10
ReAERO-5	0.05	627	35.4	0.74
Annealed		-	-	-
ReAERO-6	0.10	631	36.5	0.83
Annealed		-	-	-
ReAERO-7	0.20	631	51.8	1.18
Annealed		-	-	-

4.2 Functionalization of AlPO-5

4.2.1 Observations of AlPO-5 synthesis

A. Observations of MoAlPO-5 synthesis

In a typical synthesis using the 1-solution method, after the metal precursor was added, a clear and colorless solution was obtained. The addition of the Al(III) precursor pseudoboehmite caused the solution to turn into a thick and gel-like suspension. After vigorous stirring a white and homogeneous suspension was obtained. In the cases when MDCHA was used as SDA (sample MoAlPO5-5, MoAlPO5-13 to MoAlPO-17), as the SDA was added into the suspension, the temperature of the suspension increased, and after vigorous stirring a homogeneous suspension with pale yellow color was formed, as shown in Figure 4.20a.

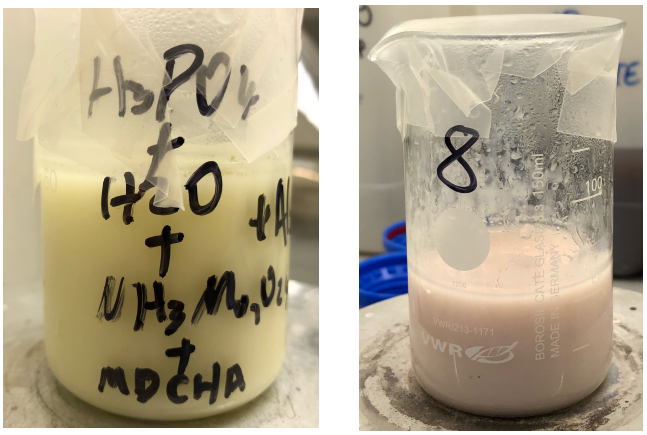

(a) **(b)**

Figure 4.20 (a). When MDCHA was used to synthesize MoAlPO-5, the suspension has a pale yellow color. (b). When TPA was used to synthesize MoAlPO-5, the suspension has a pale yellow color.

In the synthesis of sample MoAlPO5-8. when TPA was used as the SDA in 1-solution method, the suspension appeared to have a pale pink color, as shown in Figure 4.20b. The source of this color is unknown, it is possibly a complex between a polyoxomolybdate or molybdophosphate system with TPA. In all other synthesis the suspensions appeared to be white.

After the crystallization the supernatant was poured away and the solid samples were washed and centrifuged. All samples synthesized with the SDA MDCHA have a faint light blue color, and the sample synthesized with TPA is brown. After calcination, all samples synthesized with MDCHA turned into a light yellow color, while the sample synthesized

with TPA remains brown. All the other samples are while powders, and remain white powder after calcination.

B. Observations of ReAlPO-5 synthesis

For ReAlPO-5 samples, when TEA was used as the SDA, a white and homogeneous suspensions were obtained. Crystallization of the samples all yielded white solids. When TEPA was used as the SDA, the 2-solution method was followed, and the suspension has a pale yellow color.

C. Observations of GeAlPO-5 synthesis

In the synthesis of sample GeAlPO5-1, 2-solution method was used and when GeO_2 was dissolved in 40% TEAOH solution, a clear and colorless solution was obtained. In the rest of GeAlPO-5 samples, the modified 1-solution method was used with HF. Using the HF used did not completely dissolve GeO_2, possible due to the relatively small amount of HF used compares to the amount of GeO_2 (Ge : HF = 1 : 1). The mixture of HF and GeO_2 was added into the suspension of H_3PO_4, and stirred for 1 hour. Sample GeAlPO5-3 was heated to 90°C during this hour. Subsequently, the SDA (TEA) was added into the suspensions. No apparent change of color in all the suspensions was observed. After additional of 2 hours stirring, white and homogeneous suspensions were obtained.

After the crystallization and washing, all GeAlPO-5 sample appeared to be white solids. After calcination, GeAlPO5-1 remained to be a white solid, while all the rest of GeAlPO-5 samples took a light brown to gray color.

4.2.2 Powder XRD phase determination of MeAlPO-5

A. Phase determination of MoAlPO-5

In order to determine the phase of the MeAlPO-5 samples, the samples were analyzed using powder XRD. The presenting results will be categorized by the choice of SDA and synthesis methods. A summary of all the results using various SDA is shown in Table 4.6. Figure 4.21 shows the XRD patterns of MoAlPO-5 samples synthesized with the SDA TEAOH. Among them sample MoAlPO5-1 to sample MoAlPO5-4 were synthesized using the 2-solution method, and sample MoAlPO5-6 and MoAlPO5-7 were synthesized using the 1-solution method. As shown in the powder XRD patterns, none of these samples is phase pure. Sample MoAlPO5-1 and MoAlPO5-3 were synthesized using the precursor MoO_3 with 2-solution method (MoO_3 does not dissolve in aqueous solution) and contain AFI phase with other unknown phases. Other samples do not contain AFI phase, determined by the absence of the reflection at $2\theta = 7.5°$. The XRD results indicates that this synthesis route do not produce phase pure MoAlPO-5 samples using either the 1-solution or 2-solution method.

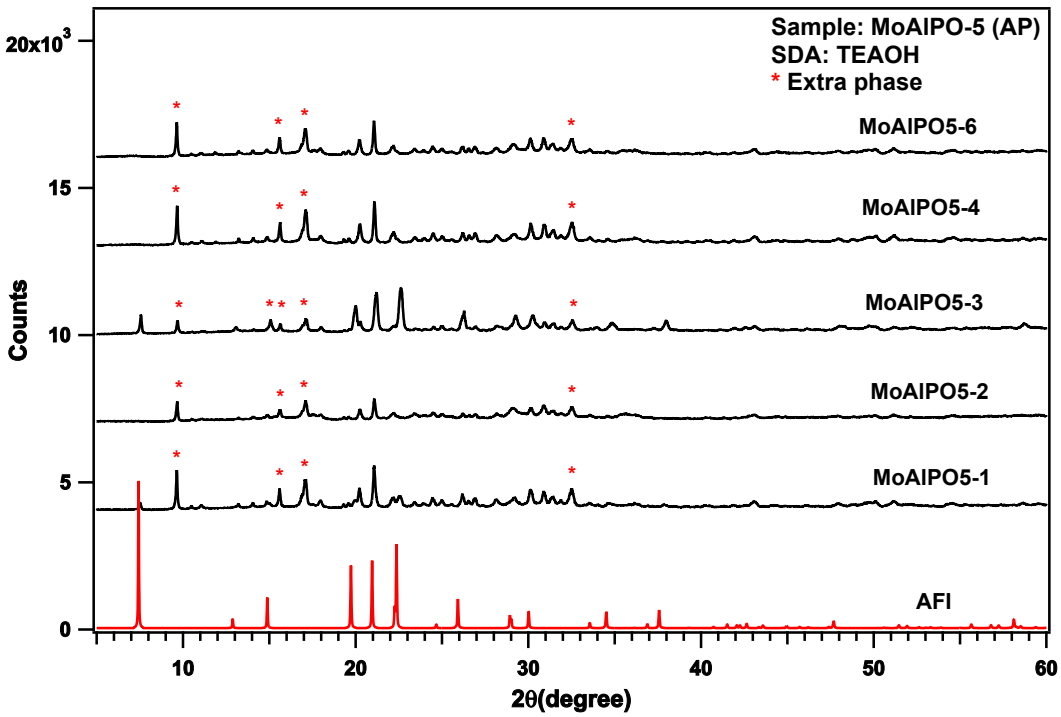

Figure 4.21 Powder XRD diffractogram of as-synthesized samples of MoAlPO5 using TEAOH as SDA. Main extra phases were labeled with asterisks in red. None of theses samples is phase pure.

Sample MoAlPO5-5, MoAlPO5-13 to MoAlPO5-17 were synthesized with the SDA MDCHA using the 1-solution method, varying crystallization temperature and crystallization time. Using this SDA phase pure AFI sample were successfully synthesized at 150°C with

all the crystallization times tested. One example of the powder XRD patterns of a phase pure sample (sample MoAlPO5-5) is shown in Figure 4.22. As shown in the patterns, both as-prepared and calcined samples are phase pure AFI. Calcination shifted some relative intensities of the peaks, but did not change the positions. Two other samples synthesized using this SDA at 150°C with different crystallization times (24 hours and 96 hours) are also phase pure AFI. The powder XRD patterns of all other samples synthesized using MDCHA are shown in Appendix Figure A.6 and Figure A.7 for the as-prepared and calcined samples, respectively.

Increasing the crystallization temperature to 200 °C, extra phases started to appear, and as the crystallization time increases, the intensity of the extra phases became more and more dominant. Although using the same SDA as preciously, none of these samples is phase pure. Calcination also did not eliminate the extra phases. The powder XRD patterns of MoAlPO-5 samples synthesized using MDCHA at 200°C are shown in Appendix Figure A.8 and Figure A.9 for the as-prepared and calcined samples, respectively.

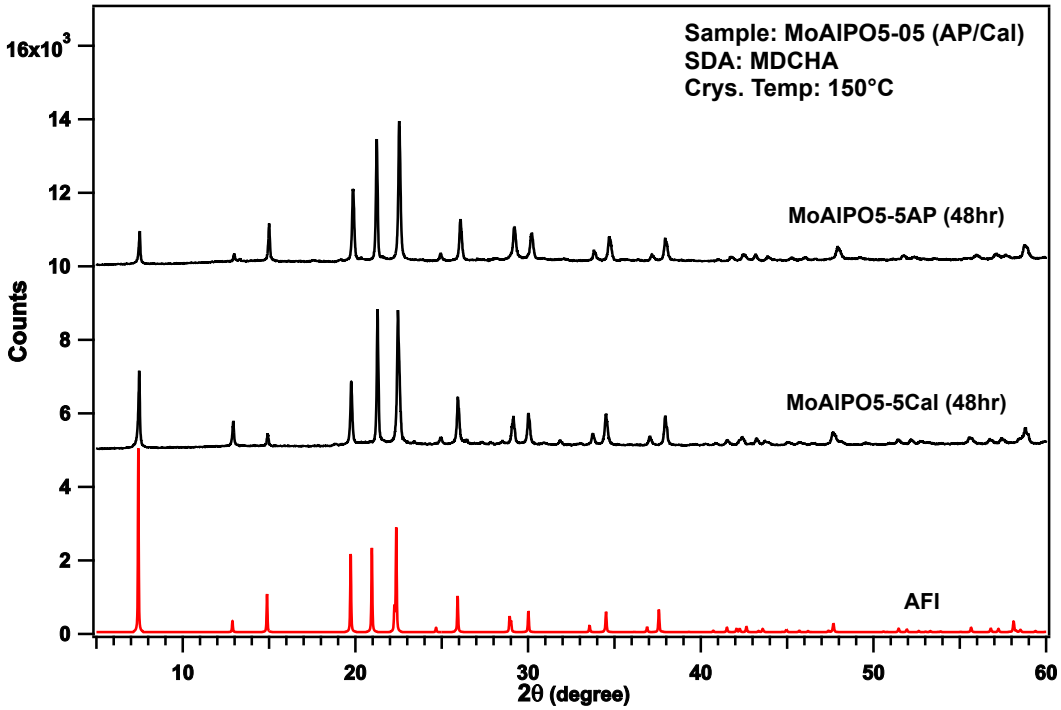

Figure 4.22 Powder XRD diffractogram of as-prepared and calcined sample MoAlPO5-5, both are phase pure AFI.

Other attempts using different SDAs, including TPA and TEA, did not produce phase pure samples. Both the as-prepared and calcined samples contain significant amount or only

extra phases. The powder XRD patterns of these samples are shown in Appendix in Figure A.10 and Figure A.11.

In general, this study shows that the choice of SDA as well as the synthesis condition have a substantial influence on the structure when the Mo precursors were added. Several SDAs that are otherwise common to direct AFI structure did not produce the phase pure product when the Mo metal precursors were present. A summary of using different SDAs with various crystallization conditions in an attempt to incorporate Mo into AlPO-5 via isomorphous substitution in this study is shown in Table 4.6. Among these synthesis only MDCHA produced the AFI structure, which also remains AFI after the calcination. When using MDCHA as the SDA to synthesize MoAlPO-5, the effects of crystallization temperature is well pronounced. Synthesis at 150°C produced phase pure AFI samples, whereas synthesis at 200°C produced significant amount of extra reflections in the powder XRD patterns.

Table 4.6 A summary of powder XRD results of MoAlPO-5 attempted using isomorphous substitution.

Sample	Mo:Al	Precursor	SDA	Method	Temp	Time	XRD
MoAlPO5-1	0.05	MTO	TEAOH	2-Sol	150°C	24 hr	Ex. phases
MoAlPO5-2	0.05	AM	TEAOH	2-Sol	150°C	24 hr	Ex. phases
MoAlPO5-3	0.05	MTO	TEAOH	2-Sol	200°C	24 hr	Ex. phases
MoAlPO5-4	0.05	AM	TEAOH	2-Sol	200°C	24 hr	Ex. phases
MoAlPO5-5	0.05	AM	MDCHA	1-Sol	150°C	48 hr	AFI
Calcined							AFI
MoAlPO5-6	0.05	AM	TEAOH	1-Sol	180°C	24 hr	Ex. phases
MoAlPO5-7	0.05	AM	TEAOH	1-Sol	180°C	48 hr	Ex. phases
MoAlPO5-8	0.05	AM	TPA	1-Sol	180°C	24 hr	Ex. phases
MoAlPO5-9	0.05	AM	TEA	1-Sol	200°C	24 hr	Ex. phases
MoAlPO5-10	0.05	AM	TEA	1-Sol	200°C	72 hr	Ex. phases
MoAlPO5-11	0.05	AM	TEA	1-Sol	200°C	96 hr	Ex. phases
MoAlPO5-12	0.05	AM	TEA	1-Sol	200°C	168 hr	Ex. phases
MoAlPO5-13	0.05	AM	MDCHA	1-Sol	150°C	24 hr	AFI
Calcined							AFI
MoAlPO5-14	0.05	AM	MDCHA	1-Sol	150°C	96 hr	AFI
Calcined							AFI
MoAlPO5-15	0.05	AM	MDCHA	1-Sol	200°C	24 hr	Ex. phases
MoAlPO5-16	0.05	AM	MDCHA	1-Sol	200°C	48 hr	Ex. phases
MoAlPO5-17	0.05	AM	MDCHA	1-Sol	200°C	96 hr	Ex. phases

B. Phase characterization of ReAlPO-5

Introduction of Re into the AlPO-5 has also been attempted using isomorphous substitution by modifying the hydrothermal synthesis method of AlPO-5, similar to that of the MoAlPO5 study. In this study the precursor Re_2O_7 been tested in combination with various SDAs and varying reaction conditions. A summary of all the powder XRD results, including as-prepared and calcined samples, are shown in Table 4.7.

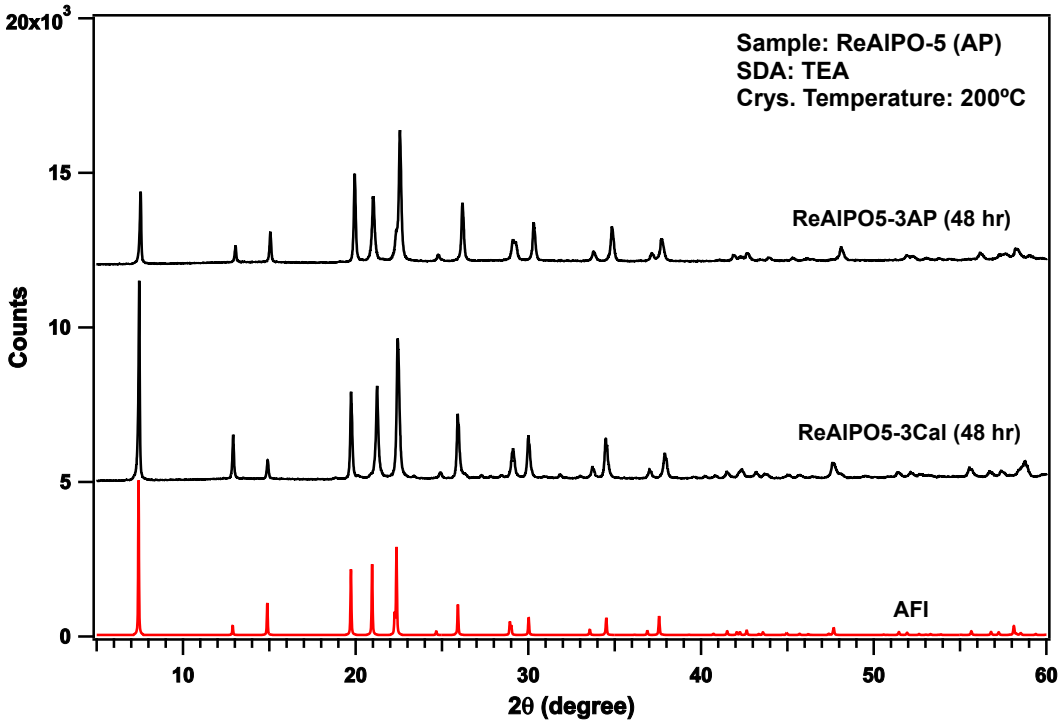

Figure 4.23 Powder XRD diffraction patterns of sample ReAlPO5-3. Both the as-prepared sample and the calcined sample have the AFI structure.

TEA was used as SDA in the first attempts using the 1-solution method with crystallization temperature at 200°C and varying crystallization time. The molar ratio was 0.05 Re : Al for all these samples unless otherwise specified. Sample ReAlPO5-5 was synthesized at 150°C for 96 hours and keeping the molar ratio the same. Sample ReAlPO5-6 was synthesized using the molar ratio Re : Al = 0.1 at 200°C for 96 hours. All of the sample synthesized using TEA as the SDA, including at various crystallization temperatures and times, yielded phase pure AFI with similar powder XRD patterns. Calcination was performed in selected samples, and did not appear to change the position of the diffraction patterns, although some of the relative intensities were altered. One example (ReAlPO5-3) of the patterns is shown in Figure 4.23, containing the diffraction patterns of both as-prepared and calcined samples.

The powder XRD patterns of other samples synthesized with the SDA TEA are shown in Appendix Figure A.12, Figure A.14, and Figure A.15.

Synthesis of ReAlPO-5 was also attempted with several other SDAs. Sample ReAlPO5-7 was synthesized using the SDA TEPA and sample ReAlPO5-8 was synthesized using the SDA TPA. Both of them were synthesized using the 2-solution method and crystallized at 200°C for 48 hours. The powder XRD diffraction patterns are shown in Appendix Figure A.16 and Figure A.17. In both the synthesis with TEPA and TPA, powder XRD patterns shown that the structure of the samples are not AFI. In the case of TEPA no matching result is found from the powder XRD database, the sample has relatively low crystallinity. In the case of TPA. the powder XRD patterns resembles the patterns produced by the dense phase aluminum phosphate rather than the molecular sieve AFI. Therefore it is obvious that TEPA and TPA alone are not suitable to use as SDA for the synthesis of ReAlPO-5 with the described parameters.

Table 4.7 Summary of powder XRD results of ReAlPO-5 samples.

Sample	Mo:Al	SDA	Sol method	Crys. Temp.	Time	Phase
ReAlPO5-1	0.05	TEA	1-sol	200°C	16 hr	AFI
ReAlPO5-2	0.05	TEA	1-sol	200°C	24 hr	AFI
ReAlPO5-3	0.05	TEA	1-sol	200°C	48 hr	AFI
Calcined						AFI
ReAlPO5-4	0.05	TEA	1-sol	200°C	96 hr	AFI
Calcined						AFI
ReAlPO5-5	0.05	TEA	1-sol	150°C	96 hr	AFI
ReAlPO5-6	0.10	TEA	1-sol	200°C	96 hr	AFI
ReAlPO5-7	0.05	TEPA	2-sol	200°C	48 hr	Extra phases
Calcined						Extra phases
ReAlPO5-8	0.05	TPA	2-sol	200°C	48 hr	Extra phases
Calcined						Extra phases

In summary, synthesis of ReAlPO-5 were attempted using different SDAs, different solution methods, and crystallization conditions. Only when TEA was used, the samples are phase pure AFI. This was not changed whether the crystallization temperature was 200°C or 150°C, at various crystallization times, or at various Re:Al molar ratio. All the synthesis with TEA produced phase pure samples. No other SDA was found to be able to direct the

AFI structure when the precursor ammonium perrhenate was added. Nevertheless, this is limited by the number of experiments attempted in this study; it is possible that other SDAs not in this study may also be able to direct the AFI structure with the presence of the rhenium precursor at certain reaction conditions (i.e. crystallization temperatures, crystallization times), or when a co-directing agent (such as HF) was added to assist the crystallization. Phase pure samples were analyzed using ICP-MS to determine the elemental composition of the samples, and the results are reported in the upcoming sections.

C. Phase characterization of GeAlPO-5

GeAlPO-5 samples were also analyzed using powder XRD to characterize the phase. A summary of results is shown in Table 4.8. The first attempt of the synthesis used the 2-solution method. This is because the Ge(IV) precursor is insoluble in aqueous solution and a solubility test confirmed that it is however soluble in 40% TEAOH (but not soluble in TEA). However this method produced a sample with relatively low crystallinity, as shown in the powder XRD patterns in Figure 4.25. The sample contains a small amount of reflections from AFI, but with significant amount of extra phases. Calcination of the sample reduced the intensity of reflections from extra phases and increase the intensity of AFI, but the AFI reflection is still weak and the sample is also not phase pure.

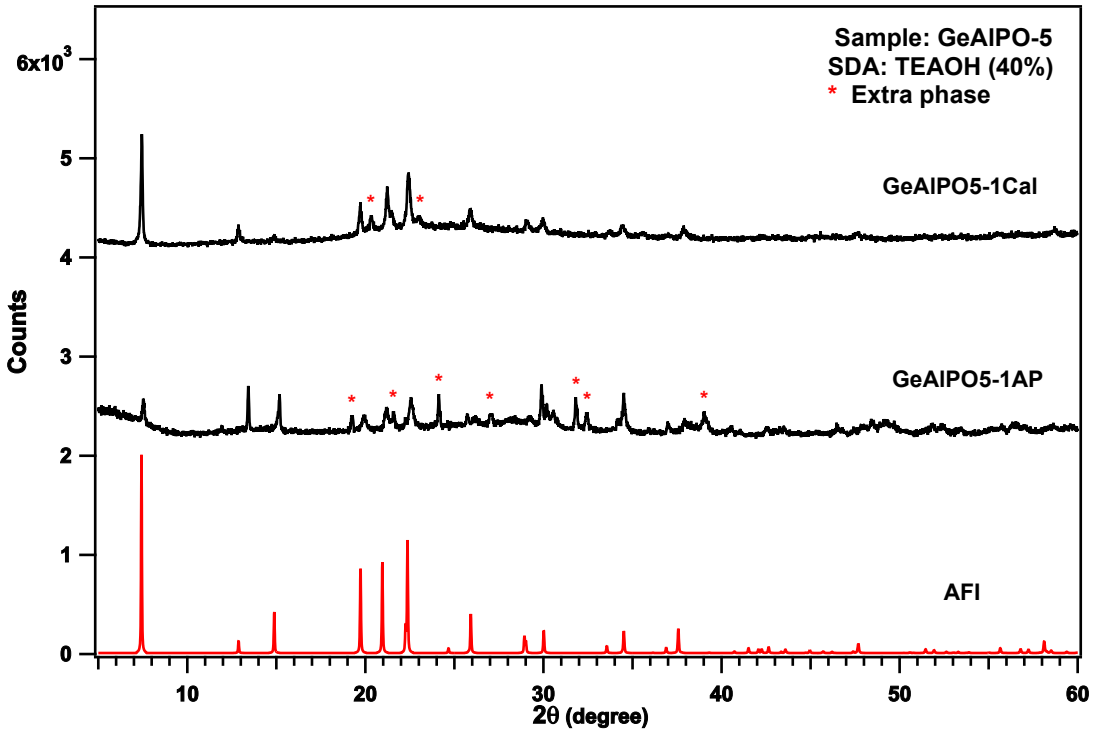

Figure 4.24 Powder XRD diffraction patterns of the as-prepared and calcined sample GeAlPO5-1. Major extra phases were labeled with red asterisks.

Sample GeAlPO5-2 to GeAlPO5-5 were synthesized using the modified 1-solution method, where HF was used to assist the dissolution of GeO_2, and TEA was used as the SDA. With the amount of HF used (Ge:HF = 1:1), GeO_2 cannot be completely dissolved. The mixture of HF and GeO_2 was however mixed with other components and proceeded for the synthesis as described in Chapter 3. The powder XRD patterns of the as-prepared and calcined samples are shown in Figure 4.25 and Figure 4.26, respectively. These patterns show that when HF was added into the reaction mixture and TEA was used as the SDA, the

synthesis produced highly crystalline phase pure AFI structure at both 180°C and 200°C. When the crystallization time is sufficiently long, as in the synthesis of sample GeAlPO5-4, an extra phase started to appear. Calcination of the phase pure samples shifted some of the relative intensities, but the reflections remain phase pure AFI. For sample GeAlPO5-4, after calcination the extra phase disappeared and the powder XRD patterns show that the calcined sample is phase pure AFI.

In summary, it has been shown that phase pure AFI samples have been obtained when the precursor GeO_2 was added into the reaction mixture before hydrothermal crystallization. This however, by itself does not mean GeAlPO-5 has been synthesized using this method. Analysis with ICP-MS is necessary to determine if the Ge content in the samples is significant.

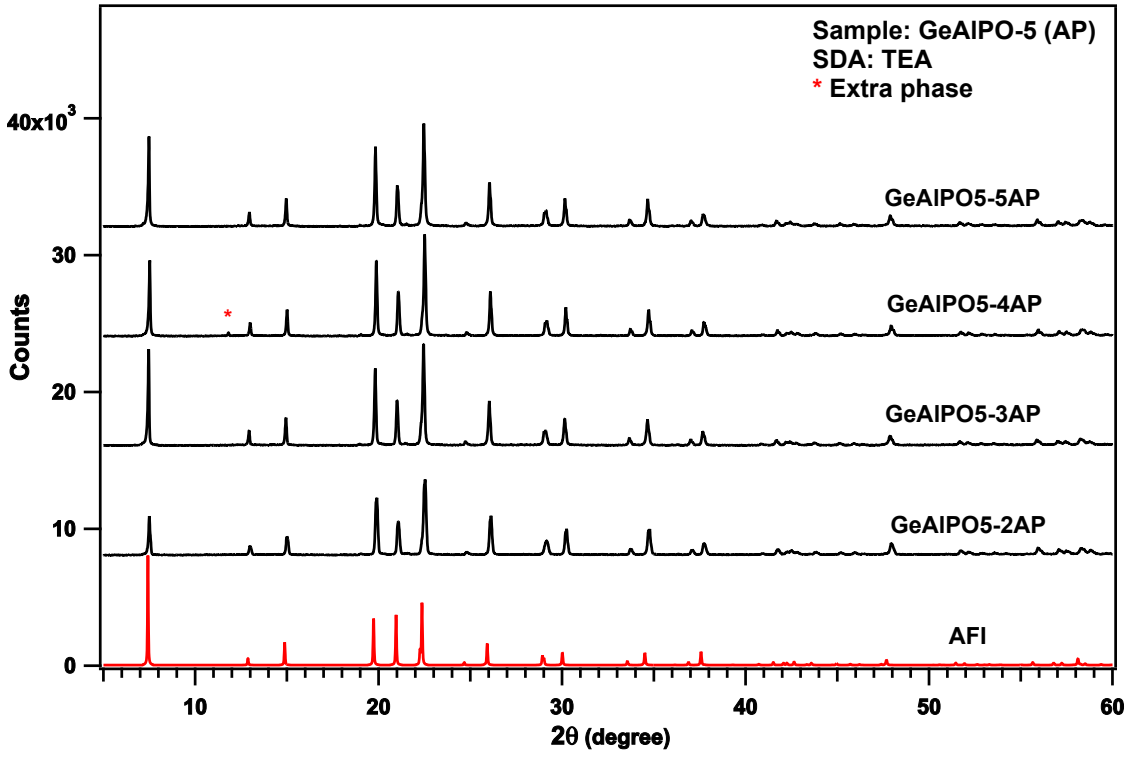

Figure 4.25 Powder XRD diffraction patterns of the as-prepared samples of GeAlPO5-2 to GeAlPO5-5. TEA was used as the SDA and HF was added into the reaction mixture. Extra phases were labeled with red asterisks.

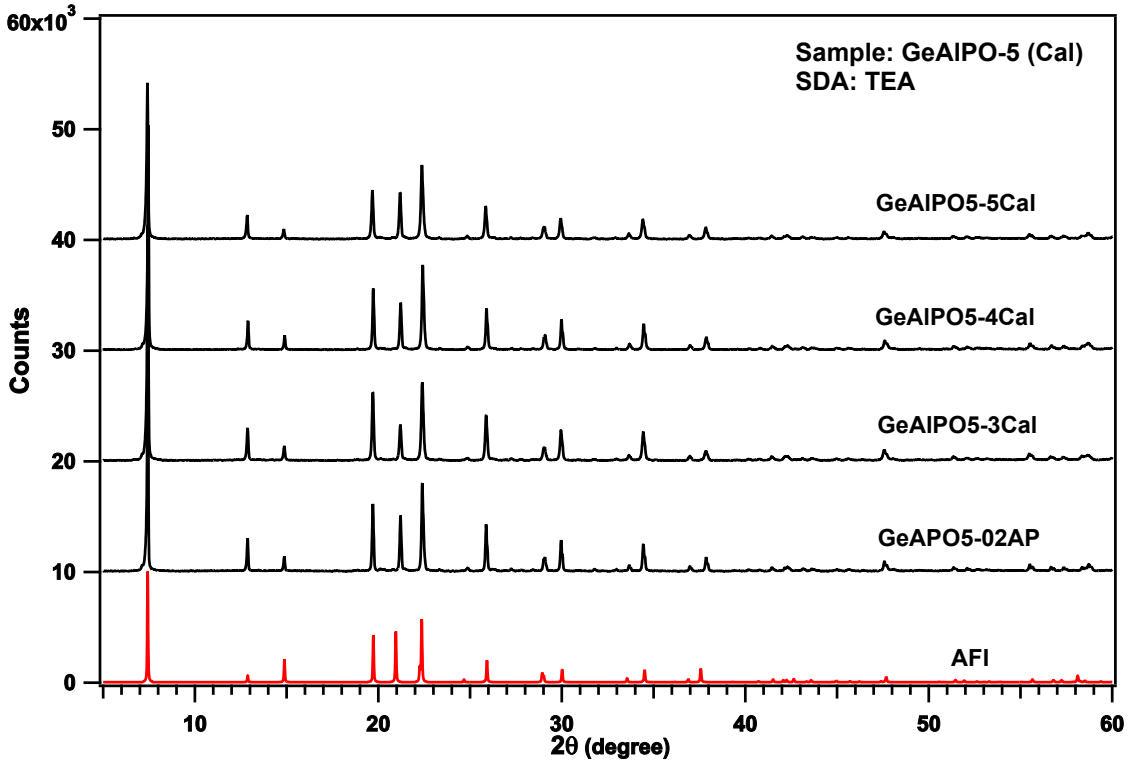

Figure 4.26 Powder XRD diffraction patterns of the calcined samples of GeAlPO5-2 to GeAlPO5-5.

Table 4.8 Summary of powder XRD results of GeAlPO-5 samples.

Sample	Ge:Al	Precursor	Sol method	Temp.	Crys. Time	Phase
GeAlPO5-1	0.10	GeO_2	2-sol	200°C	90 hr	Extra phases
Calcined						Exra phases
GeAlPO5-2	0.05	GeO_2	1-sol	200°C	90 hr	AFI
Calcined						AFI
GeAlPO5-3	0.05	GeO_2	1-sol(heat)	200°C	90 hr	AFI
Calcined						AFI
GeAlPO5-4	0.05	GeO_2	1-sol	200°C	180 hr	AFI
Calcined						AFI
GeAlPO5-5	0.05	GeO_2	1-sol	180°C	90 hr	AFI
Calcined						AFI

4.2.3 ICP-MS elemental composition analysis of MeAlPO-5

A. ICP-MS results of MoAlPO-5

Phase pure samples were analyzed using ICP-MS to determine the elemental composition of the MeAlPO-5 samples. Figure 4.27 illustrates the ICP-MS results of phase pure MoAlPO-5 samples in Mo wt.%. Clearly, the metal contents are low, and varying the crystallization time did not significantly change the uptake. A summary of the ICP-MS results of all analyzed samples is shown in Table 4.9.

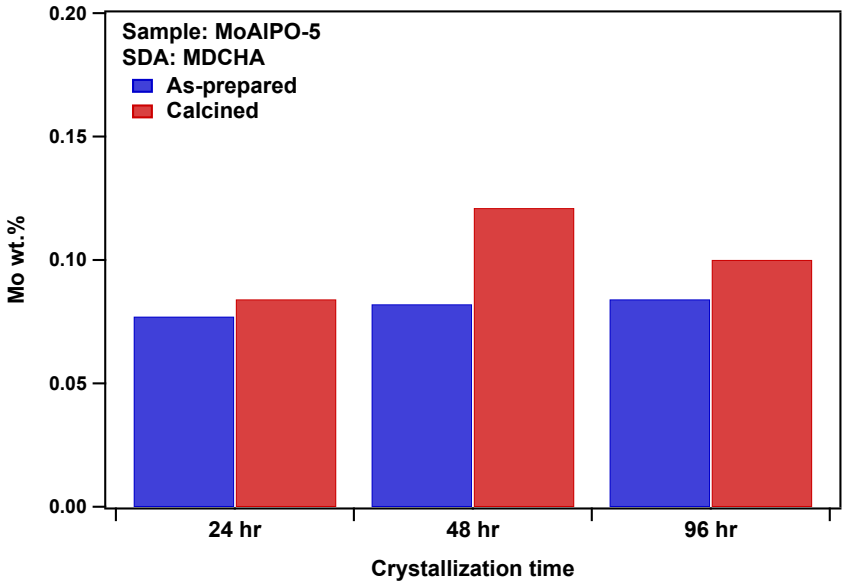

Figure 4.27 Illustration of Mo wt.% in phase pure MoAlPO-5 samples. All the samples were synthesized using the SDA MDCHA, crystallized at 150°C.

Table 4.9 ICP-MS results of MoAlPO-5. All samples were synthesized with the molar ratio 0.05Mo : Al and crystallized at 150°C

Sample	Crys. Time	Mo wt.%	Al wt.%	P wt.%
MoAlPO5-13	24 hr	0.077	19.0	17.8
Calcined		0.084	19.0	17.2
MoAlPO5-5	48 hr	0.082	18.7	16.7
Calcined		0.121	22.9	21.0
MoAlPO5-14	96 hr	0.084	18.5	18.0
Calcined		0.100	24.1	23.5

B. ICP-MS results of ReAlPO-5

All phase pure ReAlPO-5 samples were synthesized using the SDA TEA. As illustrated in Figure 4.28 and summarized in Table 4.10, all the samples contain only very low amount of rhenium. Varying the crystallization temperatures and times did not significantly affect the metal content. Increasing the molar ratio did increase the metal content, but remains too low.

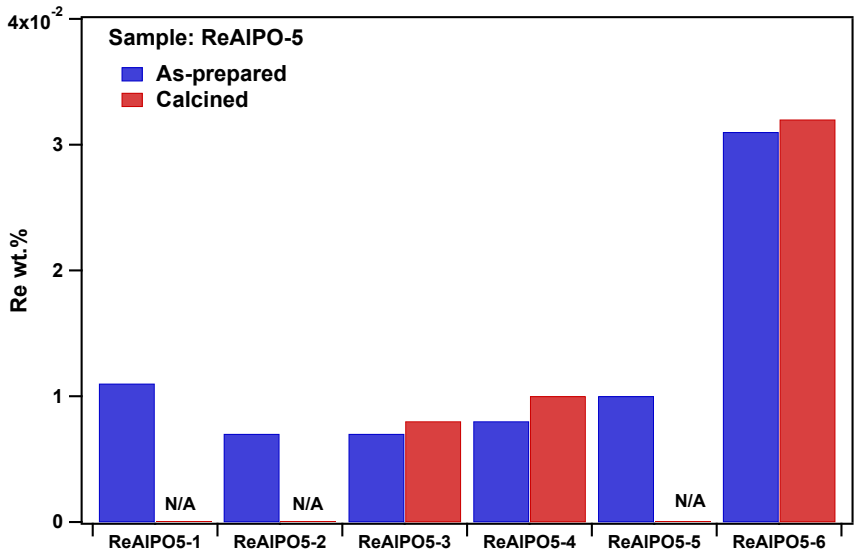

Figure 4.28 Illustration of Re wt.% in phase pure ReAlPO-5 samples.

Table 4.10 A summary of ICP-MS results of phase pure ReAlPO-5.

Sample	Re:Al	Crys. Temp.	Crys. Time	Re wt.%	Al wt.%	P wt.%
ReAlPO5-1AP	0.05	200°C	16 hr	0.011	22.7	27.6
ReAlPO5-2AP	0.05	200°C	24 hr	0.007	21.9	26.3
ReAlPO5-3AP	0.05	200°C	48 hr	0.007	19.7	24.3
Calcined				0.008	22.5	26.7
ReAlPO5-4AP	0.05	200°C	96 hr	0.008	20.4	25.0
Calcined				0.010	21.4	26.9
ReAlPO5-5AP	0.05	150°C	96 hr	0.010	25.6	29.8
ReAlPO5-6AP	0.10	200°C	96 hr	0.031	19.4	20.7
Calcined				0.032	20.7	21.8

C. ICP-MS results of GeAlPO-5

Phase pure GeAlPO-5 samples were synthesized using the TEA with HF in the reaction mixture. Figure 4.29 illustrates the results in Ge wt.%, and Table 4.11 summarized the data. GeAlPO5-1 was synthesized at 0.1 molar ratio, the uptake was good but the sample contains extra phases. Increasing the crystallization time seems to only slightly increase the uptake, but the uptake increased more clearly when heating the suspension to 90°C for 1 hour.

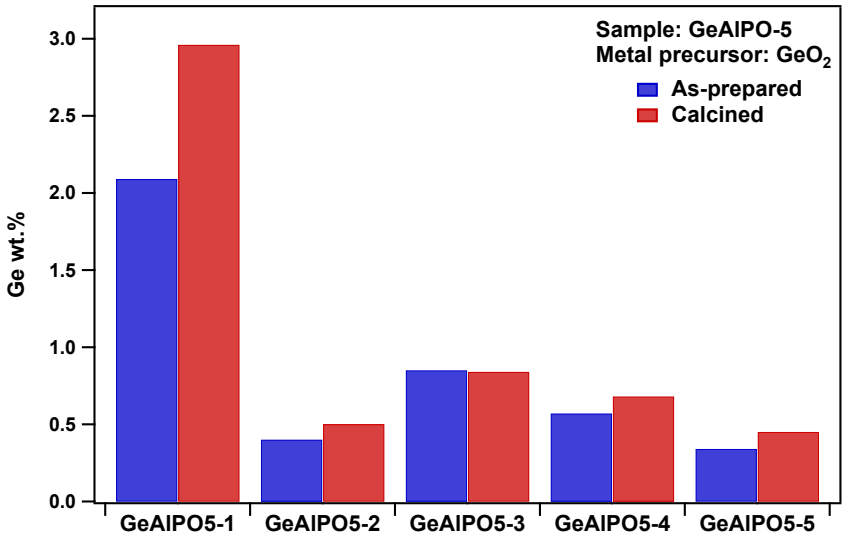

Figure 4.29 Illustration of Ge metal uptake in all GeAlPO-5 samples.

Table 4.11 ICP-MS results of all GeAlPO-5 samples.

Sample	Ge:Al	Crys. Temp.	Crys. Time	Ge wt.%	Al wt.%	P wt.%
GeAlPO5-1AP	0.10	200°C	90 hr	2.09	16.1	12.5
Calcined				2.96	22.8	17.9
GeAlPO5-2AP	0.05	200°C	90 hr	0.40	17.7	19.8
Calcined				0.50	22.0	23.5
GeAlPO5-3AP(H)	0.05	200°C	90 hr	0.85	22.9	24.7
Calcined				0.84	20.1	21.0
GeAlPO5-4AP	0.05	200°C	180 hr	0.57	17.4	18.2
Calcined				0.68	19.7	20.0
GeAlPO5-5AP	0.05	180°C	90 hr	0.34	13.7	14.7
Calcined				0.45	20.0	21.0

4.2.4 N_2 adsorption-desorption analysis of MeAlPO-5

Analysis of MoAlPO-5

The BET surface area and porosity analysis of MoAlPO-5 was performed on the calcined sample of MoAlPO5-14. The adsorption-desorption isotherms and BET surface area are shown in Figure 4.30.

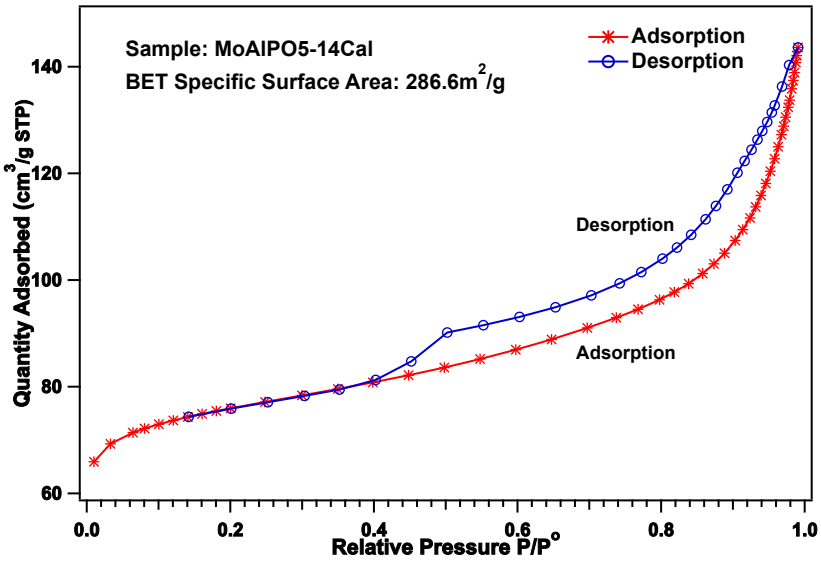

Figure 4.30 Adsorption-desorption isotherms of calcined sample MoAlPO5-14.

The N_2 adsorption-desorption isotherm shows a clear hysteresis loop, consistent with the Type H3 IUPAC classification[116]. The presence of the hysteresis loop is likely because of the inter-particle distances, since AlPO-5 is a microporous material. It also indicates that the sample is likely consist of aggregated plate-like particles with slit-shaped pores that are loosely coherent[116]. A summary of BET/BJH results is shown in Table 4.12

Table 4.12 BET/BJH analysis results of MoAlPO-5.

Sample	BET S.S.A.	Micropore area	Micropore volume	BJH pore width
MoAlPO-5	286.6 m^2/g	220.2 m^2/g	0.088 cm^3/g	86.7 Å

The BET specific surface area and micropore volume are consistent with the literature results of 277 m^2/g and 0.087 cm^3/g[127]. The average pore width is likely showing the interparticle distance, since the BJH theory cannot interpret pore size less than 1 nm[14][117]. In sum the N_2 adsorption-desorption analysis of the MoAlPO-5 sample is in good agreement with the literature analysis of AlPO-5.

Chapter 5

DISCUSSIONS

In this chapter the experimental results will be discussed with respect to how the experiments achieve the goals of this study: (1) to introduce Mo/Re into the porous supports; (2) to investigate if the introduction can be controlled for incorporation. The discussion will also focus on possible correlations between synthesis conditions and metal uptakes as well as surface properties. These results will also be compared with relevant literature value. The chapter will be divided into two sections, one to discuss the introduction into silica aerogels, and one to discuss the introduction into AlPO-5.

5.1 Introduction of Mo/Re into Silica Aerogels

The introduction of molybdenum into silica aerogels has been attempted in 6 samples. The ICP-MS results show that using the sol-gel route and ambient pressure drying method, molybdenum can be introduced into silica aerogels with low metal content. The powder XRD results show that all the as-prepared Mo-aerogels are amorphous, but it is difficult to conclude if molybdenum has been incorporated and further experiments are still needed to eliminate the possibility that molybdenum salts may be formed in small nanoparticles (< 2 nm), residing in the pores and escaped the detection of powder XRD[110]. However, the metal contents are all relatively low, compares to the similar literature studies on cobalt or copper[13][14]. The Mo-aerogel as-prepared samples in this study contain molybdenum ranging from 0.07 wt.% to 0.56 wt.% (sol Mo:Si molar ratio from 0.05 to 0.4), compares to the cobalt study in which the samples obtained have cobalt content ranging from 0.2 wt% to 11.09 wt.%, with sol Co:Si molar ratio varied from 0.0025 to 0.25[13]. Mo:Si sol molar ratio appeared to be a predominant factor for the metal uptake. As shown in Figure 5.1, when the molar ratio increased, the metal content generally increased. Beside the molar ratio, it appears that sol pH is also an influencing factor for the molybdenum uptake: as the sol

pH decreased, the metal uptake increased. This effect may be explained by the change of speciation of molybdate, which is known to form larger molybdate clusters at low pH[128], but the explanation requires a detail speciation study to provide supporting evidence.

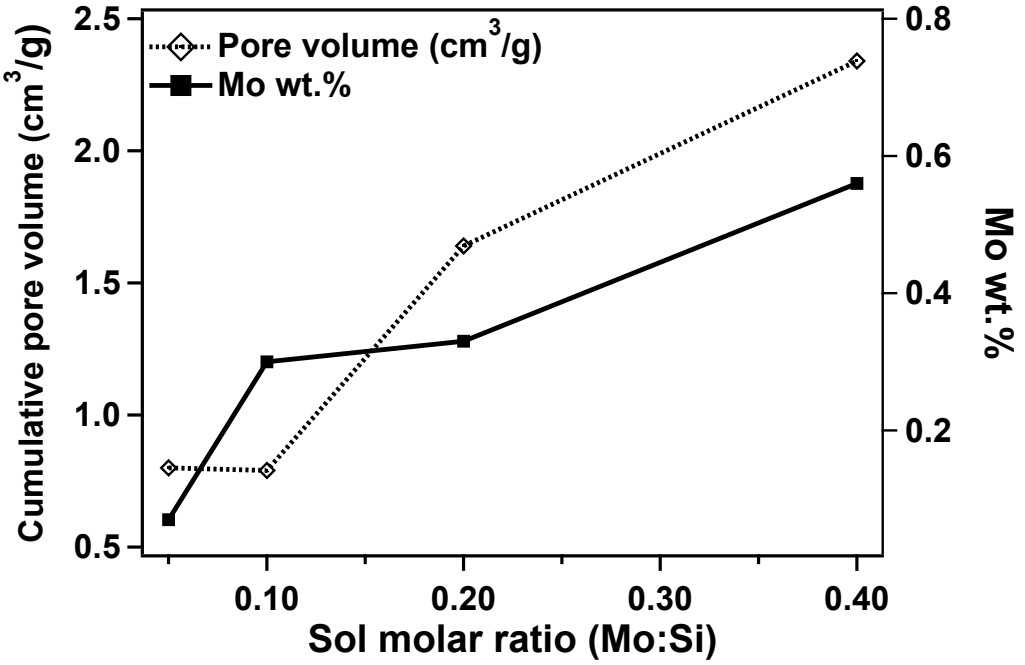

Figure 5.1 Influence of sol Mo:Si molar ratio to metal uptake and cumulative pore volume.

The BJH adsorption cumulative pore volume of the Mo-aerogel samples has shown an interesting trend. It appears that the cumulative pore volume is correlated with the sol molar ratio, as shown in Figure 5.1. The increase of pore volume with sol molar ratio is consistent with the prior work on Cu-aerogels[14]. In the copper study, it was proposed that copper cation can act as a secondary sol-gel base catalyst, although the detail mechanisms are unclear, due to the complexity of the sol-gel process[129]. From this study, similar process may also happen with the molybdate, acting as a secondary catalyst for the gelation. This may also further imply the possibility of incorporation as in the copper case[14], although more direct evidence is still needed.

Among 14 Re-aerogel syntheses, 13 aerogel samples were obtained. The ICP-MS results show that rhenium can be introduced into silica aerogels following the sol-gel route and APD method. Powder XRD results show that in all as-prepared samples, both crystalline phase and amorphous phase are present. This indicates rhenium has not been introduced in a controlled manner that can be used for incorporation, since the rhenium species exist in a separate phase, which is also further supported by the fact that after annealing or washing, the rhenium content has decreased significantly. At sol pH = 2, it appeared that using the

precursor Re_2O_7 generally has higher metal uptake than using NH_4ReO_4, as shown in Figure 5.2a. In both cases the uptake peaked at the sol molar ratio Re:Si = 0.2, and the metal content decreased at the higher molar ratio 0.4. This means that at sol pH = 2, increasing the sol molar ratio cannot introduce more rhenium into the aerogels.

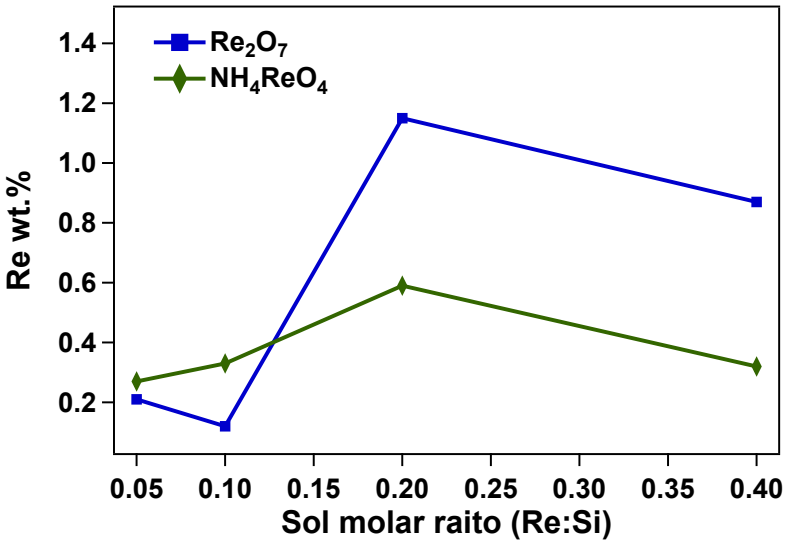

(a)

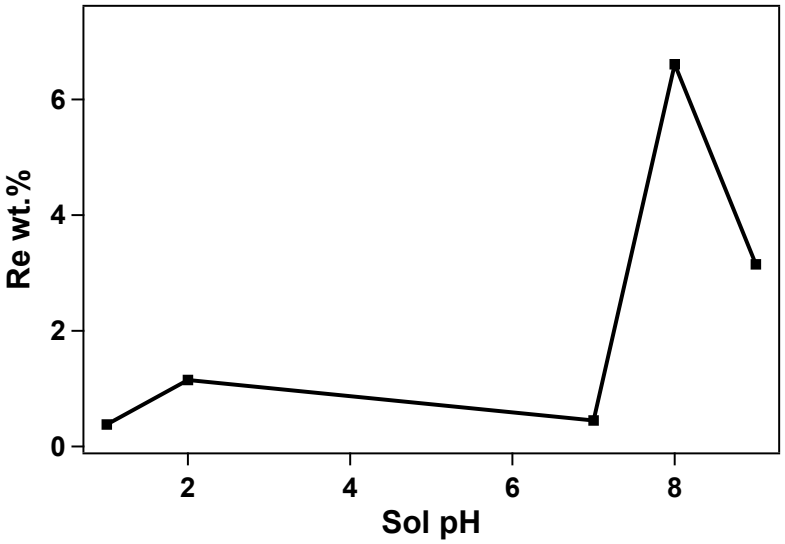

(b)

Figure 5.2 (a). Re uptake at various sol molar ratios. (b). Re uptake at various sol pH.

The dominating factor for the metal uptake of Re-aerogels appeared to be the sol pH: the uptake is generally low in acidic sols, then increased significantly at pH = 8, as plotted in Figure 5.2b. This behavior is also similar to the prior study of Cu-aerogels, in which the metal uptake peaked at sol pH = 6-7[14]. Apart from having the highest metal content, the

sample synthesized at sol pH = 8 also has the interesting behavior that the metal remained in the aerogel after annealing, while annealing resulted in significant weight loss in all other samples synthesized with the same method. Nevertheless, the sample size in this study is limited; the reproducibility of the samples needs to be further addressed. Furthermore, since the speciation of the Me-aerogels has not been studied in this work, the reasons of these behaviors are also unclear and required future works on the speciation of rhenium in the annealed samples.

The BET/BJH results of Re-aerogels show that the specific surface area did not change significantly at various molar ratios or using different precursors. The surface area of approximately 600 m^2/g is consistent with prior works with Cu-aerogels[14]. On the other hand, samples synthesized with both precursors show that as the metal content increases, the BJH pore width also increases. However, the results are also limited by the number of samples analyzed, and a clearer picture can be obtained when more samples are studied.

5.2 Introduction of Mo/Re into AlPO-5

The introduction of molybdenum into AlPO-5 by isomorphous substitution has been attempted with 17 samples. The analysis results show that molybdenum may have been introduced into AlPO-5, which is supported by two factors: (1) Phase pure calcined samples have been obtained. (2) Molybdenum is present in the phase pure samples. This study shows that the most important factors for the synthesis of MoAlPO-5 are two-fold: the choice of SDA, which has been shown that only MDCHA can lead to phase pure samples; the crystallization condition, which has been shown that phase pure samples can be obtained at 150°C but not at 200 °C.

Although the ICP-MS results show the presence of molybdenum in the phase pure samples, the metal content of approximately 0.1 wt.% is clearly not satisfactory. Changing the crystallization time between 24-96 hours did not show significant difference in the metal content. In comparison, a prior work to synthesize CuAlPO-5 with a similar Me:Al molar ratio (0.04) yielded samples with approximately 2 wt.% [33]. The challenge lies on that Mo(VI) exists in aqueous solution as an oxoanion, the molybdate, which appears to prefer staying in the aqueous phase. Furthermore, introduction of Mo(VI) may cause breakage or vacancies on the framework to allow Mo=O bonds, or otherwise positive charges will be introduced and destabilized the framework[88]. Future comprehensive works will be necessary to understand if it is possible to achieve MoAlPO-5 with higher metal uptake. The key for a potential synthesis with higher uptake would be to understand the speciation of

molybdenum in the hydrothermal suspension, as well as the nature of possible substitution sites. Understanding first the speciation of MoAlPO-5 synthesized in this work will be potentially beneficial to answer the questions: (1) Has molybdenum been incorporated into the framework. (2) If so, at what position and under what chemical environment. Obviously, the results of this work have brought up more questions than answers, and cannot provide enough evidence to point to either directions.

The introduction of rhenium into AlPO-5 was first attempted with 8 samples using the direct substitution method. The results of these experiments show that no method tested can introduce rhenium into AlPO-5. This is supported by the results that all phase pure samples contains only insignificant amount of rhenium (< 100 ppm, or 0.01 wt.%). The challenge for the introduction is similar to that of molybdenum: Re(VII) exists in aqueous solution as the oxoanion perrhenate, which has a clear preference to remain in the aqueous phase, possibly due to the difficulty of the perrhenate ion to bind with other ions in aqueous solution, because of its large size and low charge to surface area ratio[130]. Perrhenate also has a strong preference to bind with the ammine groups, which has been used for the extraction of perrhenate[130][131]. However, the attempts to first complex rhenium precursor with SDA in organic phase before crystallization did not produce phase pure sample. The alternative method to introduce rhenium through the intermediate product GeAlPO-5 has not be completed; the synthesis of GeAlPO-5 has produced phase pure samples with reasonable metal uptake, though it can still be further improved. This indirect introduction method may also be extended to the synthesis of MoAlPO-5 in the next step of the investigation.

Table 5.1 Summary of the introduction of Mo/Re into silica aerogels and AlPO-5 in this study.

Support	Metal	Method	Introduction	Control	Max. loading
Silica aerogels	Mo	Sol-gel/APD	Yes	Maybe	0.56 wt.%
Silica aerogels	Re	Sol-gel/APD	Yes	No	6.61 wt.%
AlPO-5	Mo	Isomor. subst.	Yes	Inconclusive	0.12 wt.%
AlPO-5	Re	Isomor. subst.	No	No	0.03 wt.%

A summary of the introduction of Mo/Re into silica aerogel and AlPO-5 conducted in this study is shown in Table 5.1. Clearly, there are still a lot of experiments needed for more conclusive results. In sum, the introduction of molybdenum or rhenium into silica aerogels has shown to be possible, but the control needs further investigations to confirm. Introduction of molybdenum into AlPO-5 is possible, but the metal uptake is very low. Introduction of

rhenium into AlPO-5 produced only negative results with the direct isomorphous substitution method.

Chapter 6

CONCLUSIONS

In this study the introduction of molybdenum and rhenium into silica aerogels and aluminophosphate AlPO-5 has been investigated following two main aspects: the possibility for introduction through methods developed in prior works, and the possibility to control the introduction for possible incorporation. Based on the parameter study results, the conclusions can be drawn as the following:

- Molybdenum can be introduced into silica aerogels following the sol-gel route and APD method. The as-prepared samples are amorphous, indicating the possibility of incorporation. The metal uptake was lower than expected. Mo:Si sol molar ratio and sol pH were found to be important factors for the metal content, which has shown increased uptake at higher molar ratio and at lower sol pH. BET specific surface area was relatively low compares to literature.

- Rhenium can also be introduced with the sol-gel/APD method. Relatively high metal content sample has been synthesized at sol pH = 8. Sol pH was found to be the predominating factor for the metal uptake. The presence of both crystalline and amorphous phases indicates the metal and the aerogel exist in separate structures, leading to the conclusion that the method is not likely suitable for incorporation. Among the tested samples, the BET/BJH results are consistent with literature values.

- The introduction of molybdenum into AlPO-5 by isomorphous substitution is possible, since phase pure samples containing molybdenum have been synthesized. However, the metal uptake is very low and the possibility of controlled introduction is inconclusive. The speciation of molybdenum inside the framework is also unclear at this point.

- Rhenium has not been able to introduce into AlPO-5 by isomorphous substitution directly. This may be explained by the strong stability of perrhenate ion and its inability to complex in aqueous solution as a weak ligand[126].

Although the introduction in this study have shown various degrees of success and many experiments have yet to be done, the investigation opened up a new door of possibilities and accumulated important results and for a number of potential future works, leading a step closer to achieving the higher goal to make better catalysts with molybdenum and rhenium containing porous materials.

Chapter 7

FUTURE STUDIES

Based on the results of this study, a number of future works can be done to have a better understanding of the samples and to develop potential novel routes for introduction of Mo/Re into silica aerogels and AlPO-5. The future works could focus on four potential aspects of interests:

- Acquire better understanding of speciation. Since this study has been focusing on exploring the possibility of introduction/controlled introduction, the speciation of metal ions in either silica aerogels or AlPO-5 is unknown. In particular, understanding the speciation and chemical environment of Mo-aerogels can determine if the metal has been incorporated, or can it be incorporated. The speciation is also crucial to determine if the sample can be used for ammonia decomposition. Similarly, in another material MoAlPO-5 the results of this study are inconclusive; understand the speciation of molybdenum in the samples can determine if the metal has been incorporated into the framework, and if so, how it affect the structure of the framework around it. These speciation determination may be conducted using XAS experiments.
- Complete the experiment to introduce rhenium into AlPO-5 using the indirect method through the intermediate product GeAlPO-5. This study has shown that the introduction of rhenium into AlPO-5 using the direct substitution method did not produce any desirable results. Based on a study on ITQ-33, it has been shown that germanium in a zeotype system might be exchanged by rhenium[99]. GeAlPO-5 has been synthesized in prior works as well as in this work; completing the next step to investigate the possible exchange of germanium with rhenium may be able to show a new way for the introduction of rhenium into AlPO-5.
- Test catalytic activity of the samples. A direct way to see if the samples are active toward ammonia decomposition is simply to test it. In particular, Re-aerogel should be

of high interests, since a sample with relatively high metal content has been obtained; Mo-aerogel sample may also be worth testing, although the metal content is relatively low.

- Develop new methods for metal introduction. For Mo-aerogels, the focus could be to increase the metal content, and for Re-aerogels, the focus could be to investigate other methods for possible controlled incorporation. Searching routes for the synthesis of MoAlPO-5 and ReAlPO-5 could also try using other SDA, methods, etc., that has not been attempted in this study.

References

[1] BP Statistical Review of World Energy. Technical report, June 2017.

[2] Andreas Borgschulte, Andreas Zttel, and Ursula Wittstadt. Hydrogen as a future energy carrier. Wiley-VCH Verlag GmbH & Co. KGaA, Weinheim, Germany, 2008.

[3] George A Olah, Alain Goeppert, and G K Surya Prakash. The Hydrogen Economy and its Limitations. In *Beyond Oil and Gas: The Methanol Economy*, pages 143–178. 2009.

[4] Ulrich Eberle, Bernd Mueller, and Rittmar von Helmolt. Fuel cell electric vehicles and hydrogen infrastructure: status 2012. *Energy & Environmental Science*, 5(10):8780–8798, October 2012.

[5] Satyen Baindur. Issues in Hydrogen Purity and Detection. *Ottawa Policy Research Associates, Inc.*, H2E-6-2005-6-1, 2005.

[6] Asbjørn Klerke, Claus Hviid Christensen, Jens K Nørskov, and Tejs Vegge. Ammonia for hydrogen storage: challenges and opportunities. *Journal of Materials Chemistry*, 18(20):2304–8, 2008.

[7] B Godfrey, R Dowling, M Forsyth, R Q Grafton, and I Wyld. The Role of Energy Storage in Austrilia's Future Energy Supply Mix. Technical report, November 2017.

[8] M E E Abashar. Ultra-clean hydrogen production by ammonia decomposition. *Journal of King Saud University - Engineering Sciences*, 30(1):2–11, January 2018.

[9] Steven Chiuta, Raymond C Everson, Hein W J P Neomagus, and Dmitri G Bessarabov. Hydrogen production from ammonia decomposition over a commercial Ru/Al2O3 catalyst in a microchannel reactor: Experimental validation and CFD simulation. *International Journal of Hydrogen Energy*, 41(6):3774–3785, February 2016.

[10] M Yu Kustova, S B Rasmussen, A L Kustov, and C H Christensen. Direct NO decomposition over conventional and mesoporous Cu-ZSM-5 and Cu-ZSM-11 catalysts: Improved performance with hierarchical zeolites. *Applied Catalysis B: Environmental*, 67(1):60–67, September 2006.

[11] Brian C Dunn, Paul Cole, Daniel Covington, Matthew C Webster, Ronald J Pugmire, Richard D Ernst, Edward M Eyring, Naresh Shah, and Gerald P Huffman. Silica aerogel supported catalysts for Fischer–Tropsch synthesis. *Applied Catalysis A: General*, 278(2):233–238, January 2005.

[12] Yuan Wang, Hamidreza Arandiyan, Jason Scott, Ali Bagheri, Hongxing Dai, and Rose Amal. Recent advances in ordered meso/macroporous metal oxides for heterogeneous catalysis: a review. *Journal of Materials Chemistry A*, 5(19):8825–8846, 2017.

[13] Sondre Håbrekke. Introduction of Cobalt Into Silica Aerogels, Metal Speciation and Reducibility. Master's thesis, Norwegian University of Science and Technology, Trondheim.

[14] Tina Kristiansen. *Aerogels; a new class of materials for catalytic purposes*. PhD thesis, July 2013.

[15] Karina Mathisen. *X-ray absorption spectroscopic studies on active metal sites in zeotypes during the selective catalytic reduction of NOx with propene in an oxygen rich atmosphere*. PhD thesis, Norwegian University of Science and Technology, Trondheim.

[16] T E Bell and L Torrente-Murciano. H2 Production via Ammonia Decomposition Using Non-Noble Metal Catalysts: A Review. *Topics in Catalysis*, 59(15-16):1438–1457, July 2016.

[17] Valeria Tagliazucca, Klaus Schlichte, Ferdi Schüth, and Claudia Weidenthaler. Molybdenum-based catalysts for the decomposition of ammonia: In situ X-ray diffraction studies, microstructure, and catalytic properties. *Journal of Catalysis*, 305:277–289, July 2013.

[18] J P McGeer and H S Taylor. Ammonia Decomposition and Related Phenomena on Rhenium Catalysts. *Journal of the American Chemical Society*, 73(6):2743–2751, 1951.

[19] A R Cholach, V A Sobyanin, and V V Gorodetskii. Decomposition of ammonia on rhenium I. Hydrogen adsorption on rhenium. *Reaction Kinetics and Catalysis Letters*, 18(3-4):371–375, 1981.

[20] A R Cholach, V A Sobyanin, and V V Gorodetskii. Decomposition of ammonia on rhenium II. Nitrogen adsorption on rhenium. *Reaction Kinetics and Catalysis Letters*, 18(3-4):381–385, 1981.

[21] A R Cholach, V A Sobyanin, and V V Gorodetskii. Decomposition of ammonia on rhenium III. Interaction of ammonia with rhenium. *Reaction Kinetics and Catalysis Letters*, 18(3-4):391–396, September 1981.

[22] S. S. Kistler. Coherent Expanded Aerogels. *Nature*, 127(3211):52–64, May 1931.

[23] Michel A Aegerter, Matthias M Koebel, and Nicholas Leventis. *Aerogels Handbook*. Springer New York, New York, NY, 2011.

[24] Sai S Prakash, C Jeffrey Brinker, Alan J Hurd, and Sudeep M Rao. Silica aerogel films prepared at ambient pressure by using surface derivatization to induce reversible drying shrinkage. *Nature*, 374(6521):439–443, March 1995.

[25] A. Corma and A. Martynez. Zeolites and Zeotypes as Catalysts. *Advanced Materials*, 7(2):137–144, February 1995.

[26] Tina Kristiansen, Karina Mathisen, Mari-Ann Einarsrud, Morten Bjørgen, and David G Nicholson. Single-Site Copper by Incorporation in Ambient Pressure Dried Silica Aerogel and Xerogel Systems: An X-ray Absorption Spectroscopy Study. *The Journal of Physical Chemistry C*, 115(39):19260–19268, October 2011.

[27] Gabriele Centi and Siglinda Perathoner. Nature of active species in copper-based catalysts and their chemistry of transformation of nitrogen oxides. *Applied Catalysis A: General*, 132(2):179–259, November 1995.

[28] M Wark, A Brückner, T Liese, and W Grünert. Selective Catalytic Reduction of NO by NH3over Vanadium-Containing Zeolites. *Journal of Catalysis*, 175(1):48–61, April 1998.

[29] F Meneau, G Sankar, N Morgante, S Cristol, C R A Catlow, J M Thomas, and G N Greaves. Characterization of zinc oxide nanoparticles encapsulated into zeolite-Y: An in-situ combined X-ray diffraction, XAFS, and SAXS study. *Nuclear Instruments and Methods in Physics Research Section B: Beam Interactions with Materials and Atoms*, 199:499–503, January 2003.

[30] C J G Van Der Grift, A Mulder, and J W Geus. Characterization of silica-supported copper catalysts by means of temperature-programmed reduction. *Applied Catalysis*, 60(1):181–192, January 1990.

[31] X S Zhao, Xiao Ying Bao, Wanping Guo, and Fang Yin Lee. Immobilizing catalysts on porous materials. *Biochemical Pharmacology*, 9(3):32–39, March 2006.

[32] J Kornatowski, M Sychev, G Finger, W H Baur, M Rozwadowski, and B Zibrowius. Cd, Cu, Zr, Mo and VMo Derivatives of Molecular Sieve AlPO4-5 and Their Preliminary Characterization. *Proceedings of Polish-German Zeolite Colloquium*, pages 20–26, 1992.

[33] K Mathisen, D G Nicholson, A N Fitch, and M Stockenhuber. Selective catalytic reduction of NOx over microporous CuAPO-5: structural characterisation by XAS and XRD. *Journal of Materials Chemistry*, 15(1):204–217, 2005.

[34] Tina Kristiansen. Growth Limitations of Copper Nanoparticles in Silica Aerogels: An In Situ XAS Study. Master's thesis, July 2009.

[35] Katrine Lie Boyesen and Karina Mathisen. Exposing the synergistic effect between copper and vanadium in A1P0-5 during the selective oxidation of propene. *Catalysis Today*, 229:14–22, 2014.

[36] Katrine Lie Boyesen. *Reactivity and Synergism of Vanadium in microporous Supports with Copper as a Co-cation*. PhD thesis, NTNU, Trondheim.

[37] Christianna Zenonos, Gopinathan Sankar, Furio Corà, Dewi W Lewis, Quentin A Pankhurst, C Richard A Catlow, and John Meurig Thomas. On the nature of iron species in iron substituted aluminophosphates. *Phys. Chem. Chem. Phys.*, 4(21):5421–5429, 2002.

[38] Martin Hartmann and Larry Kevan. Substitution of transition metal ions into aluminophosphates and silicoaluminophosphates: characterization and relation to catalysis. *Research on Chemical Intermediates*, 28(7-9):625–695, January 2002.

[39] Elliott P Barrett, Leslie G Joyner, and Paul P Halenda. The Determination of Pore Volume and Area Distributions in Porous Substances. I. Computations from Nitrogen Isotherms . *Journal of the American Chemical Society*, 73(1):373–380, 1951.

[40] Jeong-Gil Choi, Rane L Curl, and Levi T Thompson. Molybdenum Nitride Catalysts. *Journal of Catalysis*, 146:218–227, 1994.

[41] Michael E Wieser and Michael Berglund. Atomic Weights of the Elements 2007. De Gruyter, 2016.

[42] Carl Wilhelm Scheele. Försök med Blyerts, Molybdæna. *Kongliga Vetenskaps Akademiens Handlingar,*, 39:247–255, 1778.

[43] Peter Jacob Hjelm. Versuche mit Molybdäna, und Reduction der selben Erde. *Kongliga Vetenskaps Akademiens Handlingar,*, 49:268, 1788.

[44] Sharif Zaman and Kevin J Smith. A Review of Molybdenum Catalysts for Synthesis Gas Conversion to Alcohols: Catalysts, Mechanisms and Kinetics. *Catalysis Reviews-Science and Engineering*, 54(1):41–132, 2012.

[45] Gabriele Centi, Fabrizio Cavani, and Ferruccio Trifirò. *Selective Oxidation by Heterogeneous Catalysis*. Fundamental and Applied Catalysis. Springer US, Boston, MA, 2001.

[46] Teodóra Nagyné Kovács, Dávid Hunyadi, Alex Leandro Andrade Lucena, and Imre Miklós Szilágyi. Thermal decomposition of ammonium molybdates. *Journal of Thermal Analysis and Calorimetry*, 124(2):1013–1021, December 2015.

[47] John Rumble. *CRC Handbook of Chemistry and Physics, 98th Edition*. CRC Press, June 2017.

[48] Walter Noddack, Ida Tacke, and Otto Berg. Die Ekamangane. *Die Naturwissenschaften*, 13(26):567–574, June 1925.

[49] David A John. Rhenium: a rare metal critical in modern transportation. Technical report, 2015.

[50] William H Davenport, Valerie Kollonitsch, and Charles H Klein. Adcances In Rhenium Catalysts. *Industrial & Engineering Chemistry*, 60(11):10–19, November 1968.

[51] Karina Mathisen, Karsten Granlund Kirste, Justin S J Hargreaves, Said Laassiri, Kate McAulay, Andrew R McFarlane, and Nicholas A Spencer. An In Situ XAS Study of the Cobalt Rhenium Catalyst for Ammonia Synthesis. *Topics in Catalysis*, 61(3-4):225–239, April 2018.

[52] Bao-Lian Su, Clément Sanchez, and Xiao-Yu Yang. Insights into Hierarchically Structured Porous Materials: From Nanoscience to Catalysis, Separation, Optics, Energy, and Life Science, 2011.

[53] Ulrich Schubert and Nicola Husing. *Synthesis of Inorganic Materials*. Third, Completely Revised and Updated Edition. Wiley-VCH, 3rd edition.

[54] Sigmund M Csicsery. Shape-selective catalysis in zeolites. *Zeolites*, 4(3):202–213, July 1984.

[55] Yoshihiro Sugi and Ajayan Vinu. Shape-Selective Catalysis in the Alkylation of Naphthalene: Steric Interaction with the Nanospace of Zeolites. *Journal of nanoscience and nanotechnology*, 15(12):9369–9381, December 2015.

[56] S G Jennings. The Mean Free Path In Air. *J. Aerosol Sci.*, 19(2):159–166, 1988.

[57] J Rouquerol, D Avnir, C W Fairbridge, D H Everett, J H Haynes, N Pernicone, J D F Ramsay, K S W Sing, and K K Unger. Recommendations for the Characterization of Porous Solids. *Pure and Applied Chemistry*, 66(8):1739–1758, August 1994.

[58] J M Bennett, J P Cohen, E M Flanigen, J J Pluth, and J V Smith. Crystal-Structure of Tetrapropylammonium Hydroxide-Aluminum Phosphate Number-5. *Acs Symposium Series*, 218:109–118, 1983.

[59] M Schmidt and F Schwertfeger. Applications for silica aerogel products. *Journal of Non-Crystalline Solids*, 225:364–368, April 1998.

[60] Soleimani Dorcheh, A and Abbasi, M H. Silica aerogel; synthesis, properties and characterization. *Journal of materials processing technology*, 199(1-3):10–26, April 2008.

[61] Michele L Anderson, Catherine A Morris, Rhonda M Stroud, Celia I Merzbacher, and Debra R Rolison. Colloidal Gold Aerogels: Preparation, Properties, and Characterization. *Langmuir*, 15(3):674–681, 1999.

[62] Tomasz Błaszczyński, Agnieszka Ślosarczyk, and Maciej Morawski. Synthesis of Silica Aerogel by Supercritical Drying Method. *Procedia Engineering*, 57:200–206, 2013.

[63] Mark McHugh and Val Krukonis. *Supercritical Fluid Extraction*. Principles and Practice. Elsevier, October 2013.

[64] F Schwertfeger, D Frank, and M Schmidt. Hydrophobic waterglass based aerogels without solvent exchange or supercritical drying. *Journal of Non-Crystalline Solids*, 225:24–29, April 1998.

[65] Sharad D Bhagat, Yong-Ha Kim, Myung-Jun Moon, Young-Soo Ahn, and Jeong-Gu Yeo. A cost-effective and fast synthesis of nanoporous SiO2 aerogel powders using water-glass via ambient pressure drying route. *Solid State Sciences*, 9(7):628–635, July 2007.

[66] Jyoti L Gurav, In-Keun Jung, Hyung-Ho Park, Eul Son Kang, and Digambar Y Nadargi. Silica aerogel: synthesis and applications. *Journal of Nanomaterials*, 2010(24):23–11, January 2010.

[67] A Parvathy Rao, A Venkateswara Rao, and G M Pajonk. Hydrophobic and physical properties of the ambient pressure dried silica aerogels with sodium silicate precursor using various surface modification agents. *Applied Surface Science*, 253(14):6032–6040, May 2007.

[68] S S Prakash, C J Brinker, and A J HURD. Silica Aerogel Films at Ambient-Pressure. *Journal of Non-Crystalline Solids*, 190(3):264–275, October 1995.

[69] Fei Shi, Lijiu Wang, and Jingxiao Liu. Synthesis and characterization of silica aerogels by a novel fast ambient pressure drying process. *Materials Letters*, 60(29-30):3718–3722, December 2006.

[70] Sharad D Bhagat, Yong-Ha Kim, Young-Soo Ahn, and Jeong-Gu Yeo. Rapid synthesis of water-glass based aerogels by in situ surface modification of the hydrogels. *Applied Surface Science*, 253(6):3231–3236, 2007.

[71] C J Lee, G S Kim, and S H Hyun. Synthesis of silica aerogels from waterglass via new modified ambient drying. *Journal of Materials Science*, 37(11):2237–2241, 2002.

[72] Sharad D Bhagat, Yong-Ha Kim, Kuen-Hack Suh, Young-Soo Ahn, Jeong-Gu Yeo, and Jong-Hun Han. Superhydrophobic silica aerogel powders with simultaneous surface modification, solvent exchange and sodium ion removal from hydrogels. *Microporous and Mesoporous Materials*, 112(1-3):504–509, July 2008.

[73] Mark E Tess and James A Cox. Chemical and biochemical sensors based on advances in materials chemistry. *Journal of Pharmaceutical and Biomedical Analysis*, 19(1-2):55–68, February 1999.

[74] George Odian. *Principles of Polymerization*. John Wiley & Sons, Inc., Hoboken, NJ, USA, fourth edition, 2004.

[75] Manas Chanda. *Introduction to polymer science and chemistry: a problem-solving approach*. Boca Raton: CRC Press, Taylor & Francis Group, second edition, 2013.

[76] C J Brinker, K D Keefer, D W Schaefer, R A Assink, B D Kay, and C S Ashley. Sol-gel transition in simple silicates II. *Journal of Non-Crystalline Solids*, 63(1-2):45–59, February 1984.

[77] Zhenlü Wang, Qingsheng Liu, Jianfeng Yu, Tonghao Wu, and Guojia Wang. Surface structure and catalytic behavior of silica-supported copper catalysts prepared by impregnation and sol–gel methods. *Applied Catalysis A: General*, 239(1-2):87–94, January 2003.

[78] Jaya L Mohanan and Stephanie L Brock. Influence of Synthetic and Processing Parameters on the Surface Area, Speciation, and Particle Formation in Copper Oxide/Silica Aerogel Composites. *Chemistry of Materials*, 15(13):2567–2576, July 2003.

[79] R H Busey and O L Keller Jr. Structure of the Aqueous Pertechnetate Ion by Raman and Infrared Spectroscopy. Raman and Infrared Spectra of Crystalline KTcO 4, KReO 4, Na 2MoO 4, Na 2WO 4, Na 2MoO 4·2H 2O, and Na 2WO 4·2H 2O. *The Journal of Chemical Physics*, 41(1):215–225, July 1964.

[80] A Venkateswara Rao, E Nilsen, and M A Einarsrud. Effect of precursors, methylation agents and solvents on the physicochemical properties of silica aerogels prepared by atmospheric pressure drying method. *Journal of Non-Crystalline Solids*, 296(3):165–171, December 2001.

[81] Huijuan Liu, Wei Sha, Adrienne T Cooper, and Maohong Fan. Preparation and characterization of a novel silica aerogel as adsorbent for toxic organic compounds. *Colloids and Surfaces A: Physicochemical and Engineering Aspects*, 347(1-3):38–44, September 2009.

[82] Ae-Young Jeong, Sang-Man Koo, and Dong-Pyo Kim. Characterization of Hydrophobic SiO2 Powders Prepared by Surface Modification on Wet Gel . *Journal of Sol-Gel Science and Technology*, 19:483–487, November 2000.

[83] Sin-Kyu Kang and Se-Young Choi. Synthesis of Silica Aerogel at Ambient Pressure and Characterization (I). *Journal of the Korean Ceramic Society*, 33(12):1394–1402, 1996.

[84] Stephen T Wilson, Brent M Lok, Celeste A Messina, Thomas R Cannan, and Edith M Flanigen. Aluminophosphate molecular sieves: a new class of microporous crystalline inorganic solids. *Journal of the American Chemical Society*, 104(4):1146–1147, February 1982.

[85] C Baerlocher and L McCusker. Database of zeolite structures, 2001.

[86] Kuei-Jung Chao, Shie-Ping Sheu, and Hwo-Shuenn Sheu. Structure and chemistry of cobalt in CoAPO-5 molecular sieve. *Journal of the Chemical Society, Faraday Transactions*, 88(19):2949–2954, 1992.

[87] Ursula Lohse, Rainer Bertram, Karin Jancke, Iiona Kurzawski, Barbara Parlitz, Elke Löuffler, and Ellen Schreier. Acidity of aluminophosphate structures. Part 2.—Incorporation of cobalt into CHA and AFI by microwave synthesis. *Journal of the Chemical Society, Faraday Transactions*, 91(7):1163–1172, 1995.

[88] Laszlo Nemeth and Simon R Bare. Science and Technology of Framework Metal-Containing Zeotype Catalysts. pages 1–97. Elsevier, 2014.

[89] P R Hari Prasad Rao, Rajiv Kumar, A V Ramaswamy, and P Ratnasamy. Synthesis and characterization of a crystalline vanadium silicate with MEL structure. *Zeolites*, 13(8):663–670, 1993.

[90] G Centi, S Perathoner, F Trifiro, A Aboukais, C F Aissi, and M Guelton. Physicochemical characterization of V-silicalite. *The Journal of Physical Chemistry*, 96(6):2617–2629, March 1992.

[91] T Sen, V Ramaswamy, S Ganapathy, P R Rajamohanan, and S Sivasanker. Incorporation of Vanadium in Zeolite Lattices: Studies of the MEL (ZSM-11) System. *The Journal of Physical Chemistry*, 100(9):3809–3817, January 1996.

[92] M Huang, J Yao, S Xu, and Ch Meng. E.p.r. evidence of the unusual coordinational environment for Mo5+ in SAPO-5 molecular sieves. *Zeolites*, 12(7):810–814, September 1992.

[93] Chul Wee Lee, Thierry Saint-Pierre, Naoto Azuma, and Larry Kevan. Electron spin resonance and electron spin echo modulation studies of oxomolybdenum species in thermally reduced molybdenum-doped H-SAPO-5 and MoH-SAPO-11 silicoaluminophosphate molecular sieves: comparison of adsorbate coordination with copper-doped H-SAPO-5 and CuH-SAPO-11. *The Journal of Physical Chemistry*, 97(45):11811–11814, November 1993.

[94] J J Cruywagen. Protonation, Oligomerization, and Condensation Reactions of Vanadate(V), Molybdate(vi), and Tungstate(vi). pages 127–182. Elsevier, 1999.

[95] Stacey Borg, Weihua Liu, Barbara Etschmann, Yuan Tian, and Joel Brugger. An XAS study of molybdenum speciation in hydrothermal chloride solutions from 25-385 degrees C and 600 bar. *Geochimica Et Cosmochimica Acta*, 92:292–307, 2012.

[96] Howard H Claassen and A J Zielen. Structure of the perrhenate ion. *The Journal of Chemical Physics*, 22(4):707–709, January 1954.

[97] J Beintema. Die Kristallstruktur der Alkaliperrhenate und -perjodate. *Zeitschrift für Kristallographie - Crystalline Materials*, 97(1-6), 1937.

[98] John G Darab and and Peter A Smith. Chemistry of Technetium and Rhenium Species during Low-Level Radioactive Waste Vitrification. 8(5):1004–1021, May 1996.

[99] Øyvind Knapperholen. Incorporation of Rhenium in ITQ-33. Master's thesis, Norwegian University of Science and Technology, Norwegian University of Science and Technology, May 2016.

[100] C J Bertole, C A Mims, and G Kiss. Support and rhenium effects on the intrinsic site activity and methane selectivity of cobalt Fischer-Tropsch catalysts. *Journal of Catalysis*, 221(1):191–203, 2004.

[101] M A Ryashentseva, V P Rozhdestvenskii, Polyanskii, AB, and S Y Molina. Conversion of Hydrocarbons with Steam in the Presence of Alumino-Rhenium Catalysts. *Petroleum Chemistry*, 21(1):1–7, 1981.

[102] Edith M Flanigen, Brent M T Lok, Robert L Patton, Stephen T Wilson, and UOP LLC. Germanium-aluminum-phosphorus-oxide molecular sieve compositions. (841753):1–23, December 1989.

[103] M Tielen, M Geelen, and P A Jacobs. ChemInform Abstract: Isomorphic: Substitution in Zeolites: Its Potential Catalytic Implications. *Chemischer Informationsdienst*, 17(15):1–no, May 2016.

[104] E. M. Flsnigrn, B. M. Lok, R. L. Patton, and S. T. Wildon. Aluminophosphate Molecular-Sieves and the Periodic-Table. *Pure and Applied Chemistry*, 58(10):1351–1358, October 1986.

[105] Otto H Johnson. Germanium and its Inorganic Compounds. *Chemical Reviews*, 51(3):431–469, December 1952.

[106] Laurence Burel, Nataliia Kasian, and Alain Tuel. Quasi All-Silica Zeolite Obtained by Isomorphous Degermanation of an As-Made Germanium-Containing Precursor. *Angewandte Chemie*, 126(5):1384–1387, December 2013.

[107] Jens Als-Nielsen and Des McMorrow. *Elements of Modern X-ray Physics*. John Wiley & Sons, April 2011.

[108] Werner Massa. *Crystal Structure Determination*. Springer Berlin Heidelberg, Berlin, Heidelberg, 2nd ed. edition, 2000.

[109] David L Bish and Jeffrey Edward Post. *Modern powder diffraction*. Mineralogical Society of Amer, 1989.

[110] B S Clausen, H Topsoe, and R Frahm. Application of combined X-ray diffraction and absorption techniques for in situ catalyst characterization. *Advances in Catalysis, Vol 42*, 42(C):315–344, 1998.

[111] H R Pouretedal and M Kazemi. Characterization of modified silica aerogel using sodium silicate precursor and its application as adsorbent of Cu2+, Cd2+, and Pb2+ ions. *International Journal of Industrial Chemistry*, 3(1):20–8, 2012.

[112] S Brunauer, P H Emmett, and E Teller. Adsorption of gases in multimolecular layers. *Journal of the American Chemical Society*, 1938.

[113] I Chokendoff and J W Nimantsverdrief. Concepts of modern catalysis and kinetics 2nd, Revised and Enlarged Edition, 2007.

[114] R Pierotti and J Rouquerol. Reporting physisorption data for gas/solid systems with special reference to the determination of surface area and porosity. *Pure Appl Chem*, 1985.

[115] G Fagerlund. Determination of specific surface by the BET method. *Mat?riaux et Constructions*, 6(3):239–245, May 1973.

[116] K S W Sing. Reporting physisorption data for gas/solid systems with special reference to the determination of surface area and porosity (Recommendations 1984). *Pure and Applied Chemistry*, 57(4):603–619, 1985.

[117] Johan C Groen, Louk A A Peffer, and Javier Pérez-Ramırez. Pore size determination in modified micro- and mesoporous materials. Pitfalls and limitations in gas adsorption data analysis. *Microporous and Mesoporous Materials*, 60(1-3):1–17, 2003.

[118] Trygve Dagsloth Jakobsen. SAPO-34 with Copper: Investigation of hierarchical pore characteristics and interactions with copper for catalytic applications. Master's thesis, Norwegian University of Science and Technology, 2014.

[119] Adrian A Ammann. Inductively coupled plasma mass spectrometry (ICP MS): a versatile tool. *Journal of Mass Spectrometry*, 42(4):419–427, April 2007.

[120] Wolfgang Paul and Helmut Steinwedel. Notizen: Ein neues Massenspektrometer ohne Magnetfeld. *Zeitschrift für Naturforschung A*, 8(7), 1953.

[121] Wolfgang Paul. Electromagnetic Traps for Charged and Neutral Particles(Nobel Lecture). *Angewandte Chemie International Edition in English*, 29(7):739–748, July 1990.

[122] S D Bhagat, Y H Kim, M J Moon, Y S Ahn, and J G Yeo. A cost-effective and fast synthesis of nanoporous SiO 2 aerogel powders using water-glass via ambient pressure drying route. *Solid State Sciences*, 2007.

[123] S D Bhagat, Y H Kim, Y S Ahn, and J G Yeo. Rapid synthesis of water-glass based aerogels by in situ surface modification of the hydrogels. *Applied Surface Science*, 2007.

[124] A Venkateswara Rao, G M Pajonk, S D Bhagat, and Philippe Barboux. Comparative studies on the surface chemical modification of silica aerogels based on various organosilane compounds of the type RnSiX4−n. *Journal of Non-Crystalline Solids*, 350:216–223, 2004.

[125] Sharad D Bhagat, Yong-Ha Kim, Young-Soo Ahn, and Jeong-Gu Yeo. Textural properties of ambient pressure dried water-glass based silica aerogel beads: One day synthesis. *Microporous and Mesoporous Materials*, 96(1-3):237–244, November 2006.

[126] George Rouschias. Recent advances in the chemistry of rhenium. *Chemical Reviews*, 74(5):531–566, October 1974.

[127] M Bandyopadhyay, R Bandyopadhyay, Y Kubota, and Y Sugi. Synthesis of AlPO4-5 and AlPO4-11 molecular sieves by dry-gel conversion method. *Chemistry Letters*, 29(9):1024–1025, 2000.

[128] Jan M Coddington and Michael J Taylor. Molybdenum-95 nuclear magnetic resonance and vibrational spectroscopic studies of molybdenum(VI) species in aqueous solutions and solvent extracts from hydrochloric and hydrobromic acid: evidence for the complexes [Mo2O5(H2O)6]2+, [MoO2X2(H2O)2](X = Cl or Br), and [MoO2Cl4]2? *Journal of the Chemical Society, Dalton Transactions*, 0(1):41–47, 1990.

[129] Elizabeth I Mayo, Duke D Pooré, and A E Stiegman. Catalysis of the Silica Sol−Gel Process by Divalent Transition Metal Bis(acetylacetonate) Complexes. *Inorganic Chemistry*, 39(5):899–905, March 2000.

[130] Evgeny A Katayev, Grigory V Kolesnikov, and Jonathan L Sessler. Molecular recognition of pertechnetate and perrhenate. *Chemical Society Reviews*, 38(6):1572–16, 2009.

[131] Holger Stephan, Karsten Gloe, Werner Kraus, Hartmut Spies, Bernd Johannsen, Kathrin Wichmann, GUnter Reck, DillipK Chand, Parimal K Bharadwa, Ute Müller, WalterM Müller, and Fritz Vögtle. Binding and Extraction of Pertechnetate and Perrhenate by Azacages, 2004.

Appendix A

Powder XRD Diffraction Patterns

A.1 Me-aerogels

A.1.1 Powder XRD patterns of Re-aerogels

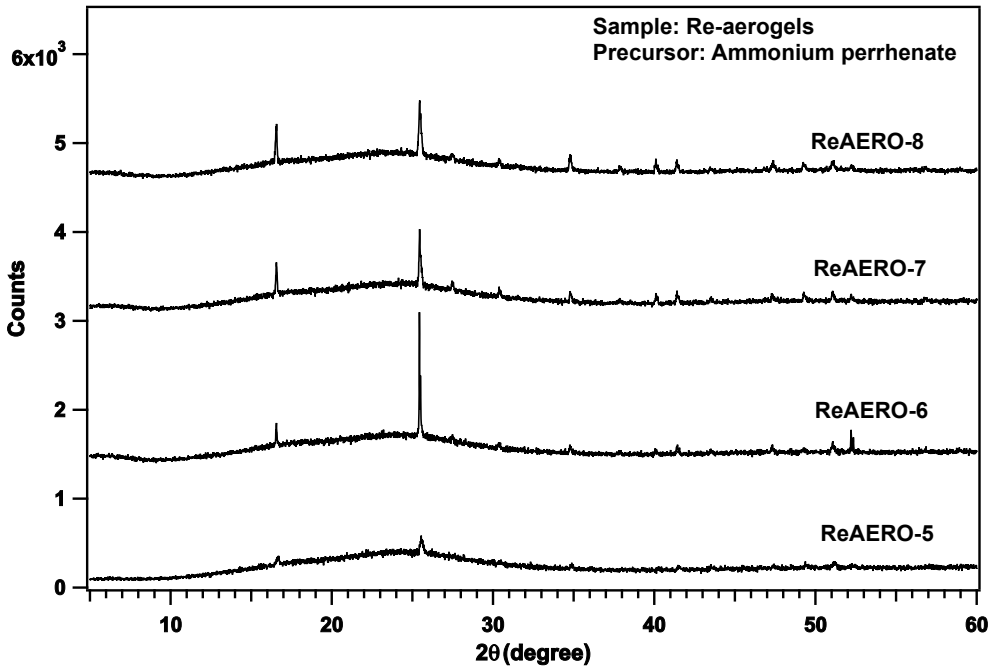

Figure A.1 Powder XRD diffractogram of samples with ammonium perrhenate as the precursor at varying molar ratios. The presence of Braggs' peaks indicating the crystalline phases in the samples.

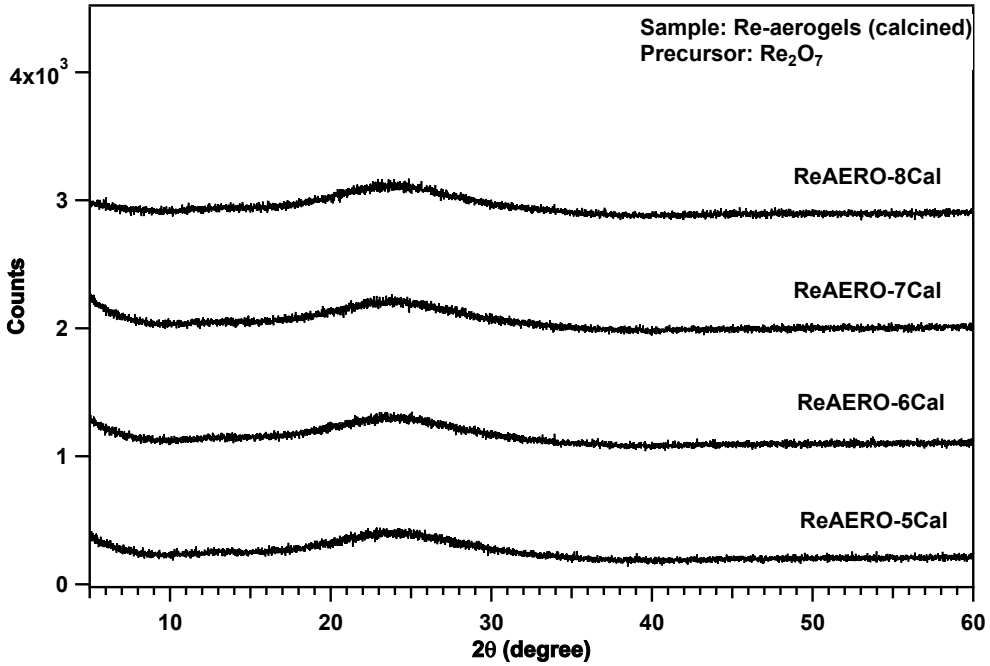

Figure A.2 Powder XRD patterns of the annealed Re-aerogel samples using ammonium perrhenate as the metal precursor and at various Re:Si molar ratios.

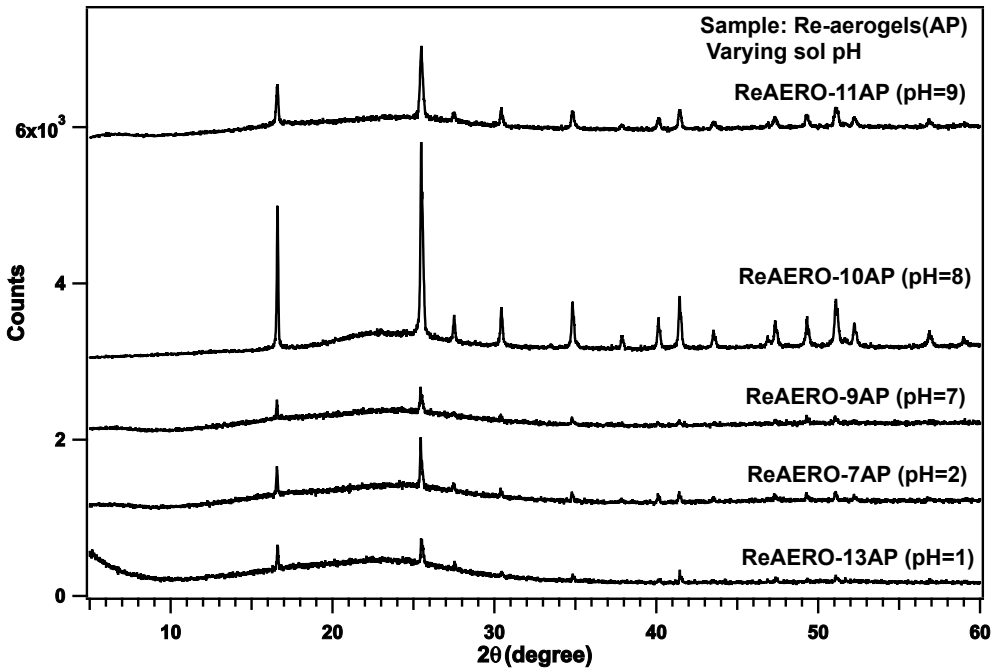

Figure A.3 Powder XRD patterns of the as-prepared Re-aerogel samples synthesized at different sol pH. Ammonium molybdate was used as the precursor and the Re:Si molar ratio was at 0.2

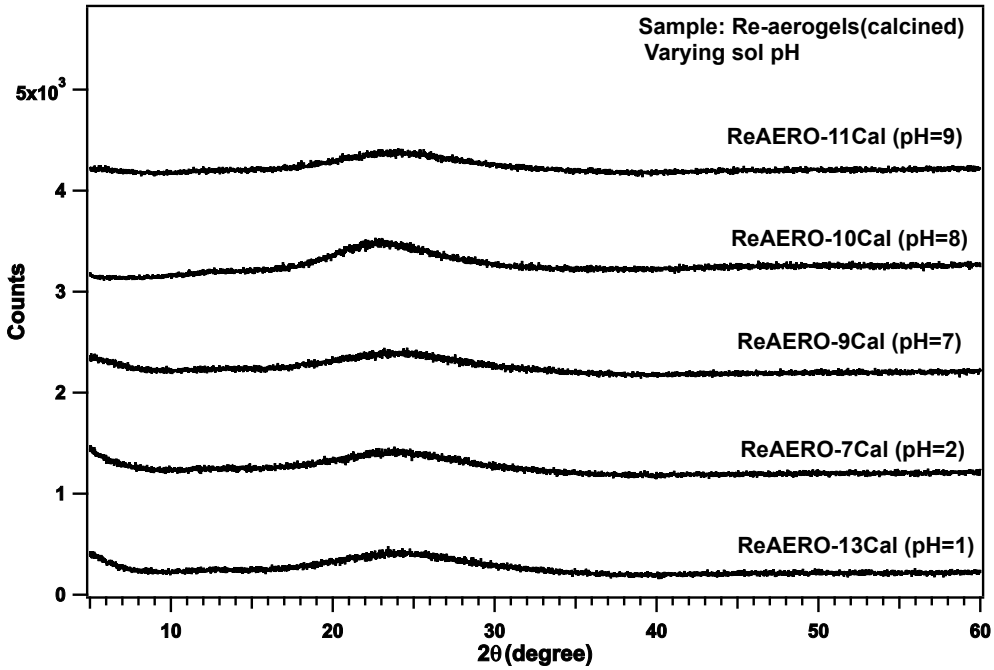

Figure A.4 Powder XRD patterns of the annealed Re-aerogel samples synthesized at different sol pH.

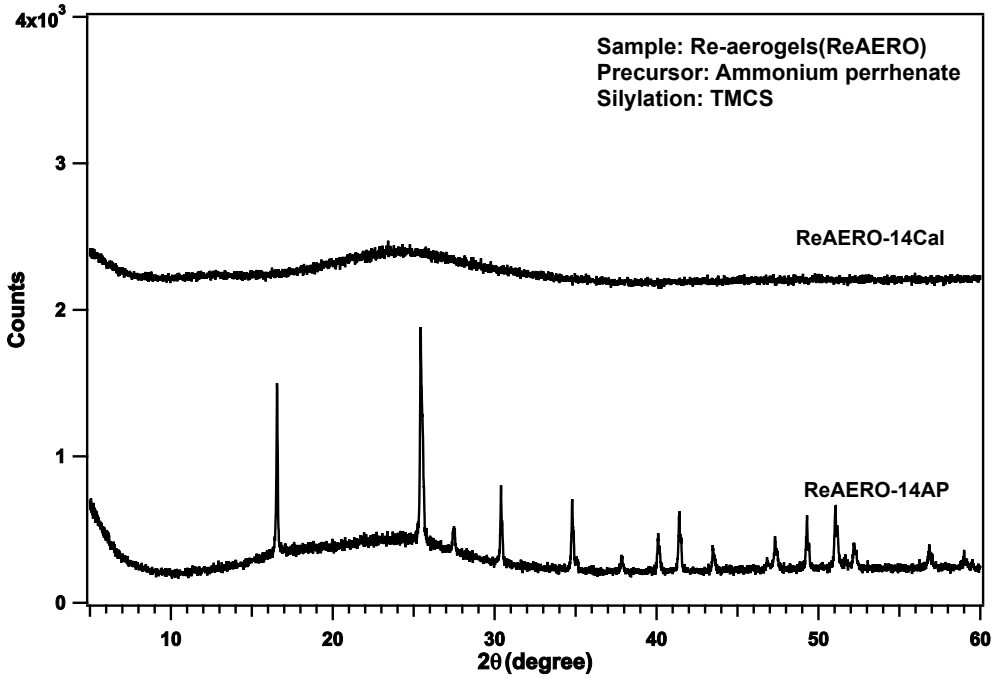

Figure A.5 Powder XRD patterns of the as-prepared and calcined Re-aerogel samples synthesized with TMCS.

A.2 MeAlPO-5

A.2.1 Powder XRD patterns of MoAlPO-5 samples

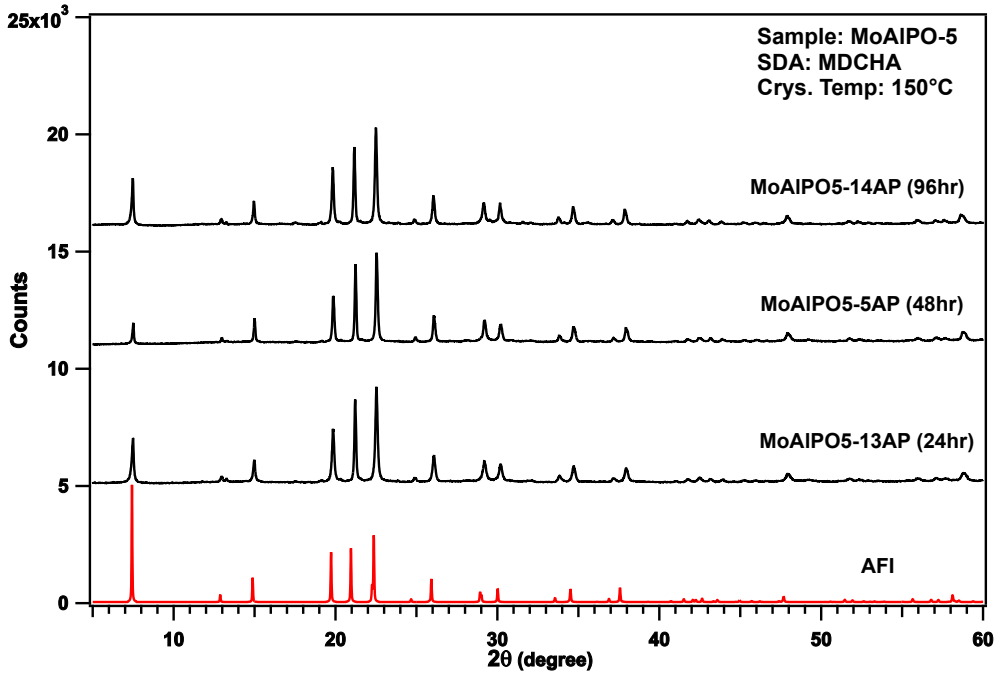

Figure A.6 Powder XRD diffractogram of as-prepared sample of MoAlPO-5 using MDCHA as SDA at 150°C. The diffraction patterns show that all the samples are phase pure AFI.

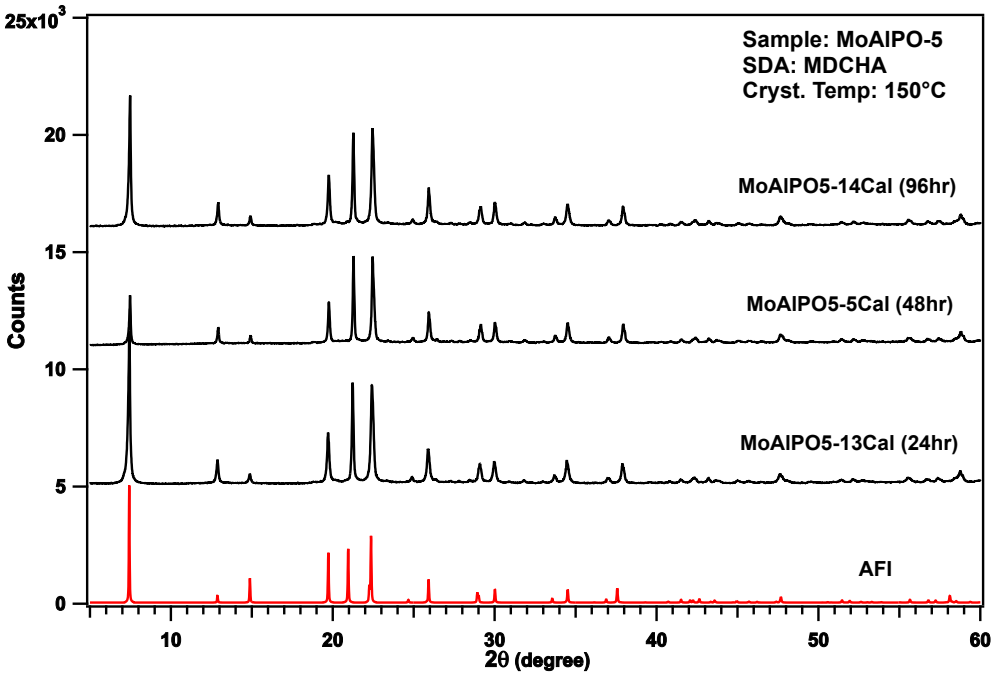

Figure A.7 Powder XRD diffractogram of calcined sample of MoAlPO-5 using MDCHA as SDA at 150°C. The diffraction patterns show that all the samples remain phase pure after calcination.

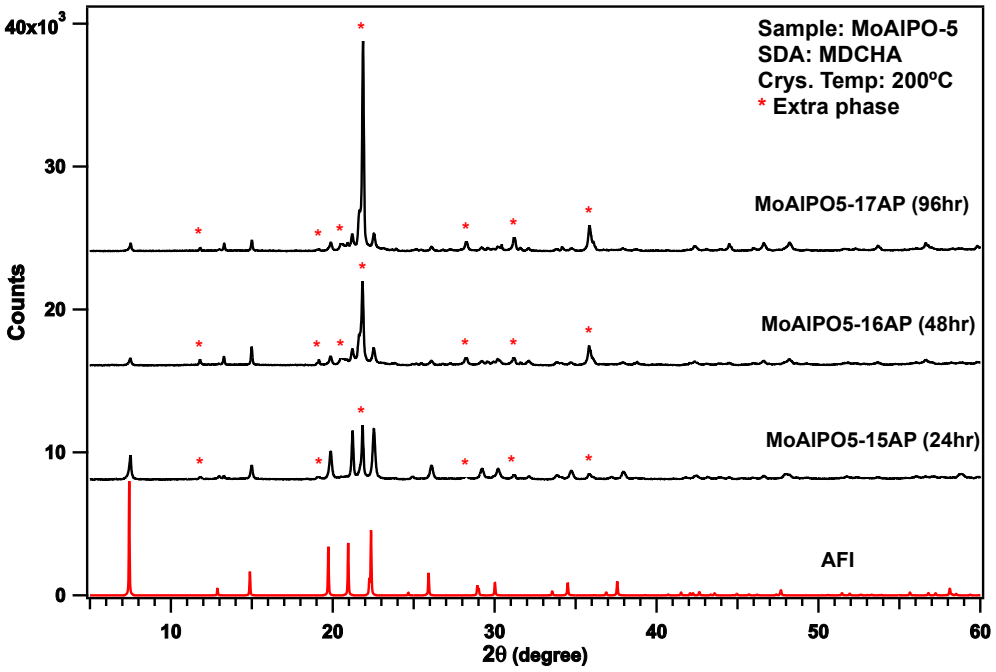

Figure A.8 Powder XRD diffractogram of as-prepared sample of MoAlPO-5 using MDCHA as SDA at 200°C. The diffraction patterns show that all the samples contain extra phases.

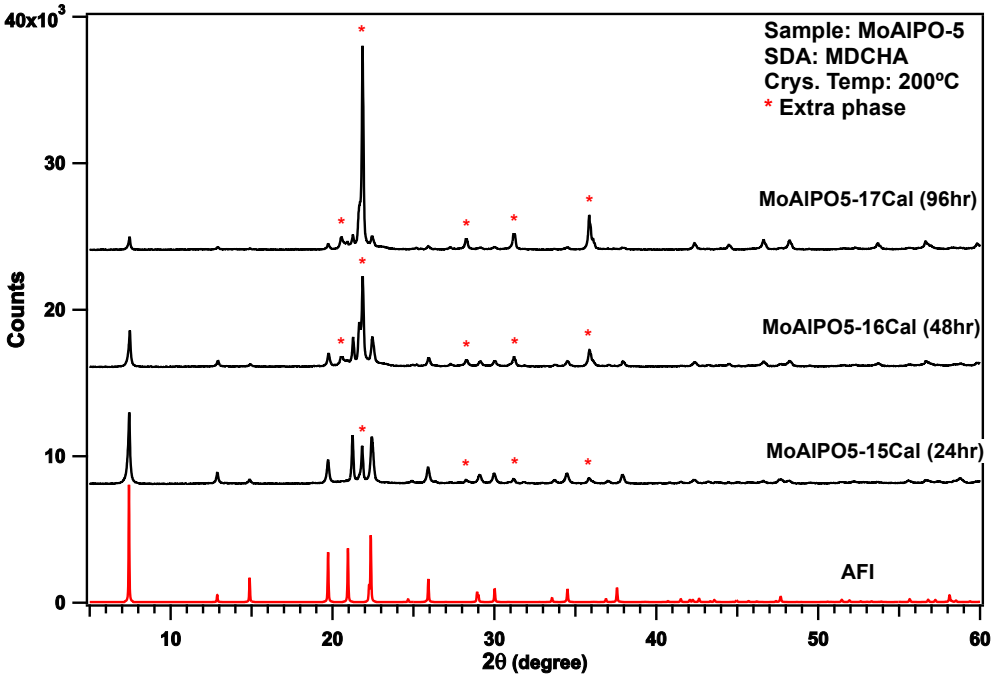

Figure A.9 Powder XRD diffractogram of calcined sample of MoAlPO-5 using MDCHA as SDA at 200°C. The diffraction patterns show that all the samples still contain extra phases.

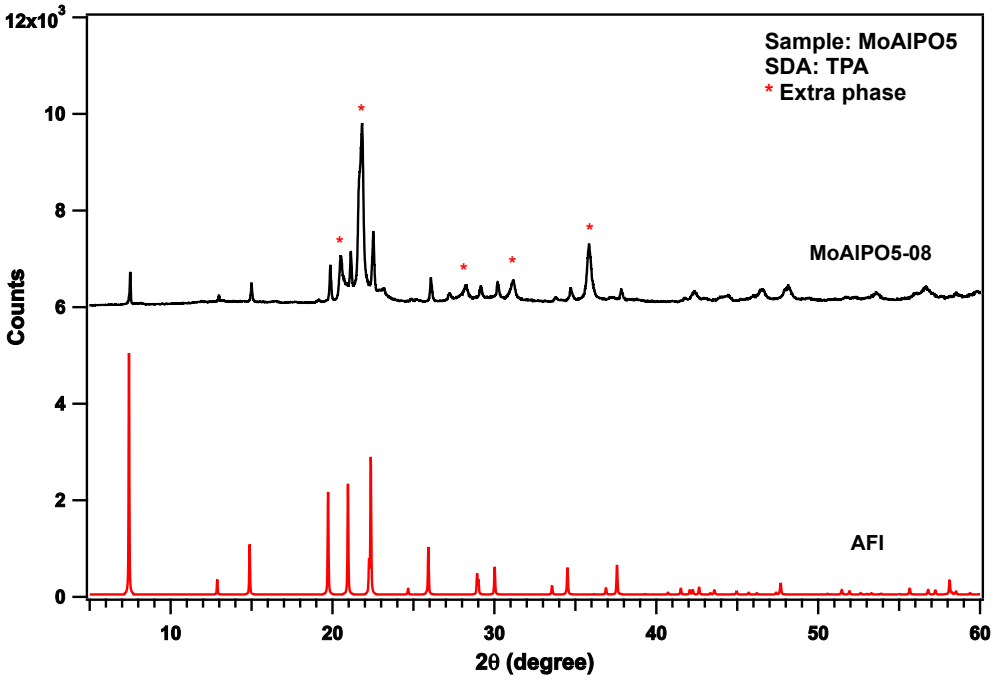

Figure A.10 Powder XRD diffractogram of the as-prepared sample of MoAlPO5-8 in which TPA was used as the SDA. Extra phases are presented.

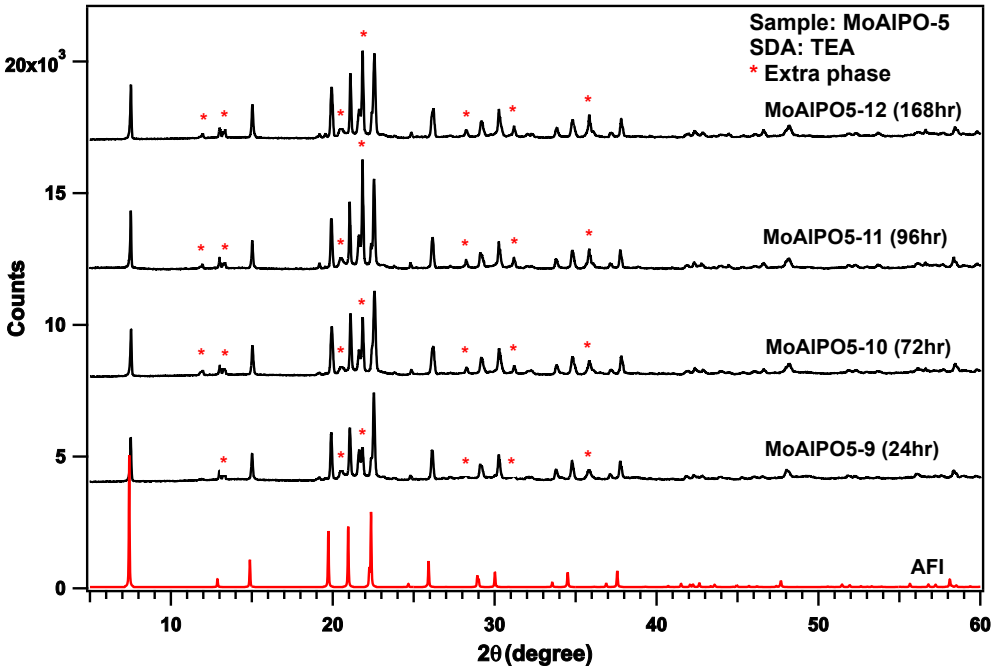

Figure A.11 Powder XRD diffractogram of the as-prepare sample of MoAlPO5-9 to MoAlPO-12 in which TEA was used as the SDA. Extra phases are presented.

A.2.2 Powder XRD patterns of ReAlPO-5 samples

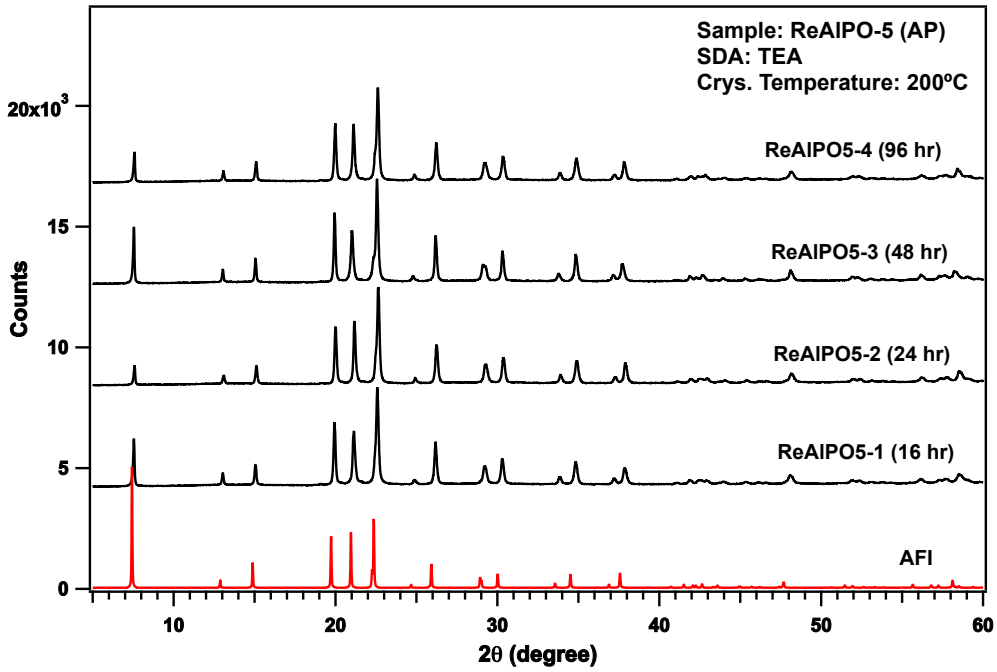

Figure A.12 Powder XRD diffractogram of the as-prepare sample of ReAlPO-5 in which TEA was used as the SDA and crystallized at 200°C. All the samples appear to be phase pure AFI.

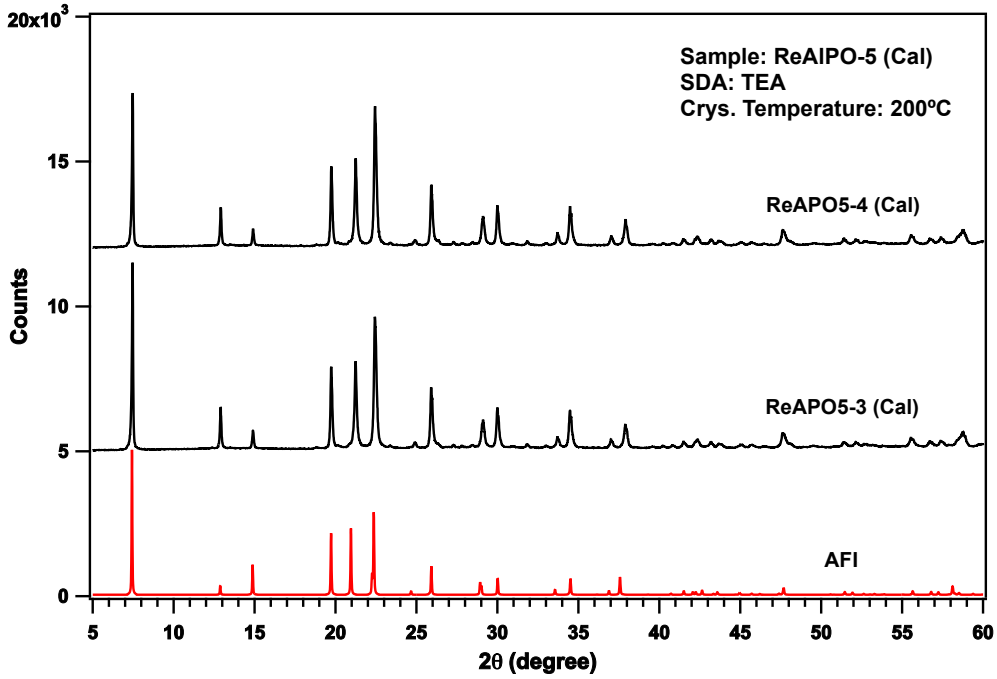

Figure A.13 Powder XRD diffractogram of the calcined sample of ReAlPO-5 in which TEA was used as the SDA and crystallized at 200°C. All the samples appear to be phase pure AFI.

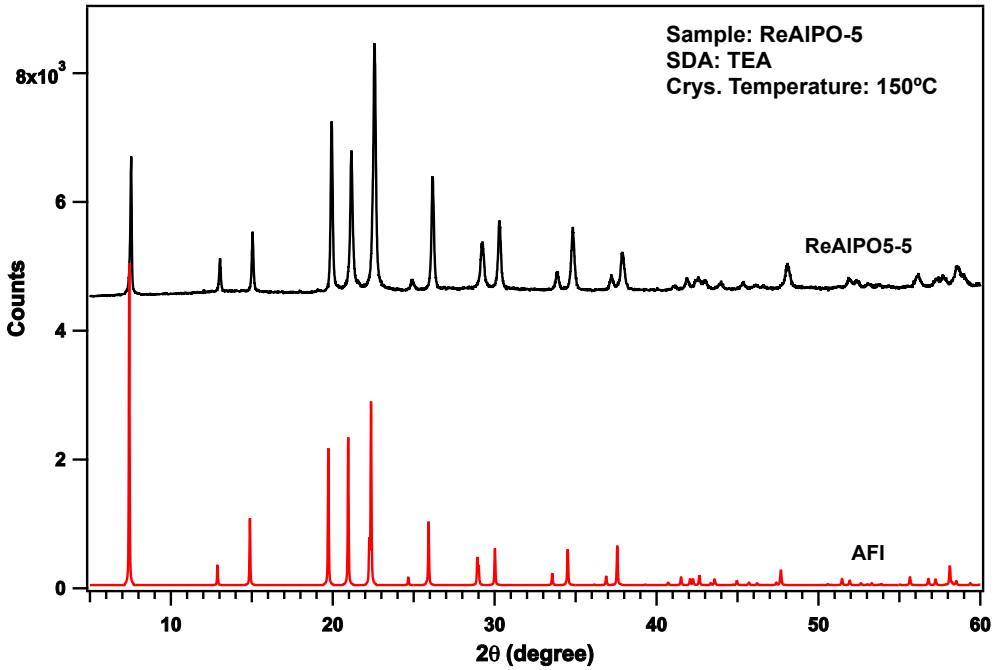

Figure A.14 Powder XRD diffractogram of the as-prepare sample of ReAlPO5-5. The crystallization temperature was adjusted to 150°C.

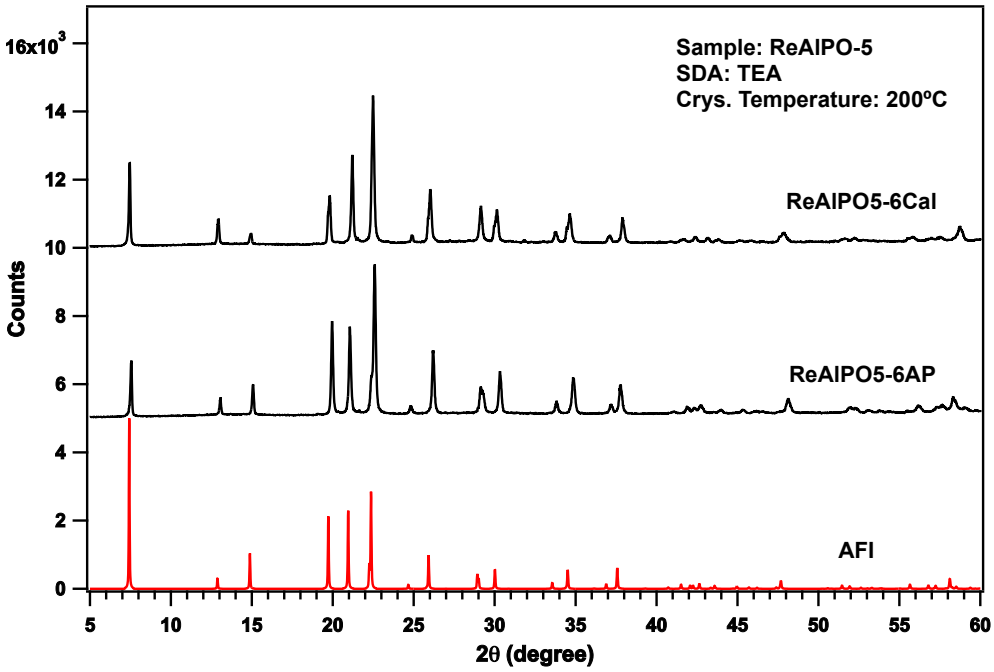

Figure A.15 Powder XRD diffraction patterns of as-prepared and calcined sample ReAlPO5-6, where the molar ratio increased to 0.10 Re : Al. Both the as-prepared sample and the calcined sample have the AFI structure.

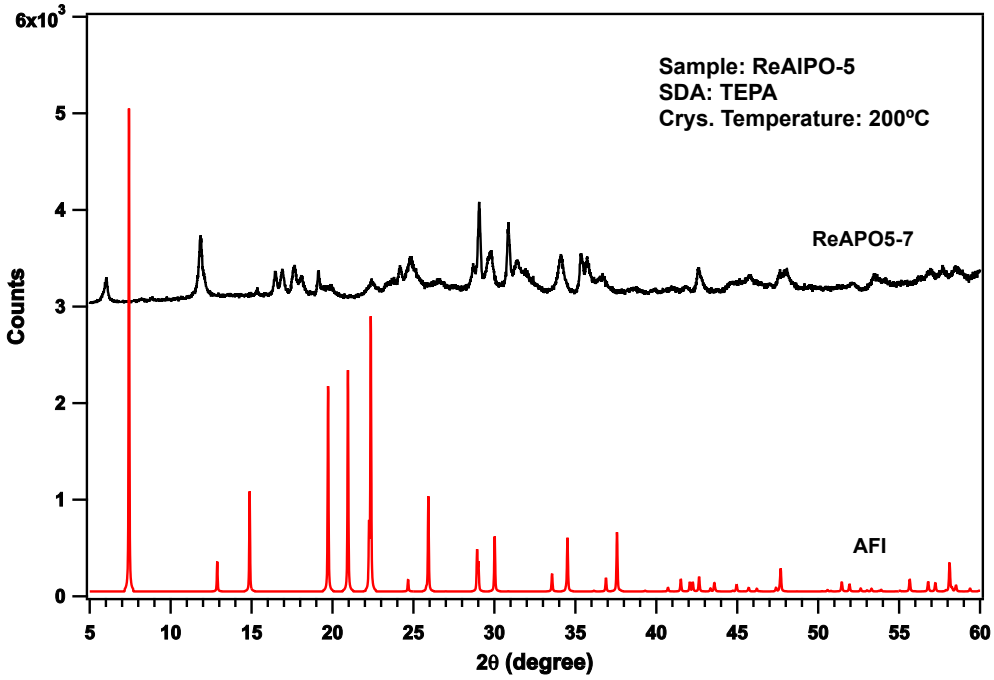

Figure A.16 Powder XRD diffraction patterns of as-prepared sample ReAlPO5-7 when TEPA was used as the SDA. The diffraction patterns show that the structure has relative low crystallinity and is not phase pure AFI.

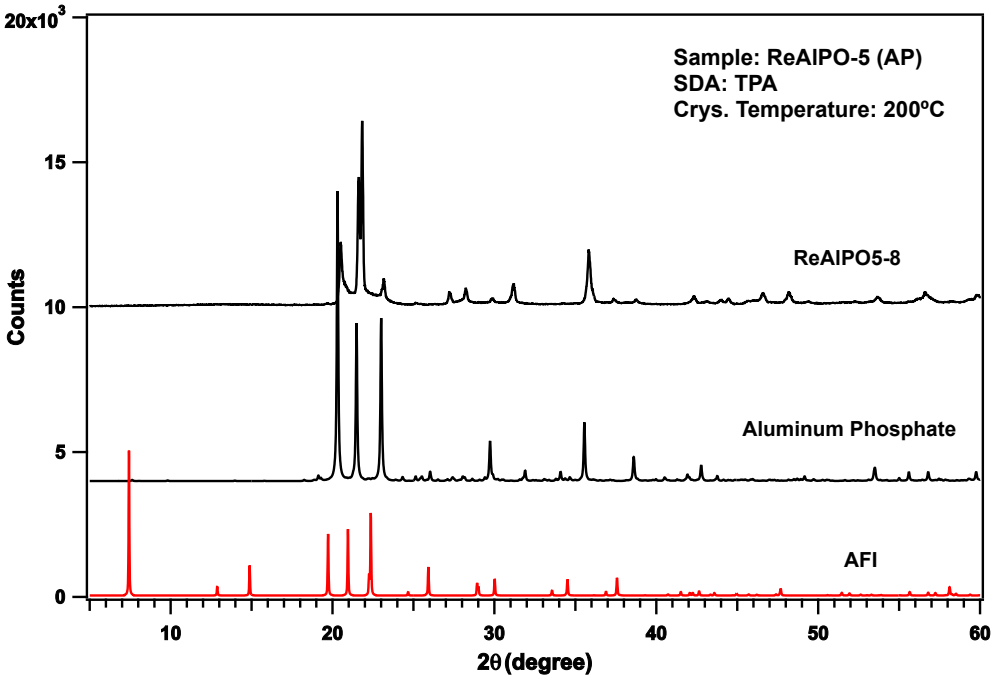

Figure A.17 Powder XRD diffraction patterns of as-prepared sample ReAlPO5-8, in which TPA was used as the SDA. The structures resembles the dense phase structure of aluminum phosphate rather than the AFI structure.

Appendix B

N_2 Adsorption-Desorption Isotherms

B.1 Isotherms of Mo-aerogels

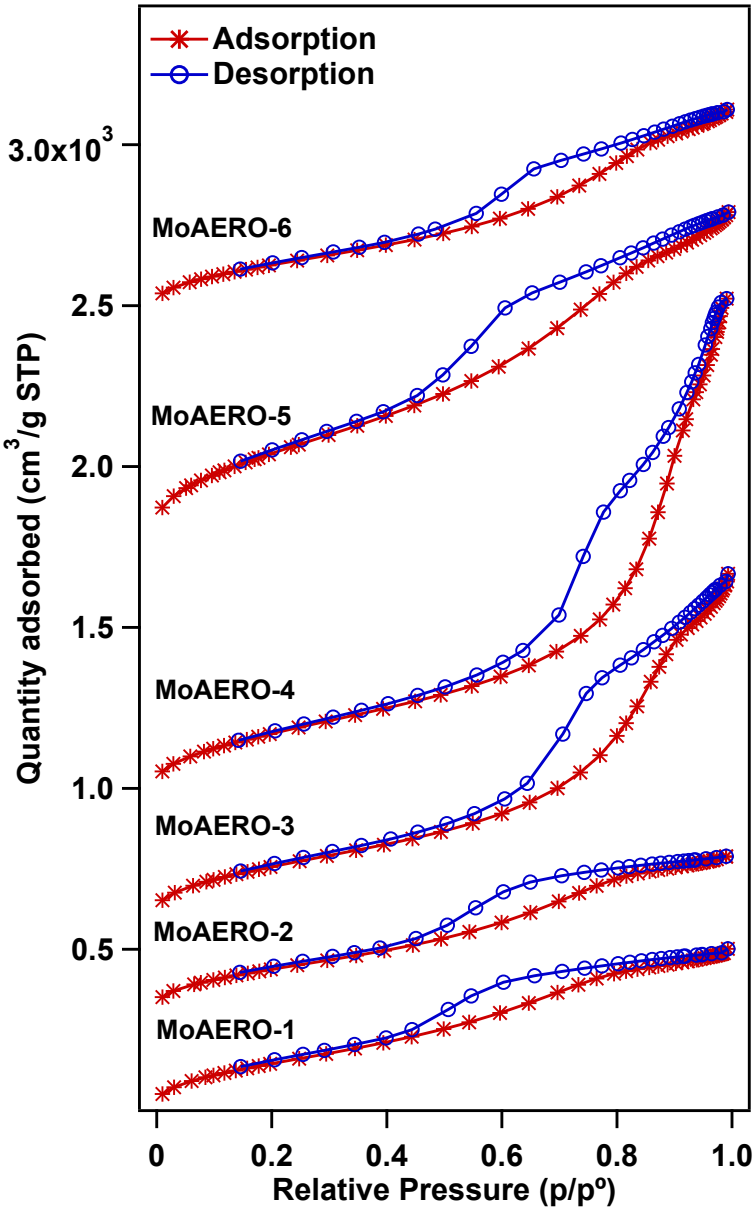

Figure B.1 Adsorption-desorption isotherms of as-prepared Mo-aerogels.

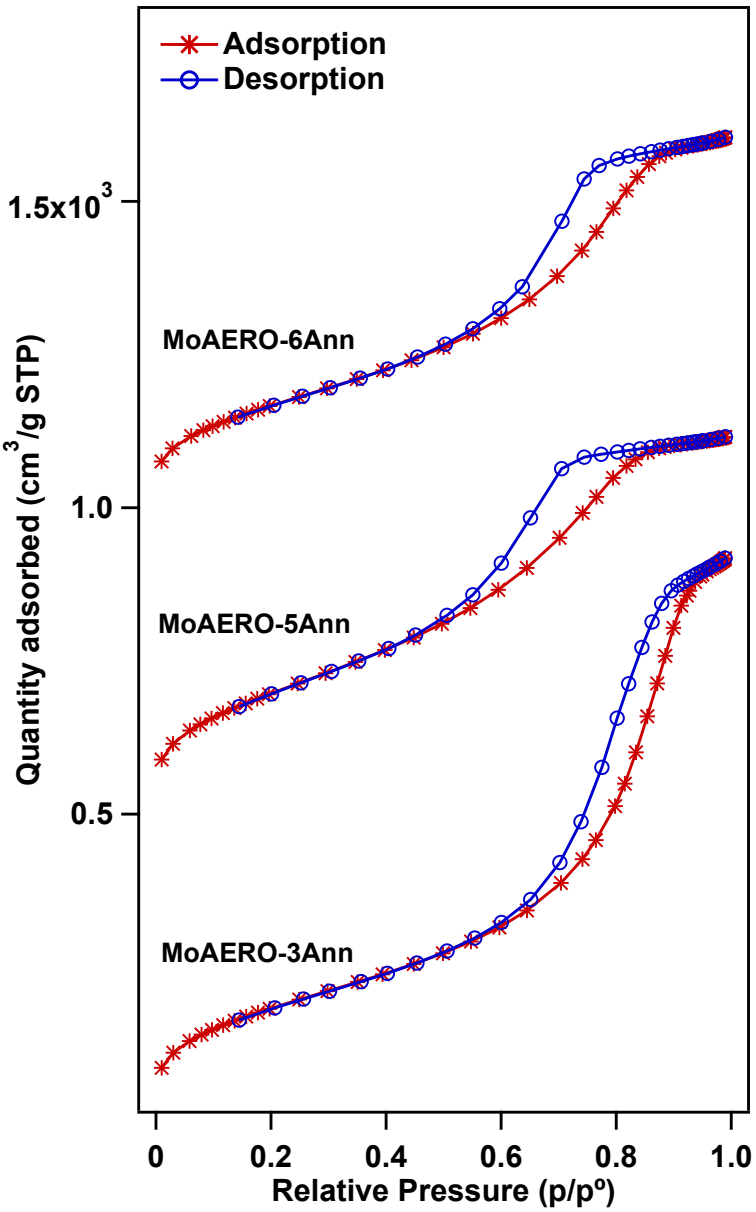

Figure B.2 Adsorption-desorption isotherms of annealed Mo-aerogels.

B.2 Isotherms of Re-aerogels

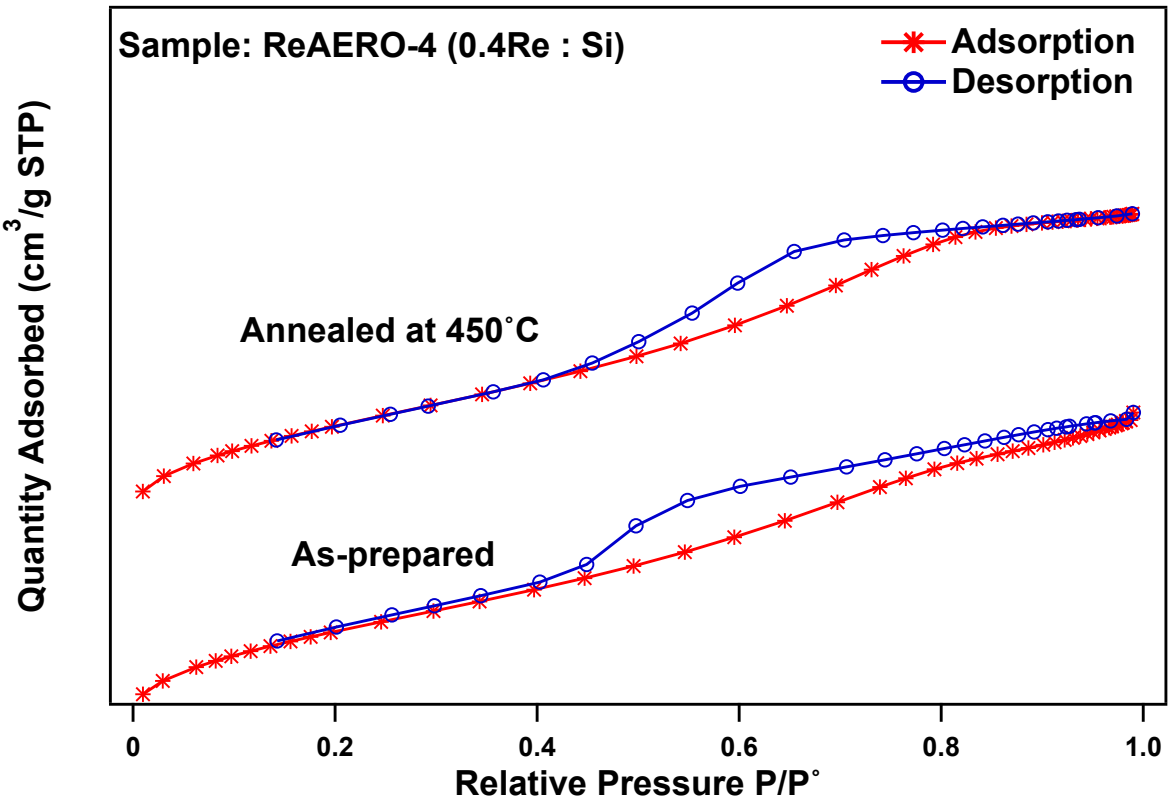

Figure B.3 Adsorption-desorption isotherms of as-prepared and annealed ReAERO-4. Isotherms of other analyzed samples have been plotted in chapter 4.